Development of New Modulation Methods Using the Pulse Valve Modulator in Multidimensional Gas Chromatography

Derrick V. Gough

A dissertation

submitted in partial fulfillment of the

requirements for the degree of

Doctor of Philosophy

University of Washington

2020

Reading Committee:

Robert Synovec, Chair

Bo Zhang

Matthew Bush

Program Authorized to Offer Degree:

Department of Chemistry

University of Washington

Abstract

Development of New Modulation Methods Using the Pulse Valve Modulator for Multi-Dimensional Gas Chromatography

Derrick V. Gough

Chair of the Supervisory Committee:
Professor Robert E. Synovec
Department of Chemistry

The potential efficiency and applicability of gas chromatography is advanced through the continued development and use of the pulse valve modulator. New advancements in modulation techniques are reported with the pulse valve modulator concurrently with the use of commercial chemometric algorithms and new data visualization techniques. First, the application of partial modulation in the negative pulse mode (NPM) is demonstrated. The NPM is developed for high-speed, one-dimensional gas chromatography (1D-GC), comprehensive two-dimensional (2D) gas chromatography (GC×GC), and comprehensive three-dimensional gas chromatography (GC^3). This modulation technique is shown to be more beneficial than previous work with partial modulation in the positive pulse mode (PPM). The NPM produces comparable analyte peak widths-at-base (w_b) as the PPM but does so with greater *S/N* and with less data processing required. In the 1D-GC mode, 8 analytes are baseline resolved ($R_s \geq 1.5$) in a 200 ms window, providing a

peak capacity, n_c, of 14 at unit resolution (R_s = 1.0). Demonstrating this higher efficiency to a GC×GC, a 20-component test mixture is separated. Analytes were separated on the second-dimension column, ^{2}D, with ^2w_b ranging from 7 to 12 ms, providing an exceptional ^{2}D peak capacity, ^2n_c of ~12 using a P_M of 100 ms. Next, the NPM is applied to a GC^3 with time-of-flight mass spectrometry detection (TOFMS). Narrow third dimension, ^{3}D, peaks ^3w_b ~ 15 ms were obtained, resulting in a GC^3 peak capacity, $n_{c,3D}$, of ~35,000, in a 45 min separation. While high peak capacity has been produced, there are challenges that needed to be addressed regarding the use of commercially available data analysis techniques to ensure method translation can occur. The NPM data has the appearance of ^{2}D separations superimposed on top of the ^{1}D separation, which is unique. Multivariate curve resolution – alternating least squares (MCR-ALS) is used to demonstrate the potential for method translation with the NPM technique. A mixture of 15 similar analytes was isothermally separated to purposefully create several scenarios of peak overlap within 20 s. Despite the high degree of overlap, the NPM data is shown to be amenable to MCR-ALS, with all 15 analytes able to be decomposed, separated, and identified. The potential for quantification is demonstrated for two representative analytes, with percent deviation values of -5.6% (± 2.2%) for 1-hexene, and 1.8% (± 3.4%) for 2-pentanone. Next, the pulse valve modulator was used in the full modulation mode to demonstrate further advancements and quantifiable gains in *S/N* with GC^3 instruments. The detector response enhancement factor (*DREF*) is a quantifiable measure of the increase in *S/N* ratio of analyte signal as the number of dimensions is increased. We calculated *DREF* values of ~ 37 for dodecene and ~ 21 for tridecane. Additionally, the ^{2}D×^{3}D peak capacity was demonstrated at 30 peaks per 1.5 s. Last, a method to visualize the ^{2}D×^{3}D chromatogram is presented, in which four successive modulations are lined up and one can “see” analytes arriving at and eluting from the TOFMS detector.

TABLE OF CONTENTS

LIST OF FIGURES

LIST OF TABLES

ACKNOWLEDGEMENTS

The research presented within this dissertation isn't merely the work of an individual, rather it is a glimpse of the collaborative work and efforts of a group of outstanding scientists and researchers that I have had the privilege to work with and learn from. First, I must thank my graduate research advisor, Dr. Robert Synovec. Thank you for taking a chance on me as a student, 8 years out of college with no research experience. Your guidance, support, and mentorship were crucial to my growth as a scientist and I will use the lessons you have taught me in my future endeavors. To my fellow members of the Synovec Research Group, thank you as well. Whether you know it or not, your friendship, dedication to research, and day-to-day talks (and groans over my dad jokes) were immeasurably helpful in taking me from a graduate student with zero research experience to a confident researcher.

Thank you to my brother, Dara, for setting the example for me. You were the first one in our family to attempt graduate school, let alone complete it and earn your Ph.D. You set an example that I could follow, albeit on my own timeline. I didn't realize it growing up, but I have always looked up to you and the example you set for me.

Last, and most importantly, thank you to my wife, Abby. I have told you before, and I cannot tell you enough, how much you and your support mean to me. I know that I would not have given myself the opportunity to go to graduate school without you being there to push me to try for new opportunities. You make me better. Thank you for being the rock that I can always lean upon.

DEDICATION

To my mom.

I know I did not take the route you preferred me to take, and that the moment you told me to do something, I was the child that did the exact opposite. I learned from you how to be headstrong and stubborn. I also learned from you how to be intelligent, fiercely independent, and courageous. You have been through some incredible tribulations to get where you are and, in the process, set an incredible example for me as a mom and person. I have taken your example to heart and I try to emulate it in my own way to make you proud. Thank you ma, I love you.

Chapter 1. Introduction to Multidimensional Gas Chromatography and the Pulse Valve Modulator.

1.1 INTRODUCTION TO GAS CHROMATOGRAPHY

1.1.1 *History of and Introduction to Gas Chromatography*

Chromatography, as an analytical technique, was introduced around 1899 by M.S. Tswett with his work studying the physico-chemical structures of plant chlorophylls.[1] All chromatography is based upon a two-phase flow system, a mobile phase and a stationary phase; separation occurs due to the differences in affinity to both phases by the chemicals being separated. Following a half century of advances into chromatographic practices and theories, a milestone study by James and Martin was published in 1952.[2] This work was the first to detail a gas-liquid partition chromatography of volatile fatty acids and helped usher in the idea of modern, high performance gas chromatography. Since its inception, gas chromatography (GC) has undergone a myriad of evolutions and breakthroughs, enabling its continued use into an ever-increasingly complex array of samples. There are numerous publications can provide a more complete history to chromatography in general and GC in particular,[3–5] in addition to the included references.

Gas chromatography is a common analytical technique that can be found in industry and research laboratories around the world.[5] Typically, the mobile phase used is an inert gas, such as hydrogen or helium, referred to as a carrier gas. Samples are injected into an inlet where they are vaporized and join the mobile phase gas. The mobile phase gas carries the analytes through a column and terminates at a detector. The column, often termed a separation column, can be made with a variety of materials, come in a variety of sizes, and contains the stationary phase. The stationary phase can be selective for a plethora of desired separation conditions, such as polarity,

chirality, and specific functional groups, to name a few. Moreover, analytes in the gas phase are amenable to a wide-variety of detectors that can be switched in and out of the GC instrumental platform depending on specific needs. One commonly used detector, the flame ionization detector (FID), measures the response of ions produced during the combustion of compounds in a hydrogen flame. This detector can be both extremely fast and quantitative. Another commonly used detector is the mass spectrometer (MS). There are many ways in which an MS can operate, but generally for GC the MS will ionize and fragment the analytes as they enter the detector via electron impact ionization, and then the fragments are separated and detected by their mass-to-charge (*m/z*) ratio. Each analyte displays a unique fragmentation pattern, enabling unknown analyte identification in addition to analyte quantification through MS techniques. Such wide-ranging applications has made GC a very attractive analytical tool that is used in nearly every industry.

1.1.2 *Comprehensive, Two-Dimensional Gas Chromatography (GC×GC)*

The first 50 years of GC instrumentation brought many improvements to the field of analytical chemistry, enhancing the separation power and broadening GC's applicability. One of the largest single jumps in GC evolution came with the advent of comprehensive, two-dimensional gas chromatography (GC×GC), first theorized by Giddings[5] and then experimentally pioneered by Lui and Phillips in 1991.[6] The general concept behind GC×GC is to use two different (i.e. orthogonal polarities) separation columns during a single GC run, thus having "two-dimensions" of separation. Essentially, the first column of a GC separation remains the same, but the effluent, as it reaches the end of the first separation column, is "re-injected" onto a shorter, quicker second column for a subsequent separation. Ideally, the second column will have either a much different type of stationary phase from the first column or a specific type of stationary phase for known functional groups.

This second separation is possible due to a new piece of equipment called a modulator. Modulators act essentially like a second injector within the GC instrument, trapping analytes as they exit the first column (^{1}D), focusing them at the point of modulation, and then reinjecting the analytes for the shorter, quicker separation on the second column (^{2}D). A more in-depth description of modulators, and modulation, will be discussed in this chapter. Visually, traditional, one-dimensional GC (1D-GC) instruments return data in which a single analyte produces a single peak that nominally looks like a Gaussian curve, with an x-axis in the time domain and the y-axis in the signal intensity domain (Figure 1.1A). The output of ^{2}D peaks for a given modulated analyte with a GC×GC instrument first appears as a series of narrower, taller Gaussians that follow the same general shape as the ^{1}D profile (Figure 1.1B). The modulations occur at constant intervals referred to as the modulation period (P_M), indicated by the dotted lines in Figures 1.1A-B. Once processed to incorporate the two time axes, by cutting and folding the modulated data at each P_M, the GC×GC data appears more akin to a topological map where the x-axis is the ^{1}D column time, and the y-axis is the ^{2}D column time (Figure 1.1C), which is equivalent to the P_M.

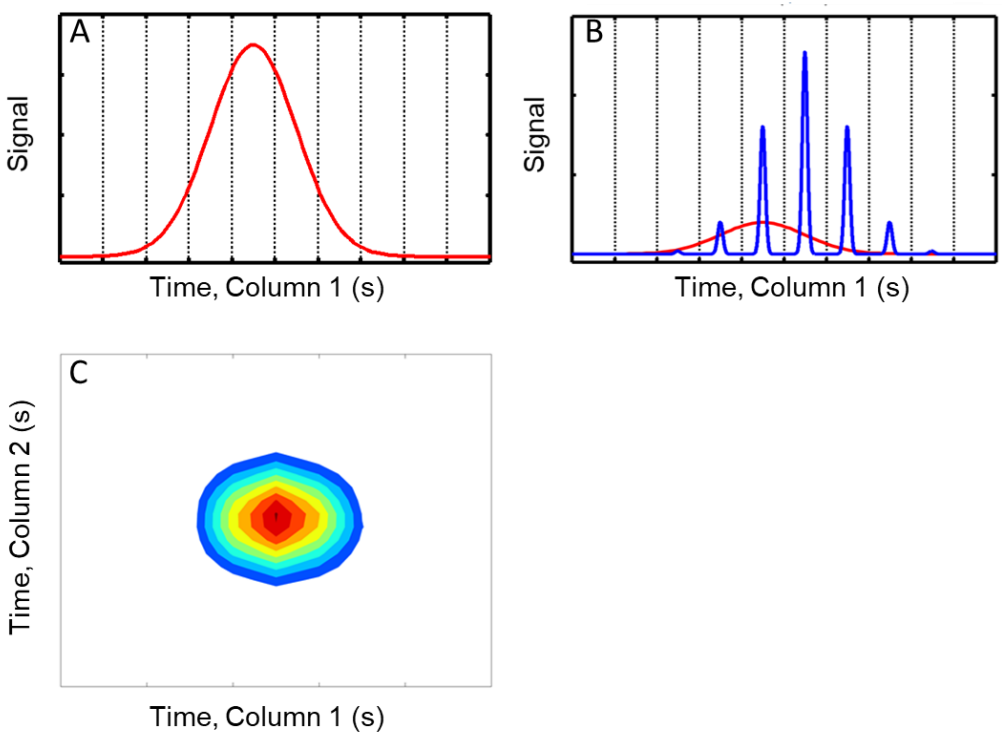

Figure 1.1. Representation of GC data. A) Modeled Gaussian curve for a 1D-GC system. B) Modeled GC×GC data (blue outline) for the curve in Figure 1.1A. Notice how the narrower, blue peaks are significantly taller than the red, 1D-GC outline. C) Processed data from Figure 1.1B. This contour plot is one means of displaying 2D GC×GC data after data processing.

1.2 Principles of Modulation

There are several types of modulators, and numerous reviews have been conducted to keep pace with their evolution.[7–13] Despite the wide variety, nearly all modulators operate by a very similar set of principles. First, the modulator traps/focuses eluate containing the analyte as it exits the ^{1}D column for a set period. Then, the modulator actuates, or releases/injects the eluate onto the ^{2}D column, and the process repeats. This period of time, that determines the frequency at which this process occurs (trap, focus, and injection), is termed the modulation period (P_M). The P_M is determined by the user and is limited by the hardware of the modulator. There are numerous

commercially available modulators, but they fall into two general categories: thermal and flow-based modulators.

Thermal modulators rely upon a difference in temperature to modulate the ^{1}D effluent. There are two sub-categories for thermal modulators: cryogen-based and cryogen-free thermal modulators. The earliest modulators were cryogen-based, and they remain popular and widely available today.[6,14–17] Cryogen-based modulators use a cryogenic fluid, like liquid nitrogen, to create a cold zone on a separation column at the point of modulation, essentially freezing effluent at this section of column. During actuation, the cold zone is turned off and a jet of hot air is used to rapidly vaporize and desorb the effluent from the ^{1}D column for subsequent separation on the ^{2}D column. There are some inherent limitations with this technique, with the prominent ones being the limited volatility range, the extra equipment and consumable materials, and increased cost required. Cryogen-free thermal modulators operate under the same principle, just without the required cryogenic liquids.[7,9,18] While this reduces the equipment footprint required, it does further decrease the volatility range of analytes that can be modulated.

Flow-based modulators use a second stream of auxiliary carrier gas to control and divert smaller aliquots of effluent from the ^{1}D column to the ^{2}D column. This can be done mechanically as in the case when implementing a suitable valve. When using a valve, effluent is trapped in a sample loop attached to the valve, and the valve is actuated periodically (per the P_M) to transfer the ^{1}D effluent from the sample loop to the ^{2}D column for separation.[19–24] This can also be done by a difference in pressures at a junction, which is broadly termed flow modulation. Flow modulators trap, compress, and divert effluent from the ^{1}D to the ^{2}D in a similar manner, but without any mechanical means as with a valve.[11,25–34] The main drawback to flow modulators is the potential lack of a total transfer of effluent (duty cycle < 1.0) from the ^{1}D to the ^{2}D, with some

modulators operating only as a low duty cycle modulator (duty cycle < 0.5).[7,9,13,35] Despite zonal compression offsetting some of this negative, this is often seen as disadvantageous as all thermal modulators have a duty cycle = 1.0 (100% mass transfer), and thus typically have a lower limit of detection (LOD) due to the higher *S/N* ratio. However, flow modulators are less equipment heavy, have a smaller footprint (no cryogenic liquids), and modulate all gas-phase analytes freely.

In 2004, a new type of modulation, coined partial modulation, was introduced by Cai and Stearn.[36] This novel method uses a flow modulator and a 3-way union to serially connect the two separation dimensions (ensuring a duty cycle = 1.0) and only modulate a fraction of the ^{1}D effluent. Until this work, all forms of modulation relied upon "full modulation," i.e. the entire analyte signal is modulated, breaking up the ^{1}D profile into a series of successive, narrower ^{2}D peaks that generally follow the same pattern as the ^{1}D profile, as illustrated in Figure 1.1. The ^{1}D profile can be mathematically reconstructed by fitting a Gaussian function to the maxima of the ^{2}D profiles for an analyte, but this does entail some undesired mathematical constraints as has been described by previous work.[37–40] By only modulating a fraction of the analyte signal, partial modulation provides the detector with information on the ^{1}D and ^{2}D profiles simultaneously. Despite the huge promise of this new modulation technique, it remained an unexplored advancement until our group recently returned to this technique with a new pulse valve modulator.[41–45]

Partial modulation can operate in two modes, the positive and negative pulse modes. As previously mentioned, a 3-way union is used the connect the ^{1}D and ^{2}D columns, with the 3rd way in the union connecting to an auxiliary supply of carrier gas through a pulse valve. The actuation of the pulse valve occurs for a user-selected period, termed the pulse width (p_w). In the positive pulse mode (PPM), the auxiliary carrier gas is kept off for the majority of the P_M, and is only turned on for a small segment, denoted by the difference in P_M - p_w. Thus, in the PPM, a pulse of

carrier gas is sent into the stream of analytes eluting from the ^{1}D column, injecting a vacancy into the ^{1}D effluent as it enters the ^{2}D column. This vacancy ultimately produces chromatographic information following the ^{2}D separation, and when combined with the principles of frontal analysis, can be analyzed as traditional GC×GC data. Previous research by the Synovec group details the steps required to conduct this analysis,[41] and is not the subject of this dissertation. In contrast, in the negative pulse mode (NPM), the auxiliary gas from the pulse valve is kept on for the majority of the P_M, and is only turned off for a small segment, denoted as the p_w. This dissertation is primarily aimed at pioneering efforts in the development of the NPM.

The NPM employs a steady stream of auxiliary carrier gas from the pulse valve that dilutes the effluent departing the ^{1}D column. During actuation for time interval p_w, the stream of auxiliary carrier gas is stopped, so a brief segment of the effluent departing the ^{1}D column is not diluted. This un-diluted segment of ^{1}D effluent, ultimately appears as a narrow ^{2}D peak on top of the ^{1}D peak profile, is then separated on the ^{2}D column. This process is explained in more detail in a subsequent chapter. The NPM provides numerous benefits over the PPM. First, it provides positive ^{2}D peaks, improving the *S/N* compared to the PPM. Secondly, the data analysis with NPM is simpler; there is no differentiation nor inversion step in handling the raw data as is the case with PPM. This enables a quicker and easier mathematical separation of the ^{1}D and ^{2}D profiles. These benefits, without any loss in ^{2}D peak widths, are a few of the reasons that the NPM is the focus of my research.

1.3 FIGURES OF MERIT FOR IMPROVED PERFORMANCE

1.3.1 *Peak Capacity*

There are a few figures-of-merit (FOM) that can be used to compare various forms of modulation, and different modulators, to each other. These FOMs are necessary in order to gauge

the overall separating strength of different types of modulation, and to see if new modulators can meet and exceed current benchmarks set by the current generation of modulators. A few FOMs have already been introduced: duty cycle, *S/N* ratio, and P_M. Modulators that connect the successive separation columns serially, such as thermal modulators and the pulse valve, have a duty cycle of 1.0. That is, all of the analyte injected onto the ^{1}D column will reach the detector with zero potential for loss due to the modulation process. This is a huge benefit to these two types of modulators, as most flow modulators, without proper synchronization, timing, or implementation, have a duty cycle of less than 1.0, meaning that some ^{1}D effluent is lost during modulation. Higher duty cycles generally lead to a higher *S/N*, which is key to lowering possible LODs with GC×GC systems. Additionally, a shorter, faster P_M is becoming possible with newer modulators and new materials, which is a key factor in my research as I seek to reduce overall separation time.

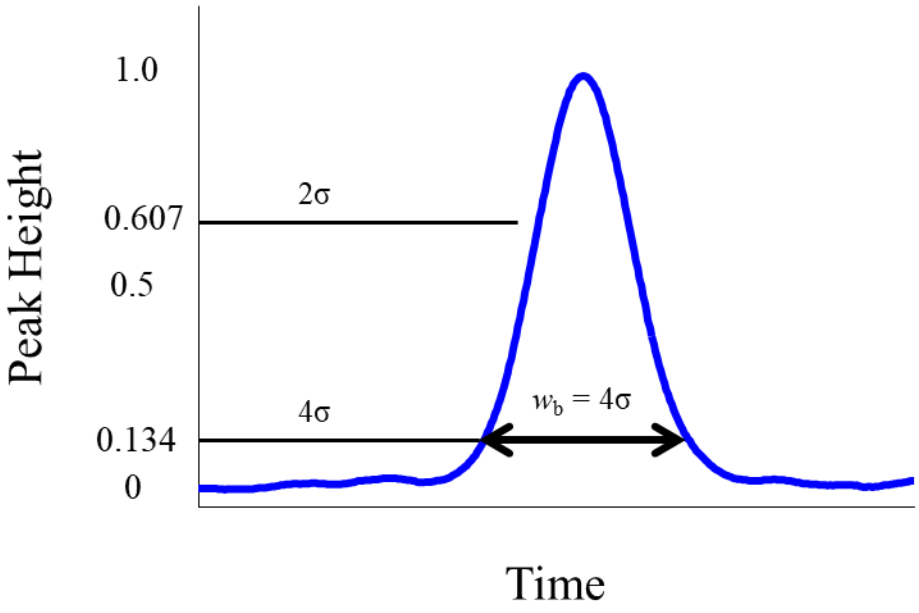

Figure 1.2. Modeled Gaussian peak with markings indicating fractional peak heights at 2σ and 4σ. All w_b measurements are done at 4σ to encompass 95% peak area.

One of the most common FOMs is a system's peak capacity, n_c. The n_c of a system can be simply thought of as the total number of peaks that can "ideally" fit in a given separation time. To calculate n_c, the separation time (t_{sep}) of a given separation dimension is divided by the average peak width-at-base (4σ), w_b, for that dimension (Equation 1.1), where the peak width is illustrated in Figure 1.2.

$$ {}^{x}n_c = \frac{{}^{x}t}{{}^{x}w_b} \tag{1.1} $$

This is an appropriate equation for all instances in which the chromatographic resolution (R_s) between any two neighboring peaks is 1.0. Equation 1.1 can be expanded for a GC×GC system by taking the product of the two dimensions to equal the total system peak capacity, $n_{c,2D}$.

$$ n_{c,2D} = {}^{1}n_c\,{}^{2}n_c \tag{1.2} $$

Substituting Equation 1.1 into Equation 1.2, we can relate the $n_{c,2D}$ to the t_{sep} of each dimension and the average w_b produced in that dimension.

$$ n_{c,2D} = \frac{{}^{1}t}{{}^{1}w_b}\frac{{}^{2}t}{{}^{2}w_b} \tag{1.3} $$

One step further, since the t_{sep} of the ^{2}D is equal to the P_M, then one obtains,

$$ n_{c,2D} = \frac{{}^{1}t}{{}^{1}w_b}\frac{{}^{1}P_M}{{}^{2}w_b} \tag{1.4} $$

This gives a relationship that can be related directly to the possible P_M of a modulator. Previous studies[37,38,40,46] have shown that to ensure a comprehensive separation, each analyte ^{1}D profile must be modulated at least twice. The number of times an analyte peak is modulated (Figure 1.3) is termed the sampling density, ρ_s, defined as the w_b/P_M. Proper ρ_s is important – too little (< 2 across a chromatogram) and the separation is not comprehensive and is not considered to properly

modulate every analyte. Too much (> 4 across a chromatogram), and the ${}^1w_b$ are too wide and total $n_{c,2D}$ is sacrificed with no offsetting gain.

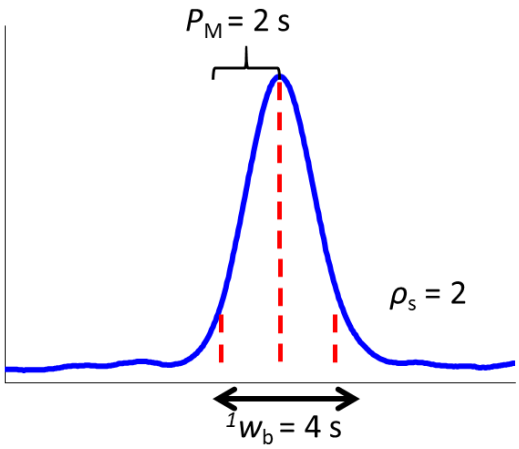

Figure 1.3. Modeled 1D-GC peak with lines denoting the P_M. In this example, a ${}^1w_b$ of 4 s, modulated every 2 s, produces a ρ_s of 2.

However, keeping in mind proper ρ_s, we find a direct relationship between the ρ_s of a separation and the total $n_{c,2D}$ achieved.

$$n_{c,2D} = \frac{1}{{}^1\rho_s}\frac{{}^1t}{{}^2w_b} \tag{1.5}$$

Equations 1.4 and 1.5 are useful as they provide a means to directly compare potential $n_{c,2D}$ between various GC×GC systems, regardless of the type of modulator or modulation technique. The equations also begin to demonstrate the value of applying a low (but not too low) ρ_s. As separations become quicker and more efficient, the ${}^1w_b$ will become narrower, and thus the P_M provided by the modulator must further reduce to maintain appropriate ρ_s to maximize $n_{c,2D}$ while providing a comprehensive separation. Additionally, another pertinent FOM for any modulator will be how narrow the peaks are that are produced, as further reductions in ${}^2w_b$ will continue to increase total $n_{c,2D}$.

This concept can be further expanded for a 3D GC system (GC^3 or GC×GC×GC) in a similar manner.

$$n_{c,3D} = {}^1n_c\,{}^2n_c\,{}^3n_c \tag{1.6}$$

Going through the same process, Equation 1.6 can be converted into Equation 1.7.

$$n_{c,3D} = \frac{1}{{}^1\rho_s}\frac{1}{{}^2\rho_s}\frac{{}^1t}{{}^3w_b} \tag{1.7}$$

Equation 1.7 shows that a GC^3 system can be considered in a similar fashion to a GC×GC system. The addition of the second modulator provides the ability to further increase the total $n_{c,3D}$ compared to $n_{c,2D}$ or ${}^1n_c$, assuming the second modulator (from the ^{2}D separation to the ^{3}D separation) is fast enough (P_M < 250 ms), which then allows for the ^{1}D and ^{2}D separations to be fully optimized as well. If the second modulator is not fast enough, then the previous dimensions cannot be optimized, and $n_{c,3D}$ will not be maximized, as previously shown.[47,48]

As mentioned, n_c is the total number of peaks ($w_b = 4\sigma$) that can fit into a separation dimension. In a 1D-GC separation, the visual representation of the ideal chromatogram appears as the number of Gaussian peaks that can fit on the x-axis of a graph at a R_S = 1. In a GC×GC separation, now there are two time axes, the x- and y-axis, and one can visualize the $n_{c,2D}$ as fitting concentric circles on a 2D plane. A GC^3 separation simply adds another time axis to this visualization of a GC×GC separation. As one goes from 1D-GC to a GC×GC separations, previous work has shown that with theoretically optimized conditions, a maximum gain in n_c of 10-20 times is possible.[49–52] Current theoretical work has not been reported regarding the gains possible in a GC^3 separation; although one can imagine a similar jump in potential $n_{c,3D}$ when compared to a 1D-GC or GC×GC.

1.3.2 *Modulation Frequency*

Gas chromatographs are incredibly efficient separation instruments. Long separation columns can help ensure complete separation of individual analytes, but they also demand extended separation run times. Additionally, the longer an analyte is on a column, under isothermal separation conditions the concentration peak profile broadens (band broadening). Thus, for a constant injected analyte concentration, quickly eluting peaks are narrower and relatively taller (i.e. higher *S/N*), while later eluting peaks will be wider and relatively shorter (i.e. lower *S/N*). Likewise, shorter separation columns lead to narrower peaks since there is less time for band broadening to occur. Keeping all other experimental parameters the same, short separation columns lead to generally narrower peaks than long separation columns. Coupling a shorter separation column (with or without a faster oven temperature ramp) and/or higher carrier gas flow rate will further reduce the band broadening experienced by analytes.

With GC×GC, the second-dimension separation provides a new time dimension to further physically separate analytes from each other, that otherwise would not be separated in a 1D-GC separation, leading to increased overall R_s between peaks. These incremental gains in shorter separations and narrower peaks on ^{2}D separations can be further advanced with the addition of a high frequency modulator. The possible frequency of operation for a modulator, or how fast it can modulate, is a key instrumental parameter for my work in shortening overall separation time without losing any chemical information. As mentioned, shortening overall separation (analysis) time leads to narrower ^1w_b. In order to maintain high system $n_{c,2D}$ (or $n_{c,3D}$), we need a modulator that can modulate at a high enough frequency to produce a ρ_s of as close to 2 as possible regardless of the analyte w_b being modulated. Most commercially available modulators operate with a P_M in the timeframe of seconds,[13,35] which means they can only modulate peaks that are generally a few

to several seconds wide. This is generally insufficient when attempting to perform a 40 min GC×GC separation in 10 min or less. Ideally, when designing a faster and more efficient GC×GC separation, the ${}^{1}n_c$ of the 10 min separation would equal the 40 min separation with minimal loss of R_S despite the condensed separation window. Commercial modulators do not easily support this goal, as their modulation frequency is too slow to produce the required peak capacity production, or peak capacity per unit time, for rapid separations. Thus, a new modulator was needed to conduct additional research into fast GC×GC (and GC^3) separations, and hopefully open new avenues of interest for using a GC as an on-line monitoring instrument.

1.4 THE PULSE VALVE MODULATOR

The pulse valve modulator has proven to be an exceptional tool for our research. Although the pulse valve was not initially developed for use with GC, it will be demonstrated to be an incredibly versatile and rugged tool that required no modifications for our use. There are many similarities between our pulse valve modulator and the home-made valve implemented by Cai and Stearns in their initial report on partial modulation. Our pulse valve is set outside the GC oven, one end connected to an auxiliary carrier gas line provided by the GC itself, and the other end connected through custom tubing to a 3-way union. The pulse valve acts as a gateway for an auxiliary flow of carrier gas into the GC instrument, controlling how much, or little, carrier gas flow is introduced to a 3-way union, depending on the desired modulation technique.

Initial research with the pulse valve modulator explored the capabilities and some initial uses[41–44] that set it and the partial modulation in the PPM apart from other modulators and modulation techniques. First, it was found that the pulse valve can consistently and reproducibly modulate as quickly as every 50 ms and produce average peak w_b of ~10 ms. This fast P_M was unheard of and enabled initial optimization of the $n_{c,3D}$ for GC^3 that was, up to that point in time,

previously unachievable. To this end, an $n_{c,3D}$ of 11,000 in 10 min of separation was reported.[42] This was a significant achievement as 1D-GC instruments typically provide a maximum n_c of ~ 600 to 900 in an hour, with most commercial GC×GC instruments then only able to provide a maximum $n_{c,2D}$ of ~ 6,000 to 9,000 in an hour separation. Subsequent research focused on sustaining the high peak capacity production (~1,000 resolvable peaks per min) to a more traditional separation time. During a 40 min separation, an $n_{c,3D}$ of ~31,000 was achieved, or a peak capacity production of ~800 per min.[44] This presented a huge gain in peak capacity production due solely to this new pulse flow modulator.

Despite the performance of the pulse flow modulator, performing partial modulation in the PPM had some drawbacks, requiring the combination of the principles of frontal analysis and vacancy chromatography (coupled with tedious data analysis steps) to arrive at data that ultimately appeared like traditional GC×GC data (and 2D plots). Thus, use of partial modulation in the PPM requires more data preprocessing to extract the pertinent chemical information that is encoded in the raw data.[41] This is a substantial barrier to the widespread acceptance and use of this new modulation approach. However, there exists a way around this barrier, which is partial modulation in the NPM. Where the PPM created local vacancies in the analyte ^{1}D peak profiles, the NPM creates localized concentration "enhancements" in the analyte ^{1}D peak profiles as they enter the ^{2}D column. Using this new mode of partial modulation in the NPM, analysts now can use a simple baseline subtraction algorithm and immediately uncouple the ^{1}D and ^{2}D peak profiles from the raw data. This powerful modulation technique will be introduced in Chapter 2 and expanded upon in Chapter 3.

1.5 CHALLENGES AND MOTIVATIONS

The pulse valve modulator has the potential to be a truly powerful tool for GC instruments, and we are only scratching the surface. Up to this point, my research centered on the PPM and the potential for increasing the data density possible (i.e. reducing total run time) and increasing peak capacity utilizing the high-speed modulation method.[42–44] This goal was even more attractive as it is built upon coupling existing commercially available GC instrumentation with an inexpensive and readily available pulse vale modulator. It has been my belief that our instruments are already incredibly powerful and efficient, but they can be combined or used in ways thus far not realized, like the pulse valve itself. Thus, using a GC system and related equipment already in our lab, I worked to improve the data we received from partial modulation. Partial modulation in the PPM with the pulse valve modulator had already shown us how powerful of a technique it can be, but the data was not user friendly and required multiple pre-processing steps to turn the data into usable information. Chapter 2 will demonstrate partial modulation in the NPM, where we discovered how to invert how the pulse valve is used to create local concentrations of analyte, as opposed to local vacancies in the PPM. Additionally, some of the additional, powerful attributes of this modulation technique for GC×GC and GC^3 instruments are demonstrated in Chapter 2. Chapter 3 will expand upon this by factoring in the use of commercially available chemometric data analysis software. Again, I believe the tools we already admirably perform, and my hypothesis was that the data produced by the NPM is ideally amenable to current chemometric tools to deconvolute, identify and quantify chromatographically overlapped analytes.

The pulse valve modulator's utility was readily apparent. However, working in the partial modulation realm, it would never have the same limits of detection for trace analysis as full modulation methods. This limited some of the potential applications until we conducted additional research into the pulse valve modulator itself, it's means of actuation, and discovered how to use

it as a more traditional flow modulator.[53] Now the pulse valve modulator provides full modulation, not just partial modulation. This concept will be further advanced from its initial publication in Chapter 4, with the potential gains in *S/N*, and thus limits of detection, highlighted.

1.6 HYPOTHESES

The following chapters describe the research performed over the past two years, which focus on new modulation techniques with the pulse valve modulator for GC×GC and GC^3, chemometric deconvolution and analysis of complex datasets with severely overlapped analyte peaks, and recent developments with the GC as a sensor concept. A brief summary of each chapter is provided below.

1.6.1 *Chapter 2: Development of Ultrafast Separations Using Negative Pulse Partial Modulation to Enable New Directions in Gas Chromatography*

Partial modulation via a pulse flow valve operated in the NPM is developed for high-speed one-dimensional gas chromatography (1D-GC), comprehensive two-dimensional (2D) gas chromatography (GC×GC), and comprehensive three-dimensional gas chromatography (GC^3). The pulse flow valve readily provides very short modulation periods, P_M, demonstrated herein at 100, 200, and 300 ms, and holds significant promise to increase the scope and applicability of GC instrumentation. The negative pulse mode creates an extremely narrow, local analyte concentration pulse. The reproducibility of the negative pulse mode is validated in a 1D-GC mode, where a pseudo-steady state analyte stream is modulated, and 8 analytes are baseline resolved ($R_s \geq 1.5$) in a 200 ms window, providing a peak capacity, n_c, of 14 at unit resolution ($R_s = 1.0$). Additionally, the pulse width, p_w, of the pulse flow valve "injection" relationship to peak width-at-base, w_b, resolution between peaks, and detection sensitivity are studied. To demonstrate the applicability to GC×GC, a high-speed separation of a 20-component test mixture

of similar, volatile analytes is shown. Analytes were separated on the second-dimension column, ^{2}D, with ^2w_b ranging from 7 to 12 ms, providing an exceptional ^{2}D peak capacity, ^2n_c of ~12 using a P_M of 100 ms. Next, a 12 min separation of a diesel sample using a P_M of 300 ms is presented. The ^1w_b is ~4 s, resulting in a ^1n_c of ~180, and ^2w_b is ~18 ms, resulting in a ^2n_c of ~17, thus achieving a $n_{c,2D}$ of ~3,000 in this rapid GC×GC diesel separation. Finally, GC^3 with time-of-flight mass spectrometry detection (TOFMS) using a P_M of 100 ms applied between the ^{2}D and ^{3}D columns is reported. Narrow third dimension, ^{3}D, peaks ^3w_b ~ 15 ms were obtained, resulting in a GC^3 peak capacity, $n_{c,3D}$, of ~35,000, in a 45 min separation.

1.6.2 *Chapter 3: Chemometric Decomposition of Comprehensive Two-Dimensional Gas Chromatography Time-of-Flight Mass Spectrometry Data Employing Partial Modulation in the Negative Pulse Mode (NPM)*

Partial modulation in the NPM was optimized for GC×GC coupled to TOFMS detection. With partial modulation in the NPM, a flow of auxiliary carrier gas is applied through a pulse valve to a T-junction joining the ^{1}D and ^{2}D columns for nearly all of the P_M. This results in dilution of the ^{1}D eluate, followed by briefly turning off the pulse valve for a specified pulse width (p_w), effectively "injecting" undiluted ^{1}D eluate onto the ^{2}D column. The raw data has the appearance of ^{2}D separations superimposed on top of the ^{1}D separation. While high peak capacity GC×GC data are produced, there are challenges that needed to be addressed regarding the use of chemometrics for analyte decomposition, identification, and quantification. Herein, these data analysis challenges are addressed using multivariate curve resolution - alternating least squares (MCR-ALS). An isothermal separation of a 15-component mixture of similar compounds is obtained in 20 s using a P_M = 250 ms and a p_w = 6 ms. Various peak overlap situations were purposely produced to facilitate the chemometric method demonstration. The MCR-ALS loadings

were used to determine retention times (t_R) and width-at-base (w_b) in both separation dimensions. MCR-ALS readily decomposed and deconvoluted $^1D \times ^2D$ regions for analytes with severe ^1D overlap if they were fully resolved on ^2D. Decomposition and deconvolution was more challenging for analytes severely overlapped on both GC×GC dimensions when their spectra were similar, though ultimately all 15 compounds were successfully separated. Additionally, the mass spectral profiles obtained by MCR-ALS were used to demonstrate that the ^2D concentration peak profiles obtained are reliable for identification and quantifiable. The predicted versus prepared concentration values are in good agreement for two representative analytes, with percent deviation values of -5.6% (± 2.2%) for 1-hexene, and 1.8% (± 3.4%) for 2-pentanone.

1.6.3 *Chapter 4: Developments in Comprehensive Three-Dimensional Gas Chromatography (GC^3) using the Pulse Valve in Full Modulation Mode*

The first three-dimensional gas chromatographic instrument was introduced by Watson et. al. in 2007. At the time, it was only useful for the gains in chemical selectivity possible with a third separation column. Now, with the pulse valve modulator, we can further increase the applicability of GC^3 instruments by realizing additional gains in peak capacity and *S/N*. The pulse valve modulator was used in the full modulation mode to demonstrate the potential increases in *S/N* when we transition from 1D-GC up to GC^3 on a TOFMS. The detector response enhancement factor (*DREF*) is used to quantify the increases in *S/N* from 1D-GC to GC×GC to GC^3. We found that the *DREF* between 1D-GC and GC^3 can be ~31, i.e., there is a gain of 31 times the signal. Additionally, the $^2D \times ^3D$ peak capacity is demonstrated at 30 peaks per 1.5 s. Last, a method to visualize the $^2D \times ^3D$ chromatogram is presented, in which four successive modulations are lined up and one can "see" analytes arriving at and eluting from the TOFMS detector.

1.7 REFERENCES

(1) Ettre, L. S. Chromatography: The Separation Technique of the 20th Century. *Chromatographia* **2000**, *51* (1), 7. https://doi.org/10.1007/BF02490689.

(2) James, A. T.; Martin, A. J. P. Gas-Liquid Partition Chromatography: The Separation and Micro-Estimation of Volatile Fatty Acids from Formic Acid to Dodecanoic Acid. *Biochem. J.* **1952**, *50* (5), 679–690.

(3) Ettre, L. S. The Development of Gas Chromatography. *J. Chromatogr. A* **1975**, *112*, 1–26. https://doi.org/10.1016/S0021-9673(00)99939-4.

(4) Ettre, L. S. Development of Chromatography. *Anal. Chem.* **1971**, *43* (14), 20A – 31a. https://doi.org/10.1021/ac60308a022.

(5) Giddings, J. C. *Unified Separation Science*; Wiley: New York, 1991.

(6) Liu, Z.; Phillips, J. B. Comprehensive Two-Dimensional Gas Chromatography Using an On-Column Thermal Modulator Interface. *J. Chromatogr. Sci.* **1991**, *29* (6), 227–231. https://doi.org/10.1093/chromsci/29.6.227.

(7) Duhamel, C.; Cardinael, P.; Peulon-Agasse, V.; Firor, R.; Pascaud, L.; Semard-Jousset, G.; Giusti, P.; Livadaris, V. Comparison of Cryogenic and Differential Flow (Forward and Reverse Fill/Flush) Modulators and Applications to the Analysis of Heavy Petroleum Cuts by High-Temperature Comprehensive Gas Chromatography. *J. Chromatogr. A* **2015**, *1387*, 95–103. https://doi.org/10.1016/j.chroma.2015.01.095.

(8) Jacobs, M. R.; Edwards, M.; Górecki, T.; Nesterenko, P. N.; Shellie, R. A. Evaluation of a Miniaturised Single-Stage Thermal Modulator for Comprehensive Two-Dimensional Gas Chromatography of Petroleum Contaminated Soils. *J. Chromatogr. A* **2016**, *1463*, 162–168. https://doi.org/10.1016/j.chroma.2016.08.009.

(9) Semard, G.; Gouin, C.; Bourdet, J.; Bord, N.; Livadaris, V. Comparative Study of Differential Flow and Cryogenic Modulators Comprehensive Two-Dimensional Gas Chromatography Systems for the Detailed Analysis of Light Cycle Oil. *J. Chromatogr. A* **2011**, *1218* (21), 3146–3152. https://doi.org/10.1016/j.chroma.2010.08.082.

(10) Tranchida, P. Q.; Purcaro, G.; Dugo, P.; Mondello, L. Modulators for Comprehensive Two-Dimensional Gas Chromatography. *TrAC, Trends Anal. Chem.* **2011**, *30* (9), 1437–1461. https://doi.org/10.1016/j.trac.2011.06.010.

(11) Seeley, J. V. Recent Advances in Flow-Controlled Multidimensional Gas Chromatography. *J. Chromatogr. A* **2012**, *1255*, 24–37. https://doi.org/10.1016/j.chroma.2012.01.027.

(12) Seeley, J. V.; Seeley, S. K. Multidimensional Gas Chromatography: Fundamental Advances and New Applications. *Anal. Chem.* **2013**, *85* (2), 557–578. https://doi.org/10.1021/ac303195u.

(13) Bahaghighat, H. D.; Freye, C. E.; Synovec, R. E. Recent Advances in Modulator Technology for Comprehensive Two Dimensional Gas Chromatography. *TrAC Trends in Anal. Chem.* **2019**, *113*, 379–391. https://doi.org/10.1016/j.trac.2018.04.016.

(14) de Geus, H.-J.; de Boer, J.; Brinkman, U. A. Th. Development of a Thermal Desorption Modulator for Gas Chromatography. *J. Chromatogr. A* **1997**, *767* (1), 137–151. https://doi.org/10.1016/S0021-9673(97)00038-1.

(15) Focant, J.-F.; Sjödin, A.; Patterson Jr., D. G. Qualitative Evaluation of Thermal Desorption-Programmable Temperature Vaporization-Comprehensive Two-Dimensional Gas Chromatography–Time-of-Flight Mass Spectrometry for the Analysis of Selected

Halogenated Contaminants. *J. Chromatogr. A* **2003**, *1019* (1–2), 143–156. https://doi.org/10.1016/j.chroma.2003.07.007.
(16) Phillips, J. B.; Ledford, E. B. Thermal Modulation: A Chemical Instrumentation Component of Potential Value in Improving Portability. *Field Anal. Chem. Technol.* **1996**, *1* (1), 23–29. https://doi.org/10.1002/(SICI)1520-6521(1996)1:1<23::AID-FACT4>3.0.CO;2-F.
(17) Mucédola, V.; Vieira, L. C. S.; Pierone, D.; Gobbi, A. L.; Poppi, R. J.; Hantao, L. W. Thermal Desorption Modulation for Comprehensive Two-Dimensional Gas Chromatography Using a Simple and Inexpensive Segmented-Loop Fluidic Interface. *Talanta* **2017**, *164*, 470–476. https://doi.org/10.1016/j.talanta.2016.12.005.
(18) Muscalu, A. M.; Edwards, M.; Górecki, T.; Reiner, E. J. Evaluation of a Single-Stage Consumable-Free Modulator for Comprehensive Two-Dimensional Gas Chromatography: Analysis of Polychlorinated Biphenyls, Organochlorine Pesticides and Chlorobenzenes. *J. Chromatogr. A* **2015**, *1391*, 93–101. https://doi.org/10.1016/j.chroma.2015.02.074.
(19) Gross, G. M.; Prazen, B. J.; Grate, J. W.; Synovec, R. E. High-Speed Gas Chromatography Using Synchronized Dual-Valve Injection. *Anal. Chem.* **2004**, *76* (13), 3517–3524. https://doi.org/10.1021/ac049909g.
(20) Lidster, R. T.; Hamilton, J. F.; Lewis, A. C. The Application of Two Total Transfer Valve Modulators for Comprehensive Two-Dimensional Gas Chromatography of Volatile Organic Compounds. *J. Sep. Sci.* **2011**, *34* (7), 812–821. https://doi.org/10.1002/jssc.201000710.
(21) Mohler, R. E.; Prazen, B. J.; Synovec, R. E. Total-Transfer, Valve-Based Comprehensive Two-Dimensional Gas Chromatography. *Anal. Chim. Acta* **2006**, *555* (1), 68–74. https://doi.org/10.1016/j.aca.2005.08.072.
(22) Sinha, A. E.; Prazen, B. J.; Fraga, C. G.; Synovec, R. E. Valve-Based Comprehensive Two-Dimensional Gas Chromatography with Time-of-Flight Mass Spectrometric Detection: Instrumentation and Figures-of-Merit. *J. Chromatogr. A* **2003**, *1019* (1–2), 79–87. https://doi.org/10.1016/j.chroma.2003.08.047.
(23) Reid, V. R.; McBrady, A. D.; Synovec, R. E. Investigation of High-Speed Gas Chromatography Using Synchronized Dual-Valve Injection and Resistively Heated Temperature Programming. *J. Chromatogr. A* **2007**, *1148* (2), 236–243. https://doi.org/10.1016/j.chroma.2007.03.029.
(24) Freye, C. E.; Mu, L.; Synovec, R. E. High Temperature Diaphragm Valve-Based Comprehensive Two-Dimensional Gas Chromatography. *J. Chromatogr. A* **2015**, *1424*, 127–133. https://doi.org/10.1016/j.chroma.2015.10.098.
(25) Seeley, J. V.; Micyus, N. J.; Bandurski, S. V.; Seeley, S. K.; McCurry, J. D. Microfluidic Deans Switch for Comprehensive Two-Dimensional Gas Chromatography. *Anal. Chem.* **2007**, *79* (5), 1840–1847. https://doi.org/10.1021/ac061881g.
(26) Seeley, J. V.; Kramp, F.; Hicks, C. J. Comprehensive Two-Dimensional Gas Chromatography via Differential Flow Modulation. *Anal. Chem.* **2000**, *72* (18), 4346–4352. https://doi.org/10.1021/ac000249z.
(27) Bueno, P. A.; Seeley, J. V. Flow-Switching Device for Comprehensive Two-Dimensional Gas Chromatography. *J. Chromatogr. A* **2004**, *1027* (1), 3–10. https://doi.org/10.1016/j.chroma.2003.10.033.

(28) Griffith, J. F.; Winniford, W. L.; Sun, K.; Edam, R.; Luong, J. C. A Reversed-Flow Differential Flow Modulator for Comprehensive Two-Dimensional Gas Chromatography. *J. Chromatogr. A* **2012**, *1226*, 116–123. https://doi.org/10.1016/j.chroma.2011.11.036.

(29) Tranchida, P. Q.; Purcaro, G.; Visco, A.; Conte, L.; Dugo, P.; Dawes, P.; Mondello, L. A Flexible Loop-Type Flow Modulator for Comprehensive Two-Dimensional Gas Chromatography. *J. Chromatogr. A* **2011**, *1218* (21), 3140–3145. https://doi.org/10.1016/j.chroma.2010.11.082.

(30) Tranchida, P. Q.; Salivo, S.; Franchina, F. A.; Mondello, L. Flow-Modulated Comprehensive Two-Dimensional Gas Chromatography Combined with a High-Resolution Time-of-Flight Mass Spectrometer: A Proof-of-Principle Study. *Anal. Chem.* **2015**, *87* (5), 2925–2930. https://doi.org/10.1021/ac5044175.

(31) Tranchida, P. Q.; Maimone, M.; Franchina, F. A.; Bjerk, T. R.; Zini, C. A.; Purcaro, G.; Mondello, L. Four-Stage (Low-)Flow Modulation Comprehensive Gas Chromatography □quadrupole Mass Spectrometry for the Determination of Recently-Highlighted Cosmetic Allergens. *J. Chromatogr. A* **2016**, *1439*, 144–151. https://doi.org/10.1016/j.chroma.2015.12.002.

(32) Boeker, P.; Leppert, J. Flow Field Thermal Gradient Gas Chromatography. *Anal. Chem.* **2015**, *87* (17), 9033–9041. https://doi.org/10.1021/acs.analchem.5b02227.

(33) Cordero, C.; Rubiolo, P.; Cobelli, L.; Stani, G.; Miliazza, A.; Giardina, M.; Firor, R.; Bicchi, C. Potential of the Reversed-Inject Differential Flow Modulator for Comprehensive Two-Dimensional Gas Chromatography in the Quantitative Profiling and Fingerprinting of Essential Oils of Different Complexity. *J. Chromatogr. A* **2015**, *1417*, 79–95. https://doi.org/10.1016/j.chroma.2015.09.027.

(34) Seeley, J. V.; Schimmel, N. E.; Seeley, S. K. The Multi-Mode Modulator: A Versatile Fluidic Device for Two-Dimensional Gas Chromatography. *J. Chromatogr. A* **2018**, *1536*, 6–15. https://doi.org/10.1016/j.chroma.2017.06.030.

(35) Prebihalo, S. E.; Berrier, K. L.; Freye, C. E.; Bahaghighat, H. D.; Moore, N. R.; Pinkerton, D. K.; Synovec, R. E. Multidimensional Gas Chromatography: Advances in Instrumentation, Chemometrics, and Applications. *Anal. Chem.* **2018**, *90* (1), 505–532. https://doi.org/10.1021/acs.analchem.7b04226.

(36) Cai, H.; Stearns, S. D. Partial Modulation Method via Pulsed Flow Modulator for Comprehensive Two-Dimensional Gas Chromatography. *Anal. Chem.* **2004**, *76* (20), 6064–6076. https://doi.org/10.1021/ac0492463.

(37) Khummueng, W.; Harynuk, J.; Marriott, P. J. Modulation Ratio in Comprehensive Two-Dimensional Gas Chromatography. *Anal. Chem.* **2006**, *78* (13), 4578–4587. https://doi.org/10.1021/ac052270b.

(38) Blumberg, L. M. Accumulating Resampling (Modulation) in Comprehensive Two-Dimensional Capillary GC (GC×GC). *J. Sep. Sci.* **2008**, *31* (19), 3358–3365. https://doi.org/10.1002/jssc.200800424.

(39) Siegler, W. C.; Fitz, B. D.; Hoggard, J. C.; Synovec, R. E. Experimental Study of the Quantitative Precision for Valve-Based Comprehensive Two-Dimensional Gas Chromatography. *Anal. Chem.* **2011**, *83* (13), 5190–5196. https://doi.org/10.1021/ac200302b.

(40) Pinkerton, D. K.; Parsons, B. A.; Synovec, R. E. Method to Determine the True Modulation Ratio for Comprehensive Two-Dimensional Gas Chromatography. *J. Chromatogr. A* **2016**, *1476*, 114–123. https://doi.org/10.1016/j.chroma.2016.11.015.
(41) Freye, C. E.; Bahaghighat, H. D.; Synovec, R. E. Comprehensive Two-Dimensional Gas Chromatography Using Partial Modulation via a Pulsed Flow Valve with a Short Modulation Period. *Talanta* **2018**, *177*, 142–149. https://doi.org/10.1016/j.talanta.2017.08.095.
(42) Bahaghighat, H. D.; Freye, C. E.; Gough, D. V.; Sudol, P. E.; Synovec, R. E. Ultrafast Separations via Pulse Flow Valve Modulation to Enable High Peak Capacity Multidimensional Gas Chromatography. *J. Chromatogr. A* **2018**, *1573*, 115–124. https://doi.org/10.1016/j.chroma.2018.08.001.
(43) Bahaghighat, H. D.; Freye, C. E.; Gough, D. V.; Synovec, R. E. Comprehensive Two-Dimensional Gas Chromatography and Time-of-Flight Mass Spectrometry Detection with a 50 Ms Modulation Period. *J. Chromatogr. A* **2019**, *1583*, 117–123. https://doi.org/10.1016/j.chroma.2018.11.027.
(44) Gough, D. V.; Bahaghighat, H. D.; Synovec, R. E. Column Selection Approach to Achieve a High Peak Capacity in Comprehensive Three-Dimensional Gas Chromatography. *Talanta* **2019**, *195*, 822–829. https://doi.org/10.1016/j.talanta.2018.12.007.
(45) Gough, D. V.; Song, D. H.; Schöneich, S.; Prebihalo, S. E.; Synovec, R. E. Development of Ultrafast Separations Using Negative Pulse Partial Modulation to Enable New Directions in Gas Chromatography. *Anal. Chem.* **2019**, *91* (11), 7328–7335. https://doi.org/10.1021/acs.analchem.9b01085.
(46) Parsons, B. A.; Pinkerton, D. K.; Synovec, R. E. Implications of Phase Ratio for Maximizing Peak Capacity in Comprehensive Two-Dimensional Gas Chromatography Time-of-Flight Mass Spectrometry. *J. Chromatogr. A* **2018**, *1536*, 16–26. https://doi.org/10.1016/j.chroma.2017.07.018.
(47) Watson, N. E.; Siegler, W. C.; Hoggard, J. C.; Synovec, R. E. Comprehensive Three-Dimensional Gas Chromatography with Parallel Factor Analysis. *Anal. Chem.* **2007**, *79* (21), 8270–8280. https://doi.org/10.1021/ac070829x.
(48) Watson, N. E.; Prebihalo, S. E.; Synovec, R. E. Targeted Analyte Deconvolution and Identification by Four-Way Parallel Factor Analysis Using Three-Dimensional Gas Chromatography with Mass Spectrometry Data. *Anal. Chim. Acta* **2017**, *983*, 67–75. https://doi.org/10.1016/j.aca.2017.06.017.
(49) Klee, M. S.; Cochran, J.; Merrick, M.; Blumberg, L. M. Evaluation of Conditions of Comprehensive Two-Dimensional Gas Chromatography That Yield a near-Theoretical Maximum in Peak Capacity Gain. *J. Chromatogr. A* **2015**, *1383*, 151–159. https://doi.org/10.1016/j.chroma.2015.01.031.
(50) Davis, J. M.; Giddings, J. Calvin. Statistical Theory of Component Overlap in Multicomponent Chromatograms. *Anal. Chem.* **1983**, *55* (3), 418–424. https://doi.org/10.1021/ac00254a003.
(51) Davis, J. M.; Giddings, J. C. Statistical Method for Estimation of Number of Components from Single Complex Chromatograms: Theory, Computer-Based Testing, and Analysis of Errors. *Anal. Chem.* **1985**, *57* (12), 2168–2177. https://doi.org/10.1021/ac00289a002.

(52) Davis, J. M. Statistical Theory of Spot Overlap for N-Dimensional Separations. *Anal. Chem.* **1993**, *65* (15), 2014–2023. https://doi.org/10.1021/ac00063a015.
(53) Trinklein, T. J.; Gough, D. V.; Warren, C. G.; Ochoa, G. S.; Synovec, R. E. Dynamic Pressure Gradient Modulation for Comprehensive Two-Dimensional Gas Chromatography. *J. Chromatogr. A* **2019**, 460488. https://doi.org/10.1016/j.chroma.2019.460488.

Chapter 2. Development of Ultrafast Separations using Negative Pulse Partial Modulation to Enable New Directions in Gas Chromatography

This chapter was reproduced from D.V. Gough, D.H. Song, S. Schöneich, S.E. Prebihalo, and R.E. Synovec, "Development of Ultrafast Separations using Negative Pulse Partial Modulation to Enable New Directions in Gas Chromatography" *Anal. Chem.* 91 (2019) 7328-35.

2.1 INTRODUCTION

Comprehensive, two-dimensional (2D) gas chromatography (GC×GC) has evolved a great deal since its first description by Giddings[1] and first implementation by Lui and Phillips.[2] Over the past 25-plus years, great strides have been made to improve and broadly apply GC×GC to a host of ever-more complicated samples.[3–5] Availability of a wide range of stationary phases ensure that complementary separations can be readily provided, greatly increasing the utility of GC×GC compared to one-dimensional (1D) GC. Several reviews[6–13] have been conducted to capture advancements within this field, enabling researchers to maintain awareness of recent advances in instrumentation and chemometric data analysis techniques.

The heart of the GC×GC instrument is the modulator, facilitating the conversion of the 1D separation to a comprehensive 2D separation. Design and implementation of most modern GC×GC instrumentation relies on the use of "full modulation." During full modulation, each second-dimension separation (^{2}D) peak arises from an isolated fraction of the larger first-dimension separation (^{1}D) peak following elution from the ^{1}D column. Typically, each isolated analyte fraction is trapped, compressed, and re-injected onto the ^{2}D column. This is true whether the modulated amount of eluate is 100% (duty cycle = 1.0) or if only a fraction of the eluate makes it through the modulator (duty cycle < 1.0). Either way, the analyte ^{1}D profile is divided

into evenly spaced, narrower ^{2}D peaks that follow the same general shape of the analyte concentration profile as it departs from the ^{1}D column. Thus, a ^{1}D peak profile can be reconstructed, mathematically, by fitting a Gaussian function to the maxima of the ^{2}D peaks for a given analyte.[14,15] Absent placing a detector prior to the modulator, what has largely been omitted from the practice of GC×GC is the ability to simultaneously obtain the complementary ^{1}D and ^{2}D separations without forfeiting the integrity of the ^{1}D analyte peak profile. This is due to application of separation conditions that result in a low sampling density (fewer points to fit a Gaussian function), where sampling density is defined as the number of modulations across the ^{1}D peak width-at-base. However, this challenge should be readily addressable using partial modulation pioneered by Cai and Stearns.[16]

As the name implies, the main difference between partial and full modulation lays in the amount of analyte modulated relative to the peak concentration profile eluting from the ^{1}D column. In contrast to full modulation, with partial modulation only a portion of the analyte composition eluting from the ^{1}D column is modulated, simultaneously leaving a suitable fraction of analyte composition unmodulated also entering the ^{2}D column. One can imagine this as skimming off the top of an analyte peak and only modulating and separating on the ^{2}D column that portion skimmed. As originally illustrated with simulated data, use of partial modulation provides the possibility of retaining the ^{1}D peak profile for an analyte while adding a ^{2}D separation on top of the ^{1}D profile.[16] This form of modulation remains in its infancy in development despite showing the promise for some truly unique and beneficial attributes.

We previously studied one form of partial modulation, in the “positive pulse” mode, where a small pulse of carrier gas, determined with a user-selected injection pulse width was injected at a T-union between the ^{1}D and ^{2}D columns.[17–20] Using a “pulse flow valve,” each pulse

of carrier gas created a local vacancy in the analyte concentration profile. Combining the principles of vacancy chromatography and frontal analysis chromatography, the raw data produced required differentiation and inversion to produce what were termed an "apparent" peaks (a detailed explanation to this is provided in a previous report).[17] The apparent peaks were shown to be amenable to being presented in traditional chromatographic plots such as 1D-GC, GC×GC, and even comprehensive three-dimensional GC (GC^3).[17–20] These apparent peaks, especially when the GC×GC is combined with time-of-flight mass spectrometry (TOFMS) detection and chemometrics, have been shown to provide reproducible and quantitative results.[19] Hence, use of partial modulation in the positive pulse mode has shown great promise in GC×GC and GC^3 due to the robustness of the modulator, the ultrafast modulation capability (modulation period, $P_M \geq 50$ ms), and the narrow peak widths-at-base, w_b (4 standard deviation width, as low as single-digit ms. High peak capacity, n_c, has been obtained for either ^{2}D separations in GC×GC (~11,000 in 11 min), or ^{3}D separations in GC^3-FID (~31,000 in 40 min).[18,20]

While previous reports are promising, the performance of the partial modulation in the positive pulse mode resulted in critical shortcomings in the concentration profiles of the modulated peaks. Specifically, the need to differentiate the data to obtain the apparent peaks (chromatographic information) resulted in a substantial loss in signal-to-noise ratio (*S/N*), and in general is non-ideal for wide acceptance of the technology. To address this shortcoming, we have begun exploring an alternative form of partial modulation, the "negative pulse" mode.[16] Partial modulation in the negative pulse mode has hereto remained undeveloped beyond the original report, especially for ultrafast GC separations, and will be the focus of this report.

It is hypothesized that use of the negative pulse mode will eliminate the need to differentiate the data, thus substantially reducing the data processing requirements and increasing

the *S/N*. Additionally, it is hypothesized that application of a suitable baseline correction algorithm will be more amenable to the naturally produced positive peaks from the negative pulse mode than to the vacancies produced by the positive pulse mode. In this report, the basic principles and key applications of partial modulation in the negative pulse mode are reported. First, with a 1D-GC study, we demonstrate the ability to obtain replicate chromatograms at a high sampling frequency by introducing a steady-state analyte test mixture for continuous analysis by the system. Applied herein, fast modulations ($P_M \geq 50$ ms) are readily achieved with the pulse flow valve. We then study how the injected pulse width, p_w, affects the detected peak widths and signal intensity in the context of GC×GC. Next, the benefits of this technology for GC×GC separations are demonstrated with a test mixture and diesel. Finally, GC^3-TOFMS with pulse flow valve modulation in the negative pulse mode is demonstrated using a P_M of 100 ms applied between the ^{2}D and ^{3}D columns. A 90-component test mixture is used for this demonstration. By adding the pulse flow valve and ^{3}D column to the end of a commonly applied thermally modulated GC×GC-TOFMS instrument, high peak capacity GC^3 separations are achieved[18,20] with TOFMS detection.[21,22]

2.2 Basic Principles

In their original study, Cai and Stearns used a homemade pulsed flow modulator which alternated between a high and low flow (not zero) of carrier gas at a Y-junction between the ^{1}D and ^{2}D in GC×GC.[16] We have modified the negative pulse method described in this original report in one subtle, yet key way: the auxiliary flow of carrier gas at a T-union is alternated between either a fixed value or zero flow. This was done in order to use a commercially available pulse flow valve that required zero adjustments aside from connections to the GC instrument. In the positive pulse mode, a pulse of carrier gas is introduced into the main analyte stream. In the

negative pulse mode, a complete *absence* of the auxiliary carrier gas flow at the T-union is "introduced" into the main analyte stream (Figure 2.1).

During normal operation (Figure 2.1A), the pulse flow valve is left open, allowing a stream of auxiliary carrier gas to enter at the T-union and "dilute" the analyte stream coming from the ^{1}D column onto the ^{2}D column. During modulation, the pulse flow valve closes (Figure 2.1B), and there is now no flow of auxiliary carrier gas. This enables a section of analyte stream from the ^{1}D column to enter the ^{2}D column without being diluted at the T-union. Next, the pulse valve reopens (Figure 2.1C), and the stream of carrier gas resumes. The auxiliary carrier gas returns the majority of the ^{1}D profile back to its "diluted" state, while simultaneously creating a local concentration of the "injected" portion of the analyte stream. An example of peaks obtained using the negative pulse mode for four p_w can be compared in an overlay plot (Figure 2.1D), which could be observed in either a 1D-GC, GC×GC, or GC^{3} separation.

These data provide an impetus for the first two studies in this report, as there is a marked impact of p_w on w_b and signal intensity. Indeed, the "injected" portion of the analyte stream produces a narrow ^{2}D peak (e.g., in a GC×GC context), since it is the only segment of the analyte stream to undergo visible separation on the ^{2}D column. The rest of the analyte stream remains "unmodulated" and essentially retains its ^{1}D profile. The complementary ^{1}D and ^{2}D separations are simultaneously obtained without forfeiting the integrity of the ^{1}D analyte peak profiles, even if a low modulation sampling density is applied (Figure A1). A simple baseline correction algorithm can be applied to the raw negative pulse mode data (Figure A1A-C) to isolate each ^{1}D peak and the series of ^{2}D peaks obtained are readily converted into the traditional 2D contour plot for GC×GC (Figure A1D). Note that the "unmodulated" (diluted) portion of the analyte

stream (Figure 2.1C) will also produce negative "peaks" due to a subtle vacancy modulation effect.

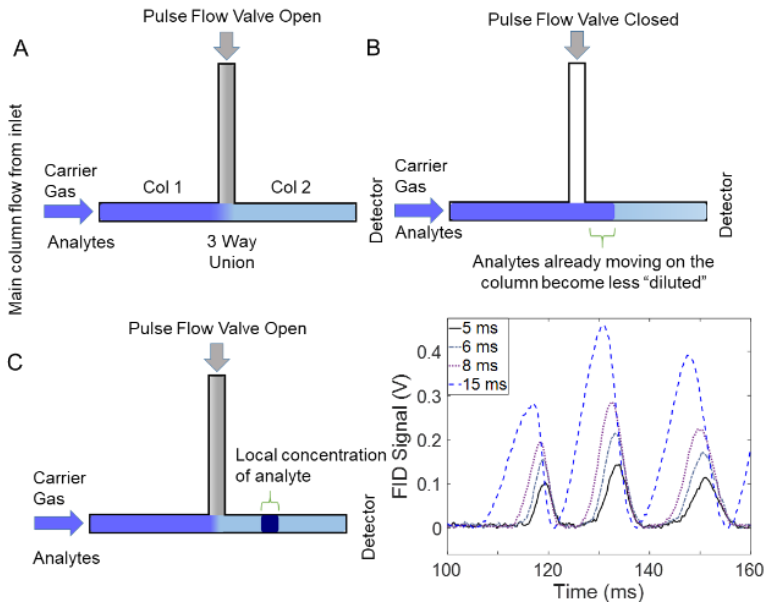

Figure 2.1. Illustration of the interaction of gas flows at the 3-way union during partial modulation using the pulse flow valve in the negative pulse mode for GC×GC. (A) Most of the time, the pulse flow valve is open, allowing an auxiliary flow of carrier gas into the ^{2}D column, diluting the carrier gas effluent entering the union. (B) When the pulse flow valve is actuated to close, the flow of auxiliary carrier gas at the flow junction is temporarily stopped using a user-selected pulse width, p_w, and the carrier gas effluent entering the union is not diluted. (C) When the pulse flow valve is actuated to open, the flow of auxiliary carrier gas returns to re-dilute the analyte stream. (D) Baseline corrected data of four specified p_w. Only the "injected" pulse is visibly separated on the ^{2}D column while the main flow of analyte from the ^{1}D column continues through the ^{2}D column providing the baseline signal.

There are two extremes for partial modulation, the negative pulse and positive pulse modes, with injection pulse widths defined by p_w and P_M-p_w, respectively. When P_M-p_w >>p_w, as

in the negative pulse mode, positive peaks are obtained, as observed herein, and shallow negative peaks are not readily observed and are essentially removed by the baseline correction. Conversely, when P_M-p_w<< p_w, a narrow pulse of carrier gas is "injected" by the pulse flow valve, the system would then be operating in the positive pulse mode.[16–20]

Further development of partial modulation in the negative pulse mode demands validation of its theory of operation and the reproducibility of the data. At its core, a modulator can be viewed as a secondary injector, taking the effluent from a previous dimension and re-injecting it onto a successive dimension in a multidimensional GC instrument. Taking this a step further, a modulator can be simply viewed as an injection system,[23–25] and one can study the modulator performance and characteristics for continuous 1D-GC separations. Previous work focused on improving the ability of injectors/modulators to inject narrow pulses of sample/effluent to reduce the overall band-broadening. Expanding upon this idea, we examine the pulse flow valve in the negative pulse mode by rapidly performing successive modulations onto a pseudo steady-state analyte test mixture stream, to mimic continuous process monitoring. Each modulation provides an injection for a high-speed 1D-GC separation.

The flow ratio between the pulse flow valve modulator and the inlet column flow was previously shown to impact the ^{2}D signal intensity relative to the ^{1}D signal, and the total amount of analyte partially modulated.[16] This was studied at a constant p_w of 30 ms. The p_w dependence in the negative pulse mode was studied in more detail (Figure A2 and Table A3). A steady pressure ratio (and thus flow ratio) was maintained between the pulse flow valve and the inlet column flow for each experiment, while the size of the p_w was varied. The flow ratio is a critical factor, and with the column sets (ID and length) applied herein the auxiliary flow pressure must be held slightly higher than the column inlet pressure in order to obtain optimal results. Larger p_w

correlated to larger w_b for a given analyte, as a larger analyte portion (i.e., volume and/or mol) eluting from the ^{1}D column became "undiluted" and then was "re-injected" and separated on the ^{2}D column. The data obtained was analyte w_b and signal height, both as a function of p_w. A "sweet spot" in the p_w dependency was observed (p_w in the 6 to 10 ms range), below which the w_b is barely affected since chromatographic band broadening due to the column dominates, and above which the w_b significantly increases with p_w.[23] This sweet spot concurrently provided an optimal signal height without introducing substantial peak broadening due to the injection. Finding the sweet spot provided suitable conditions without modifying flow ratios for the high-speed 1D-GC, GC×GC, and GC^3 studies presented.

2.3 EXPERIMENTAL

Two GC instrumental configurations, one for 1D-GC (Figure 2.2A) and the other for GC×GC (Figure 2.2B), were based upon an Agilent 7890A GC and 7683B auto-injector (Agilent Technologies, Palo Alto, CA, USA) with a flame ionization detector (FID). The stock electrometer for the Agilent FID was replaced with a high-speed electrometer, built in-house, allowing the data to be collected at 100 kHz, then boxcar averaged to 1 kHz. The electrometer was interfaced to a data acquisition board, and the resulting data was collected using an in-house written LabVIEW program (National Instruments, Austin, TX, USA). Post-run data processing was performed in MATLAB R2017b (The Mathworks, Inc., Natick, MA, USA). Two solvents, acetone and hexane (Fisher Scientific, Hampton, NH, USA), were used in between experiments for rinses. Ultra-high purity hydrogen (Grade 5, 99.999%) was used as the carrier gas (Praxair,

Seattle, WA, USA). All experiments utilized an inlet temperature of 175 °C and FID temperature of 255 °C. For all studies using a GC×GC configuration, the column sets were located in the same oven and subjected to the same temperature conditions.

Both GC configurations were fitted with a high-speed pulse flow valve (Model 009-0347-900, Parker Hannifin, Hollis, NH, USA). The pulse flow valve was mounted outside the oven (Figure 2.2B), with a custom-built fitting to connect a 125 µm- inner diameter (ID) stainless steel tubing (VICI model T5C5D, Valco Instruments Company Inc., Houston, TX, USA) to a 3- way T-union (Model MT.5CXS6, Valco Instruments Company Inc., Houston, TX, USA) mounted inside the oven. The 3-way T-union served as the point of modulation for the pulse flow valve. The pulse flow valve was controlled by an Iota One Microfluidic Valve Driver (Model 060-

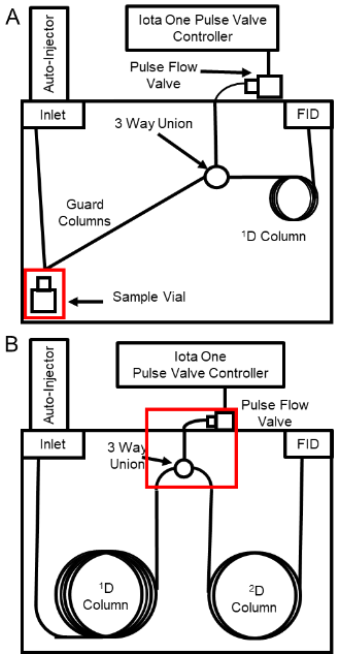

Figure 2.2 Schematic of the two instrumental configurations used for the studies. (A) 1D-GC in a headspace sampling mode. The highlighted region depicts the setup used to create the steady-state analyte mixture stream that is introduced to the T-union. (B) GC×GC mode. The highlighted region contains the custom tubing linking the pulse flow valve to the T-union.

0010-900, Parker Hannifin, Hollis, NH, USA). All pressures and flow rates were controlled by the stock gauges in the GC platform.

The 1D-GC configuration (Figure 2.2A) was implemented using a pseudo steady-state analyte test mixture (Table A1A). Lists of all four analyte test mixtures used are provided in Supporting Information (Tables A1A-D). A guard column (Restek, 25 cm ×100 µm ID) was used to connect the auto-injector to a headspace sampling vial (Part Number 8010-0412, Agilent Technologies, Palo Alto, CA, USA), and a second guard column (Restek, 25 cm ×100 µm ID) connected the vial to the 3-way T-union, followed by the separation column (DB-5, 1.0 m × 100 µm d_c × 0.10 µm d_f). Isothermal conditions were applied at 90 °C. The inlet flow rate was set to 6.5 mL/min, equating to 47.6 psig at the inlet. The auxiliary flow from the pulse flow valve was set to 49.0 psig with a p_w of 6 ms. The auto-injector for the GC was utilized to inject 5 µL of the analyte test mixture ten times (totaling 50 µL injected) to establish a pseudo steady-state analyte stream emitted from the headspace vial.

The GC×GC study with the 20-component test mixture (Table A1C) used a "normal" column configuration, with a non-polar ^{1}D column (DB-5, 3.0 m × 100 µm ^1d_c × 0.10 µm ^1d_f) followed by a polar ^{2}D column (DB-WAX, 1.0 m × 100 µm ^2d_c × 0.10 µm ^2d_f). An isothermal temperature of 90 °C was applied. The inlet flow rate was set to 3.0 mL/min, equating to 52.6 psig at the inlet, with a split of 100:1. The split ratios in this study were selected to provide adequate *S/N*. The auxiliary flow from the pulse flow valve was set to 52.6 psig with a p_w of 10 ms.

The pulse width study and the diesel GC×GC separation study used the same GC×GC "reverse" column configuration, with a polar ^{1}D column (DB-WAX, 3.0 m × 100 µm ^1d_c × 0.10 µm ^1d_f) followed by a non-polar ^{2}D column (DB-5, 1.0 m × 100 µm ^2d_c × 0.10 µm ^2d_f). For the

pulse width study, an isothermal temperature of 90 °C was applied. The inlet flow rate was set to 3.0 mL/min, equating to 52.6 psig at the inlet, with a split of 300:1. The pulse flow valve auxiliary pressure was set to 49.0 psig with variable pulse widths. For the GC×GC diesel study, a temperature program was used. The oven was initially set to 40 °C for 1 min, ramped at 20 °C/min to 240 °C, and held for 2 min. The inlet flow rate was held at 1 mL/min, going from 21.8 psig to 38.1 psig, with a split of 10:1. Auxiliary flow from the pulse flow valve was set to a pressure ramp to match the ^{1}D column inlet, going from 22.5 psig to 38.7 psig at 1.62 psi/min.

Finally, the pulse flow valve and column assembly were attached to the end of a GC×GC but prior to a TOFMS, creating a GC^{3}-TOFMS instrument based on an Agilent 6890N GC and LECO Pegasus III TOFMS (LECO Corporation, St. Joseph, MI). The ^{1}D column was non-polar (DB-5 ms, 40.0 m × 180 µm $^{2}d_{c}$ × 0.18 µm $^{2}d_{f}$) followed by a semi-polar ^{2}D column (RTX-200, 2.5 m × 180 µm $^{2}d_{c}$ × 0.18 µm $^{2}d_{f}$), followed by a more polar ^{3}D column (DB-HeavyWax, 1.0 m × 180 µm $^{2}d_{c}$ × 0.18 µm $^{2}d_{f}$). The switch from 100 µm to 180 µm ID columns ensured adequate flow rates could be used within the allowable parameters of the GC instrument and the TOFMS vacuum. The pulse flow valve was mounted as previously described, but in between the ^{2}D and ^{3}D columns, with the stock thermal modulator between the ^{1}D and ^{2}D columns. The oven was set to 40 °C for 1 min, ramped by 5 °C/min to 250 °C and held for 2 min. The inlet flow rate was held at 1.1 mL/min, going from 31.4 to 67.7 psig. The pulse flow valve auxiliary pressure was ramped from 6 to 14 psig at 0.19 psi/min. The GC^{3}-TOFMS study utilized a 90-component test mixture (Table A1D).

2.4 Results and Discussion

We begin by studying partial modulation in the negative pulse mode using the 1D-GC configuration (Figure 2.2A), to demonstrate the ability to obtain replicate chromatograms at a

high sampling frequency using a pseudo steady-state analyte test mixture. In doing so, each partial modulation "reinjects" a small portion (p_w of 6 ms applied) of the steady-state analyte stream onto the GC column while a large fraction of the stream remains relatively unchanged for the raw data of 7 representative and reproducible replicate chromatograms (i.e. injections) prior to baseline correction (Figure 2.3A), and for one chromatogram (Figure 2.3B). The "baseline" FID signal of 2.0 V is from the pseudo steady-state analyte stream that is constantly evaporating from the ~50 µL injected into the headspace vial. Using an in-house written code, the original chromatogram (Figure 2.3B) is baseline corrected (Figure 2.3C). The separating and resolving capability using partial modulation in the negative pulse mode is apparent. The 8 analytes in the test mixture (Table A1A) are separated with baseline resolution (i.e. a resolution $R_s \geq 1.5$) between them. Following baseline correction, the $w_{1/2}$ and retention time, t_R, for each analyte was measured for the 7 displayed chromatograms (Figure 2.3A). The w_b (1.7 $w_{1/2}$) and retention factors, k', were calculated in relation to acetone, which is taken as an unretained analyte (Table A2). Next, a plot of w_b as a function of k' was obtained (Figure 2.3D). As expected for an isothermal separation,[26] later eluting analytes are wider (w_b ~26 ms for benzyl alcohol versus ~6.5 ms for acetone), and the w_b increases linearly with k' (R^2 of 0.9778). Using this linear fit, one can estimate the peak capacity, n_c, at unit resolution ($R_s = 1$).[27] Indeed, a remarkable n_c of 14 is achieved for this 200 ms separation window. If used in GC×GC mode, a P_M of 200 ms could be applied and this high peak capacity would be provided.

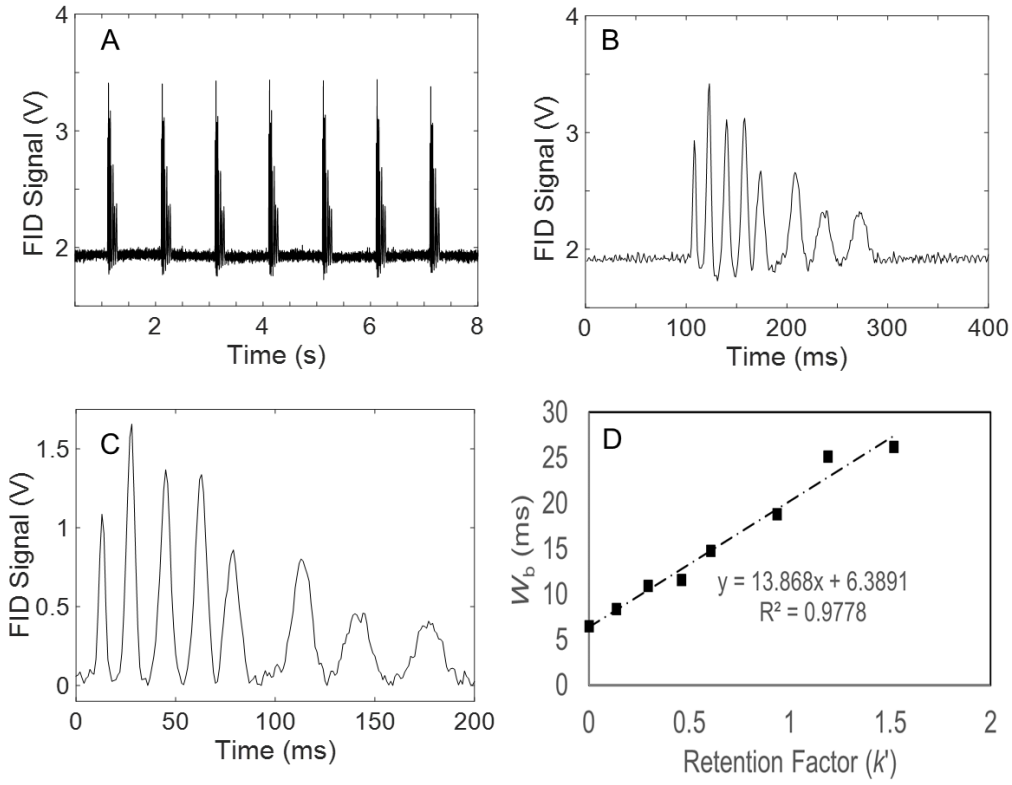

Figure 2.3. With partial modulation in the negative pulse mode, the pulse flow valve acts as an "injector" on a steady-state analyte mixture stream (Figure 2.1A, Table A1A). (A) Raw data of 7 successive "injections" of the steady-state analyte stream. (B) Zoomed in view of the first injection. The 8 analytes in the test mixture emerge within 200 ms of each other with baseline resolution. Order of elution for the analytes is: acetone, heptane, octane, chlorobenzene, nonane, butyl benzene, decane, benzyl alcohol. (C) Each chromatogram is baseline corrected using an in-house algorithm (rolling ball minimum). (D) Plot of w_b as a function of k' for the 8 analytes (data summarized in Table A2).

This 1D-GC study presents an intriguing way to envisage the use of high-speed GC separations for continuous monitoring and related measurement applications. In this study, enough analyte is initially injected into the headspace vial to maintain a pseudo steady-stream of

signal that was modulated to investigate the repeatability of this modulation approach. Viewing this another way, any chemical reaction, or process, that emits volatiles (or semi-volatiles) could be monitored by a GC in such a way. Modifications to the headspace vial setup to divert a stream of volatile products from a reaction or process to this modulator could enable near-real time analyses to be performed. This is an area that we intend to continue to explore.

Evaluation of high-speed partial modulation in the negative pulse mode for GC×GC was performed next, using a 20-component test mixture (Table A1C), a P_M of 100 ms, and a p_w of 8 ms (Figure 2.4). The raw data (Figure 2.4A) appears to exhibit ~5 ^{1}D peaks (everything below the modulated ^{2}D peaks) in this 12 s separation region. Baseline correction was applied to the raw data (Figure A1) to provide the typically appearing, modulated GC×GC data in the unfolded ^{1}D format (Figure 2.4B). A 1 s window, centered at 32 s, shows 6 modulated ^{2}D chromatograms (Figure 2.4C). Five analytes are separated in a 60 ms window in each ^{2}D separation, while they are all co-eluting on the ^{1}D separation: methylcyclopentane, hexyne, benzene, thiophene, and 1,2-dichloromethane. Cutting and folding the raw data in the traditional GC×GC format (Figure 2.4B) provides a 2D contour plot (Figure 2.4D). Identification of each analyte was determined through serial addition of each analyte prior to the combination of the test mixture. The ^2w_b obtained are quite narrow (Figure 2.4D). Indeed, ^2w_b ranged from 7 ms (acetone, isopropyl alcohol) to 12 ms (thiophene, toluene), providing a remarkable ^2n_c of ~12 with a P_M of only 100 ms. This GC×GC separation illustrates the power of partial modulation in the negative pulse mode.

Nonetheless, the ^{1}D peaks in Figure 2.4 are oversampled relative to most GC×GC applications. Each analyte is between 1-2 s wide on ^{1}D, resulting in about 10-20 modulations per analyte. Typically with GC×GC, ^{1}D peaks are (should be) sampled between 2-4 times by the

modulator,[28] enabling the analyst to maximize the 2D peak capacity, $n_{c,2D}$, while still providing comprehensive separations. Oversampling generally means that ^{1}D peaks are excessively wide, and the analyst is losing ^{1}D peak capacity as a result. However, that is not the case here. One may infer that the use of partial modulation is not producing oversampling for the same reason. In fact, the performance of the modulator speaks to the need to improve the performance of GC so much more efficient ^{1}D separations are achieved, such as providing ^1w_b ~200-400 ms concurrently with a P_M of ~100 ms, so the sampling density is more appropriate. Recent advances in GC technology have been very promising in this regard,[29,30] such as

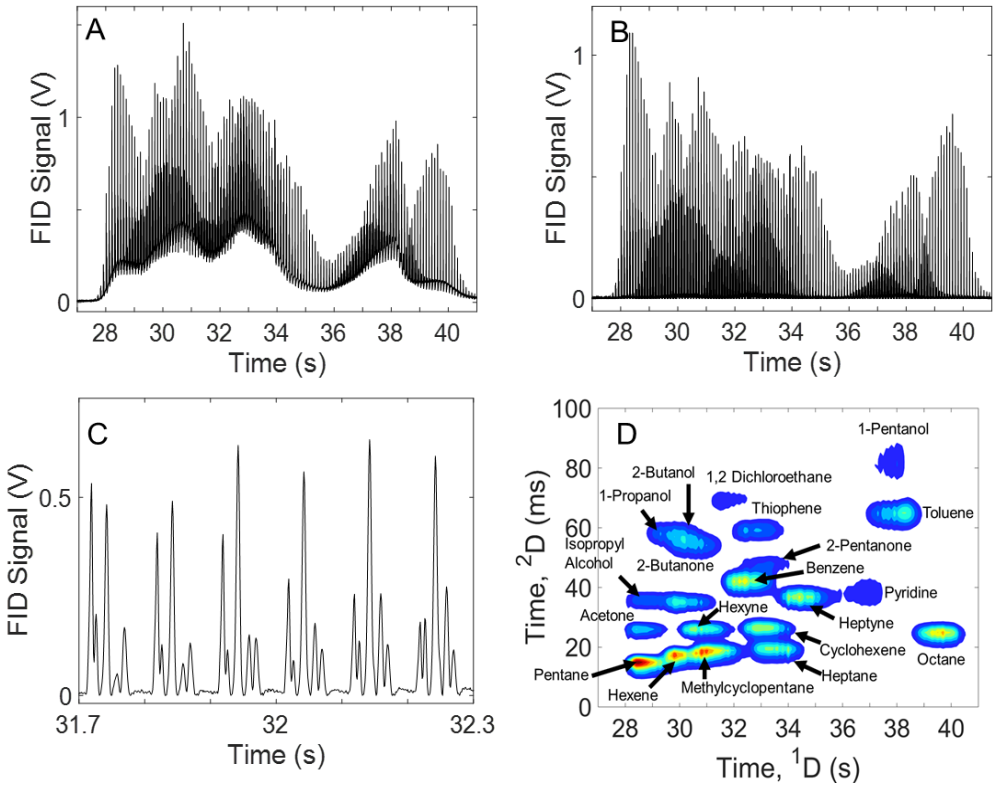

Figure 2.4. GC×GC separation of the 20-component mixture (Table A1C). (A) Raw data collected showing the ^{2}D peaks riding on top of the ^{1}D chromatographic profile. (B) Baseline corrected data where the ^{1}D chromatographic profile is subtracted. (C) Zoom-in view of (B) at

the 32 s mark in a complex region showing 6 modulations with a P_M = 100 ms, to highlight the performance of partial modulation in the negative pulse mode. (D) The data in (B) is cut and fold into a traditional GC×GC chromatogram. The ^2w_b range is ~7-12 ms, resulting in a ^2n_c ~12.

resistively heated temperature programming,[27,31,32] with extension to micro-GC formats.[33–35] Developments in axial thermal gradient GC[36] and flow field thermal gradient GC[37] are also very promising platforms for potential integration with pulse flow valve modulation. Additionally, modulation from the ^{2}D to ^{3}D dimensions in GC^3 is naturally well suited to take advantage of partial modulation, as the second dimension peaks of ^2w_b ~200 to 400 ms are readily achieved.[7,18,20] Indeed, this direction with GC^3-TOFMS is reported herein.

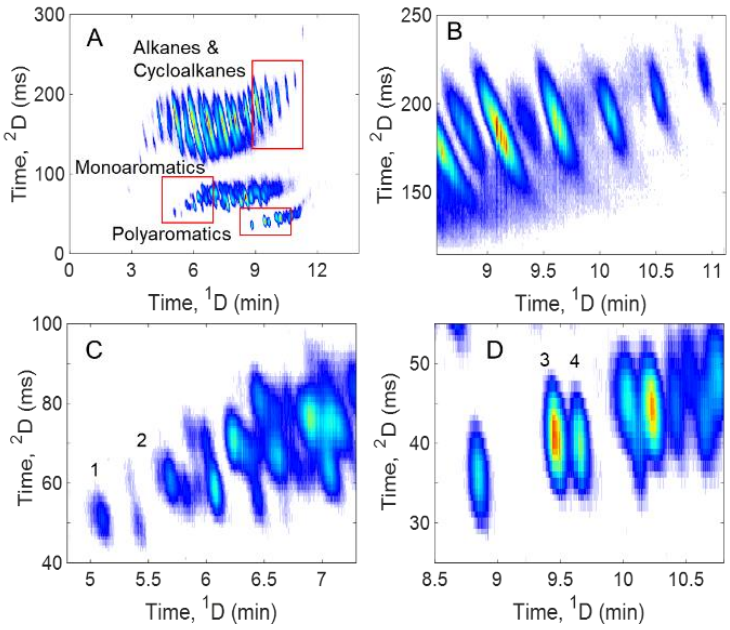

Figure 2.5. (A) GC×GC chromatogram of a diesel sample. (B) A zoom in of the highlighted area in the top right corner of the alkane and cycloalkane band. (C) A zoom in of the beginning of the monoaromatic band. (D) A zoom in of the beginning of the polyaromatic band. Individual

analyte ^2w_b ranges (numbered 1-4 in (C) and (D)) from 16-19 ms (average of ~18 ms). This affords us an approximated ^2n_c of ~17 per 300 ms modulation period.

Next, a more extreme test of the separating power using partial modulation in the negative pulse mode was performed on a diesel sample. A rapid (12 min) GC×GC separation with a reverse column configuration and a P_M of 300 ms is provided (Figure 2.5). Distinct compound classes within the fuel are separated (Figure 2.5A). The large band at the top (most retained on the ^{2}D) includes the alkanes and the cycloalkanes, the middle band includes the monoaromatics, and the lower band (least retained on the ^{2}D) contains the polyaromatics. For additional insight, Figures 2.5B-D provide a zoom in view of highlighted regions of the separation (Figure 2.5A). In each zoomed-in region, single analyte peaks are visible for additional examination. Of note, since the alkane and cycloalkane band is comprised of very wide ^{2}D peaks, with a range of ~60-100 ms, a majority of these peaks are likely not single analytes, but rather closely eluting isomers. Clearly resolved individual analyte peaks were retrieved from the two aromatic regions (numbered 1-4, Figure 2.5C-D) to provide estimates for ^1w_b and ^2w_b for the sake of estimating peak capacities. The ^1w_b range is 3.5-4 s (average of 4 s, ^1n_c of ~180) and ^2w_b range is 16-19 ms (average of 18 ms, ^2n_c of ~17) for the aromatic bands, resulting in a $n_{c,2D}$ of ~3,000 in this high-speed GC×GC separation. The raw data for this separation, as well as two zoomed in regions, are also provided (Figure A3).

Finally, GC^3-TOFMS with pulse flow valve modulation between the ^{2}D and ^{3}D columns (P_M of 100 ms) is demonstrated using a 90-component test mixture (Table A1D). The full, 45-min separation in the raw, 1D vector format and traditional ^{1}D×^{2}D GC×GC (TIC) chromatogram, with the ^{3}D summed away, are provided (Figures 2.6A-B). A zoom in of 9 modulations (18 s)

near the 15 min ^{1}D time is also provided (Figure 2.6C), revealing four analytes in a 3D isosurface plot. Alternatively, the analyst can sum away the ^{1}D time data, and utilize the mass spectral data provided. Doing so, we can plot all four analytes in a ^{2}D×^{3}D GC×GC chromatogram, using selective *m/z* for each analyte (Figure 2.6D). This format is easier to view and analyze than the 3D isosurface plot format.

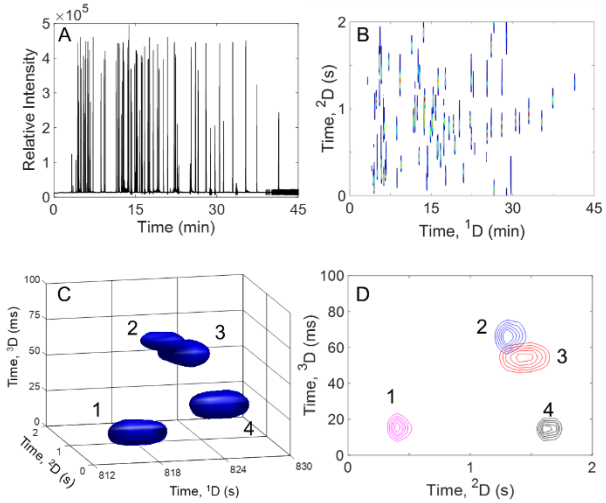

Figure 2.6. (A) Raw, vector chromatogram for the GC^{3}-TOFMS separation of the 90-component sample (Table A1D). (B) A traditional, ^{1}D×^{2}D GC×GC (TIC) chromatogram where the ^{3}D data is summed away. (C) A zoom-in of 9 modulations on the ^{1}D (i.e. 18 s), where four test analytes elute with unique $^{1}t_{R}$, $^{2}t_{R}$, and $^{3}t_{R}$. (D) Using the mass spectral data, selective *m/z* for each analyte were used to create a ^{2}D×^{3}D overlay, displaying the selectivity afforded by this 4D data set. These four analytes, with their selective *m/z* are: (1) 5-decyne (*m/z* 55), (2) methyl caproate (*m/z* 74), (3) anisole (*m/z* 78), and (4) cyclooctane (*m/z* 56).

In addition to the gains in chemical selectivity provided by three separation dimensions with GC^{3}, a substantial peak capacity is also provided. Using representative peak width data (Table A4), for the ^{1}D separation time (45 min) producing average $^{1}w_{b}$ of 4 s, a near optimal 1D-

GC peak capacity ${}^{1}n_c$ of 675 was obtained. This high ${}^{1}n_c$ was achieved concurrent with reasonably high peak capacities for the ^{2}D and ^{3}D separations. For each ^{2}D separation with a run time of 2 s, an average ${}^{2}w_b$ of 255 ms produced a ${}^{2}n_c$ of 8. Thus, the ideal GC×GC peak capacity, taken as the product ${}^{1}n_c \times {}^{2}n_c$ is 5,400, which is near optimal. Similarly, for each ^{3}D separation with an average ${}^{3}w_b$ of 15 ms, a ${}^{3}n_c$ of 6.5 was achieved. The product ${}^{1}n_c \times {}^{2}n_c \times {}^{3}n_c$ provides a total 'ideal" peak capacity for GC^3, $n_{c,3D}$, of 35,100,[18] now with TOFMS detection. This impressive $n_{c,3D}$ is made possible by coupling an optimized GC×GC instrument with high speed 100 ms modulations to the ^{3}D column, which produced extremely narrow ^{3}D peaks.

2.5 CONCLUSION

In this study, further development of partial modulation in the negative pulse mode was reported. With GC×GC, partial modulation provided the ability to readily obtain the peak profiles of the ^{1}D peaks without requiring peak fitting. As the ^{2}D peaks are superimposed upon the ^{1}D profile, the ^{2}D peaks were uncoupled from the ^{1}D peaks via baseline subtraction. The negative pulse mode produced consistently narrow peaks (w_b in the 6-20 ms range). While this study focused on a P_M range of 100-300 ms, a P_M of 50 ms can be applied.[17,18] The pulse flow valve was also used to create a GC^3-TOFMS instrument to demonstrate effective use of the short P_M. In doing so, the peak capacity produced for a 45 min separation was 35,100. Since the ^{3}D peak widths were typically ~ 15 ms, a P_M of 100 ms provided a peak capacity approaching 10, which has been determined to be the optimal theoretical and experimental gain in peak capacity if comprehensive separation conditions are optimized.[38–41] While the pulse flow valve and associated hardware is straight forward to implement, there is much room for continued exploration into the properties of, and uses for, partial modulation (and pulse flow valve

modulation) for 1D-GC (continuous monitoring), high-speed GC×GC, GC^3, and related methods.

2.6 REFERENCES

(1) Giddings, J. C. *Unified Separation Science*; Wiley: New York, 1991.

(2) Liu, Z.; Phillips, J. B. Comprehensive Two-Dimensional Gas Chromatography Using an On-Column Thermal Modulator Interface. *J. Chromatogr. Sci.* **1991**, *29* (6), 227–231. https://doi.org/10.1093/chromsci/29.6.227.

(3) Dimitriou-Christidis, P.; Bonvin, A.; Samanipour, S.; Hollender, J.; Rutler, R.; Westphale, J.; Gros, J.; Arey, J. S. GC×GC Quantification of Priority and Emerging Nonpolar Halogenated Micropollutants in All Types of Wastewater Matrices: Analysis Methodology, Chemical Occurrence, and Partitioning. *Enviro. Sci. Technol.* **2015**, *49* (13), 7914–7925. https://doi.org/10.1021/es5049122.

(4) Megson, D.; Kalin, R.; Worsfold, P. J.; Gauchotte-Lindsay, C.; Patterson, D. G.; Lohan, M. C.; Comber, S.; Brown, T. A.; O'Sullivan, G. Fingerprinting Polychlorinated Biphenyls in Environmental Samples Using Comprehensive Two-Dimensional Gas Chromatography with Time-of-Flight Mass Spectrometry. *J. Chromatogr. A* **2013**, *1318*, 276–283. https://doi.org/10.1016/j.chroma.2013.10.016.

(5) Welke, J. E.; Manfroi, V.; Zanus, M.; Lazzarotto, M.; Zini, C. A. Differentiation of Wines According to Grape Variety Using Multivariate Analysis of Comprehensive Two-Dimensional Gas Chromatography with Time-of-Flight Mass Spectrometric Detection Data. *Food Chem.* **2013**, *141* (4), 3897–3905. https://doi.org/10.1016/j.foodchem.2013.06.100.

(6) Pierce, K. M.; Kehimkar, B.; Marney, L. C.; Hoggard, J. C.; Synovec, R. E. Review of Chemometric Analysis Techniques for Comprehensive Two Dimensional Separations Data. *J. Chromatogr. A* **2012**, *1255*, 3–11. https://doi.org/10.1016/j.chroma.2012.05.050.

(7) Prebihalo, S. E.; Berrier, K. L.; Freye, C. E.; Bahaghighat, H. D.; Moore, N. R.; Pinkerton, D. K.; Synovec, R. E. Multidimensional Gas Chromatography: Advances in Instrumentation, Chemometrics, and Applications. *Anal. Chem.* **2017**. https://doi.org/10.1021/acs.analchem.7b04226.

(8) Seeley, J. V.; Seeley, S. K. Multidimensional Gas Chromatography: Fundamental Advances and New Applications. *Anal. Chem.* **2013**, *85* (2), 557–578. https://doi.org/10.1021/ac303195u.

(9) Seeley, J. V. Recent Advances in Flow-Controlled Multidimensional Gas Chromatography. *J. Chromatogr. A* **2012**, *1255*, 24–37. https://doi.org/10.1016/j.chroma.2012.01.027.

(10) Bahaghighat, H. D.; Freye, C. E.; Synovec, R. E. Recent Advances in Modulator Technology for Comprehensive Two Dimensional Gas Chromatography. *TrAC, Trends Anal. Chem.* **2018**. https://doi.org/10.1016/j.trac.2018.04.016.

(11) Marriott, P. J.; Chin, S.-T.; Maikhunthod, B.; Schmarr, H.-G.; Bieri, S. Multidimensional Gas Chromatography. *TrAC, Trends Anal. Chem.* **2012**, *34*, 1–21. https://doi.org/10.1016/j.trac.2011.10.013.

(12) Edwards, M.; Boswell, H.; Górecki, T. Comprehensive Multidimensional Chromatography. *Curr. Chromatogr.* **2015**, *2*, 80–109. https://doi.org/10.2174/2213240602666150722232236.
(13) Pierce, K. M.; Kehimkar, B.; Marney, L. C.; Hoggard, J. C.; Synovec, R. E. Review of Chemometric Analysis Techniques for Comprehensive Two Dimensional Separations Data. *J. Chromatogr. A* **2012**, *1255*, 3–11. https://doi.org/10.1016/j.chroma.2012.05.050.
(14) Khummueng, W.; Harynuk, J.; Marriott, P. J. Modulation Ratio in Comprehensive Two-Dimensional Gas Chromatography. *Anal. Chem.* **2006**, *78* (13), 4578–4587. https://doi.org/10.1021/ac052270b.
(15) Siegler, W. C.; Fitz, B. D.; Hoggard, J. C.; Synovec, R. E. Experimental Study of the Quantitative Precision for Valve-Based Comprehensive Two-Dimensional Gas Chromatography. *Anal. Chem.* **2011**, *83* (13), 5190–5196. https://doi.org/10.1021/ac200302b.
(16) Cai, H.; Stearns, S. D. Partial Modulation Method via Pulsed Flow Modulator for Comprehensive Two-Dimensional Gas Chromatography. *Anal. Chem.* **2004**, *76* (20), 6064–6076. https://doi.org/10.1021/ac0492463.
(17) Freye, C. E.; Bahaghighat, H. D.; Synovec, R. E. Comprehensive Two-Dimensional Gas Chromatography Using Partial Modulation via a Pulsed Flow Valve with a Short Modulation Period. *Talanta* **2018**, *177*, 142–149. https://doi.org/10.1016/j.talanta.2017.08.095.
(18) Bahaghighat, H. D.; Freye, C. E.; Gough, D. V.; Sudol, P. E.; Synovec, R. E. Ultrafast Separations via Pulse Flow Valve Modulation to Enable High Peak Capacity Multidimensional Gas Chromatography. *J. Chromatogr. A* **2018**. https://doi.org/10.1016/j.chroma.2018.08.001.
(19) Bahaghighat, H. D.; Freye, C. E.; Gough, D. V.; Synovec, R. E. Comprehensive Two-Dimensional Gas Chromatography and Time-of-Flight Mass Spectrometry Detection with a 50 Ms Modulation Period. *J. Chromatogr. A* **2018**. https://doi.org/10.1016/j.chroma.2018.11.027.
(20) Gough, D. V.; Bahaghighat, H. D.; Synovec, R. E. Column Selection Approach to Achieve a High Peak Capacity in Comprehensive Three-Dimensional Gas Chromatography. *Talanta* **2019**, *195*, 822–829. https://doi.org/10.1016/j.talanta.2018.12.007.
(21) Watson, N. E.; Bahaghighat, H. D.; Cui, K.; Synovec, R. E. Comprehensive Three-Dimensional Gas Chromatography with Time-of-Flight Mass Spectrometry. *Anal. Chem.* **2017**, *89* (3), 1793–1800. https://doi.org/10.1021/acs.analchem.6b04112.
(22) Watson, N. E.; Prebihalo, S. E.; Synovec, R. E. Targeted Analyte Deconvolution and Identification by Four-Way Parallel Factor Analysis Using Three-Dimensional Gas Chromatography with Mass Spectrometry Data. *Anal. Chim. Acta* **2017**. https://doi.org/10.1016/j.aca.2017.06.017.
(23) Gross, G. M.; Prazen, B. J.; Grate, J. W.; Synovec, R. E. High-Speed Gas Chromatography Using Synchronized Dual-Valve Injection. *Anal. Chem.* **2004**, *76* (13), 3517–3524. https://doi.org/10.1021/ac049909g.
(24) van Deursen, M. M.; Beens, J.; Janssen, H.-G.; Leclercq, P. A.; Cramers, C. A. Evaluation of Time-of-Flight Mass Spectrometric Detection for Fast Gas Chromatography. *J. Chromatogr. A* **2000**, *878* (2), 205–213. https://doi.org/10.1016/S0021-9673(00)00300-9.

(25) Klemp, M. A.; Akard, M. L.; Sacks, R. D. Cryofocusing Inlet with Reverse Flow Sample Collection for Gas Chromatography. *Anal. Chem.* **1993**, *65* (18), 2516–2521. https://doi.org/10.1021/ac00066a020.
(26) Wilson, R. B.; Hoggard, J. C.; Synovec, R. E. High Throughput Analysis of Atmospheric Volatile Organic Compounds by Thermal Injection – Isothermal Gas Chromatography – Time-of-Flight Mass Spectrometry. *Talanta* **2013**, *103*, 95–102. https://doi.org/10.1016/j.talanta.2012.10.013.
(27) Fitz, B. D.; Mannion, B. C.; To, K.; Hoac, T.; Synovec, R. E. Evaluation of Injection Methods for Fast, High Peak Capacity Separations with Low Thermal Mass Gas Chromatography. *J. Chromatogr. A* **2015**, *1392*, 82–90. https://doi.org/10.1016/j.chroma.2015.03.009.
(28) Pinkerton, D. K.; Parsons, B. A.; Synovec, R. E. Method to Determine the True Modulation Ratio for Comprehensive Two-Dimensional Gas Chromatography. *J. Chromatogr. A* **2016**, *1476*, 114–123. https://doi.org/10.1016/j.chroma.2016.11.015.
(29) Wang, A.; Tolley, H. D.; Lee, M. L. Gas Chromatography Using Resistive Heating Technology. *J. Chromatogr. A* **2012**, *1261*, 46–57. https://doi.org/10.1016/j.chroma.2012.05.021.
(30) Jacobs, M. R.; Hilder, E. F.; Shellie, R. A. Applications of Resistive Heating in Gas Chromatography: A Review. *Anal. Chim. Acta* **2013**, *803*, 2–14. https://doi.org/10.1016/j.aca.2013.04.063.
(31) Luong, J.; Gras, R.; Hawryluk, M.; Shellie, R. A.; Cortes, H. J. Multidimensional Gas Chromatography Using Microfluidic Switching and Low Thermal Mass Gas Chromatography for the Characterization of Targeted Volatile Organic Compounds. *J. Chromatogr. A* **2013**, *1288*, 105–110. https://doi.org/10.1016/j.chroma.2013.02.084.
(32) Dong, H.; Zhang, F. J.; Wang, F. Y.; Wang, Y. Y.; Guo, J.; Kanhar, G. M.; Chen, J.; Liu, J.; Zhou, C.; Yan, M.; et al. Simultaneous On-Line Monitoring of Propofol and Sevoflurane in Balanced Anesthesia by Direct Resistive Heating Gas Chromatography. *J. Chromatogr. A* **2017**, *1506*, 93–100. https://doi.org/10.1016/j.chroma.2017.05.001.
(33) Ghosh, A.; Foster, A. R.; Johnson, J. C.; Vilorio, C. R.; Tolley, L. T.; Iverson, B. D.; Hawkins, A. R.; Tolley, H. D.; Lee, M. L. Stainless-Steel Column for Robust, High-Temperature Microchip Gas Chromatography. *Anal. Chem.* **2019**, *91* (1), 792–796. https://doi.org/10.1021/acs.analchem.8b04174.
(34) Ghosh, A.; Johnson, J. E.; Nuss, J. G.; Stark, B. A.; Hawkins, A. R.; Tolley, L. T.; Iverson, B. D.; Tolley, H. D.; Lee, M. L. Extending the Upper Temperature Range of Gas Chromatography with All-Silicon Microchip Columns Using a Heater/Clamp Assembly. *J. Chromatogr. A* **2017**, *1517*, 134–141. https://doi.org/10.1016/j.chroma.2017.08.036.
(35) Reid, V. R.; McBrady, A. D.; Synovec, R. E. Investigation of High-Speed Gas Chromatography Using Synchronized Dual-Valve Injection and Resistively Heated Temperature Programming. *J. Chromatogr. A* **2007**, *1148* (2), 236–243. https://doi.org/10.1016/j.chroma.2007.03.029.
(36) Wang, A.; Hynynen, S.; Hawkins, A. R.; Tolley, S. E.; Tolley, H. D.; Lee, M. L. Axial Thermal Gradients in Microchip Gas Chromatography. *J. Chromatogr. A* **2014**, *1374*, 216–223. https://doi.org/10.1016/j.chroma.2014.11.035.
(37) Boeker, P.; Leppert, J. Flow Field Thermal Gradient Gas Chromatography. *Anal. Chem.* **2015**, *87* (17), 9033–9041. https://doi.org/10.1021/acs.analchem.5b02227.

(38) Klee, M. S.; Cochran, J.; Merrick, M.; Blumberg, L. M. Evaluation of Conditions of Comprehensive Two-Dimensional Gas Chromatography That Yield a near-Theoretical Maximum in Peak Capacity Gain. *J. Chromatogr. A* **2015**, *1383*, 151–159. https://doi.org/10.1016/j.chroma.2015.01.031.
(39) Davis, J. M. Statistical Theory of Spot Overlap for N-Dimensional Separations. *Anal. Chem.* **1993**, *65* (15), 2014–2023. https://doi.org/10.1021/ac00063a015.
(40) Davis, J. M.; Giddings, J. Calvin. Statistical Theory of Component Overlap in Multicomponent Chromatograms. *Anal. Chem.* **1983**, *55* (3), 418–424. https://doi.org/10.1021/ac00254a003.
(41) Davis, J. M.; Giddings, J. C. Statistical Method for Estimation of Number of Components from Single Complex Chromatograms: Theory, Computer-Based Testing, and Analysis of Errors. *Anal. Chem.* **1985**, *57* (12), 2168–2177. https://doi.org/10.1021/ac00289a002.

Chapter 3. Chemometric Decomposition of Comprehensive Two-Dimensional Gas Chromatography Time-of-Flight Mass Spectrometry Data Employing Partial Modulation in the Negative Pulse Mode

This chapter was reproduced from D.V. Gough, S. Schöneich, R.E. Synovec, "Chemometric Decomposition of Comprehensive Two-Dimensional Gas Chromatography Time-of-Flight Mass Spectrometry Data Employing Partial Modulation in the Negative Pulse Mode" accepted in *Talanta*, in press.

3.1 INTRODUCTION

Gas chromatography (GC) is a powerful separation tool that enables the gas phase separation of volatile and semi-volatile analytes. The efficacy of GC has significantly increased with the advent of comprehensive, two-dimensional (2D) gas chromatography (GC×GC) pioneered by Liu and Phillips,[1] since significantly more peak capacity[2] and chemical selectivity[3–5] are provided by GC×GC relative to one-dimensional GC. GC×GC instruments require a modulator between two successive capillary columns in order to comprehensively couple the second dimension (^{2}D) separation to the first dimension (^{1}D) separation.[6–8] Furthermore, the ^{2}D column must be equipped with a stationary phase sufficiently different from the ^{1}D column so as to provide orthogonal selectivity.[5] The growth of GC×GC has been significant in recent years, especially when coupled with time-of-flight mass spectrometry (TOFMS) detection.[5,6,9–16]

The modulator is the key instrument component that enabled the jump from one-dimensional GC to GC×GC. Currently, there are two broad categories of modulators: thermal and flow-based modulators.[6,8,12,17–21] Both modulator categories generally provide "full" modulation,[17] resulting in a series of ^{2}D peaks for a given ^{1}D peak in which baseline is observed

between adjacent ^{2}D peaks for a given analyte. The series of narrow ^{2}D peaks follow the same general shape of the ^{1}D peak. When each analyte is modulated at least 2 or more times, the GC×GC separation is considered "comprehensive" as it retains the ^{1}D separation peak profiles.[5,22,23] The number of times an analyte is modulated, defined as the ^{1}D width-at-base ($^{1}W_b$) divided by the modulation period (P_M), is termed the sampling density (ρ_s),[23] or alternatively the modulation ratio (M_R).[5,22] Currently, modulators typically run in the seconds timeframe,[5,6,8,9,12] though some have been able to operate as quickly as every 250-500 ms.[8,24,25] Further research towards shorter and more efficient GC×GC separations to expand applicability requires a modulator capable of operating at a suitably higher frequency.

Recently, we have been exploring an alternative modulation approach, referred to as partial modulation,[17] that employs a pulse valve and is capable of higher frequency sampling rates with P_M as low as 50 ms.[26–29] As the name implies, partial modulation differs from full modulation by only modulating a portion of the ^{1}D eluate. The fraction of a modulated analyte becomes a series of ^{2}D peaks superimposed on the ^{1}D peak profile. Overall, the ^{1}D separation is comprehensively obtained by ^{2}D separations, simultaneous with also measuring the ^{1}D separation. Note that although the ^{1}D eluate is only partially modulated, the duty cycle is technically 100% since all of the ^{1}D eluate is detected.

Partial modulation can be operated in two modes, either the negative pulse mode (NPM), or the positive pulse mode (PPM).[17,29] With partial modulation in the NPM, a flow of auxiliary carrier gas at a suitable pressure (P_{aux}) is applied through a pulse valve to a T-junction joining the ^{1}D and ^{2}D columns for nearly all of the P_M, resulting in dilution of the ^{1}D eluate. This is followed by briefly turning off the pulse valve for a specified pulse width (p_w), effectively "injecting" undiluted ^{1}D eluate onto the ^{2}D column. The resulting raw data has the appearance of

^{2}D separations superimposed on top of the ^{1}D separation.[29] Application of a rolling ball minimum baseline correction to the raw data uncouples the ^{2}D separation from the ^{1}D separation, and the uncoupled ^{2}D chromatograms can then be cut and folded into a GC×GC chromatogram. Extremely narrow ^{2}D peak widths-at-base ^2W_b (4σ) of about 10 ms with a P_M of 100 ms were obtained.[29] In contrast, in the PPM, the flow of auxiliary carrier gas from the pulse valve is turned off for nearly all of the P_M (p_w approaching P_M), and then is briefly turned on for a short time interval of P_M - p_w, creating a local analyte vacancy in the ^{1}D eluate as it enters the ^{2}D column. Although the raw data collected in the PPM can be converted into traditional appearing GC×GC chromatograms, the data analysis steps were overly complex and the resulting signal-to-noise ratio (*S/N*) suffered.[26–28] The overall consensus was that the partial modulation in the NPM has superior potential relative to the PPM, by achieving extremely narrow peaks using a very short P_M, concurrent with a much higher *S/N* post data processing. In the recent report, we introduced the potential for coupling GC×GC using partial modulation in the NPM to a TOFMS.[29] In this initial report we did not address the challenges that would arise due to the necessity to uncouple the ^{1}D and ^{2}D contributions to the overall detected signal at each mass channel (*m/z*) for overlapped peaks. In this current study we focus our attention on this challenge by employing chemometric decomposition.[10,30–33]

The data produced by GC×GC-TOFMS instruments is inherently complex. Numerous computational tools (broadly termed chemometrics) have been developed to adequately and quickly process and analyze the data. There are numerous useful chemometric tools available for use.[10,33–38] For GC×GC-TOFMS, using partial modulation in the NPM, the data are inherently not trilinear because of the nature in which the ^{1}D separation is coupled to the ^{2}D separations prior to applying chemometric decomposition. Essentially, in the workflow the signal as a

function of *m/z* for each analyte must first be separated from the other analytes and/or interferences. Following this step, the ^{1}D separation can be uncoupled from the ^{2}D separations using a rolling ball minimum baseline correction step. For this purpose multivariate curve resolution – alternating least squares (MCR-ALS) is ideally suited for the chemometric decomposition step of the workflow.[31,38–44] While partial modulation in the NPM is a chromatographically efficient method that produces narrow peaks, the potential drawback is that the GC×GC data produced is intrinsically non-bilinear. MCR-ALS is robust to shifts in ^{2}D retention time shifts and less sensitive to peak shape differences than other chemometric techniques that require the data to be bilinear, which makes it an advantageous algorithm to use for the non-bilinear data produced by this modulation technique. MCR-ALS also allows for the use of common constraints such as non-negativity, unimodality, convergence, and selectivity across the entire data set or just selected components, as desired. An important consideration when applying MCR-ALS is that the solutions are subject to rotational ambiguity. This can often be minimized by applying harsher constraints, building augmented data matrices, and hard modeling.[45] Augmented data matrices can be built by concatenating each unfolded 2D data array either column-wise or row-wise. Uniqueness of the solutions may be evaluated by various methods including MCR-BANDS[45] software or other soft modelling methods.[46]

MCR-ALS splits the instrumental response of the sample matrix into the concentration peak profiles and the spectral information, and uses the alternating least-squares process to fit the data.[42–44] The algorithm calculates the total variance explained in the data set as well as the residuals, or the part of the data set that was not modeled. An initial estimate of the pure analytes is first determined and the ALS process adjusts the elution profiles and spectra iteratively to maximize the explained variance of the data being modeled.[40] GC×GC-TOFMS data can be

decomposed computationally by MCR-ALS along the ^{1}D elution time (^1t_R), ^{2}D elution time (^2t_R), and mass spectral data dimensions. In addition to selecting a time window of the raw sample data, the number of chemical components present in this selected region must be estimated prior to decomposition, though knowing the identity of the components is not necessary.[44] This assigns the number of response profiles the model generates and the number of predicted chemical components that can be edited according to the modeled results. Computing an MCR-ALS model decomposes the raw data matrix into a matrix containing the ^{1}D and ^{2}D elution peak profiles, herein referred to as the loadings, for each analyte.[28,40,45] These loadings contain the concentration information of the pure response peak profiles that allows for the quantification of analytes that are susceptible to co-elution with similar compounds. The MCR-ALS model also provides a matrix containing the mass spectral profiles, corresponding to each loading, that can be matched to established libraries to identify analytes. An advantage of including spectral data as one of the model variables includes the ability to chemometrically decompose complex samples based upon selective *m/z*. The details of this algorithm and its applications are described more extensively in the literature.[31,39,42–44]

GC×GC-TOFMS using more "traditional" modulation approaches produces a series of modulated peaks that follow the same general shape of the ^{1}D analyte peak profile. From a single ^{1}D analyte peak, a series of ^{2}D peaks are produced, which can be summed for quantification. Partial modulation in the NPM creates a similar set of modulated ^{2}D peaks, but also retains the ^{1}D peak profile underneath the ^{2}D peak profile. These ^{2}D peaks were shown to be reproducible with very narrow ^2W_b, and the ^{2}D peaks are relatively easily isolated from the ^{1}D peaks for comparison and calculation of figures-of-merit.[29] However, analyte quantification, either with or without peak overlap, was not previously addressed. A goal of the current study is to determine if

data produced using partial modulation in the NPM is quantifiable using a chemometric decomposition approach. The quantification task at hand bares similarity to that presented by Carabahal et al.[47] that describes an elegant method using MCR-ALS to quantify data with two coupled instrumental modes. They reported an approach that models augmented data matrices containing concatenated test samples and calibration samples, whereby the peak area under the entire resolved concatenated profiles is calculated for quantification. In our study, the ^{1}D peak for each analyte is modulated by the same ratio, the resulting ^{2}D peak areas can be summed (without concern for the remaining, overlapped ^{1}D signals) in a similar manner as traditional one-dimensional GC and GC×GC data, and yield reliable identification and accurate quantification.[48] For this purpose, an isothermal separation of a 15-component mixture of similar compounds is studied, with a 20 s separation time window using a P_M of 250 ms and a short pulse width p_w of 6 ms in order to produce very narrow ^{2}D peaks. Various peak overlap situations were purposely produced to facilitate the chemometric method demonstration.

3.2 EXPERIMENTAL

The GC×GC-TOFMS instrument using partial modulation in the NPM was based upon an Agilent 6890N GC (Agilent Technologies, Palo Alto, CA, USA) and a LECO Pegasus III TOFMS (LECO Corporation, St. Joseph, MI), with the schematic provided in Fig. 3.1. The carrier gas (Praxair, Seattle, WA, USA) was ultra-high purity helium (Grade 5, 99.999%). The inlet

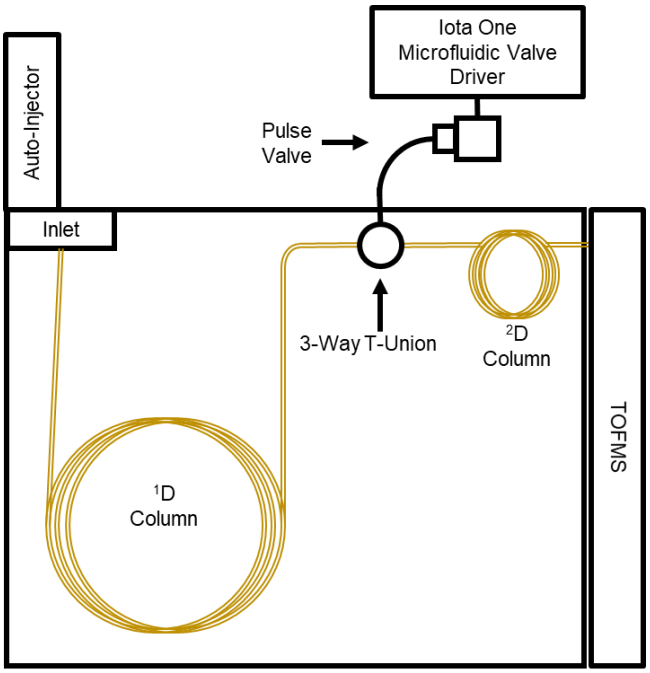

Figure 3.1. Schematic of the GC×GC-TOFMS instrumental setup used for all data collection. Partial modulation in the negative pulse mode by the pulse valve occurs at the 3-way T-union, where eluate from the ^{1}D column is "re-injected" onto the ^{2}D column.

temperature was 175 °C and the transfer line temperature was 240 °C. The oven temperature was set to 100 °C. Post-run data processing was performed in MATLAB R2017b (The Mathworks, Inc., Natick, MA, USA). The Agilent 6890N GC was fitted with a high-speed pulse valve (Model 009-0347-900, Parker Hannifin, Hollis, NH, USA) to facilitate the GC×GC operation. The pulse valve was mounted outside the oven (Fig. 3.1), with a custom-built fitting to connect a 0.005-inch inner diameter (ID) stainless steel tubing (VICI model T5C5D, Valco Instruments Company Inc., Houston, TX, USA) to a 3-way T-union (Model MT.5CXS6, Valco Instruments Company Inc., Houston, TX, USA) mounted inside the oven. The 3-way T-union served as the point of modulation for the pulse valve, coupling the ^{1}D and ^{2}D columns. The pulse valve was

controlled by an Iota One Microfluidic Valve Driver (Model 060-0010-900, Parker Hannifin, Hollis, NH, USA). The auxiliary pressure was controlled by the Agilent 6890N GC.

The study was conducted with a 15-component mixture (Table 3.1) measured by volume in octane. Octane served as a common solvent that did not elute in the same ^{1}D time window as

Peak Number	Analyte Name	Boiling Point (°C)
1	Pentane	36.1
2	Acetone	56
3	Isopropyl Alcohol	82.6
4	1-Hexene	62-63
5	1-Hexyne	69-71
6	2-Butanone	79.6
7	2-Butanol	98
8	Methylcyclopentane	71.8
9	1,2-Dichloroethane	83
10	Heptane	98.4
11	Cyclohexene	83
12	Benzene	80.1
13	2-Pentanone	101
14	Thiophene	84
15	1-Heptyne	98-99

Table 3.1. The fifteen-component test mixture is listed here, with peak number and boiling point for each analyte. The analytes are ordered by $^{2}t_{R}$ within the time window input for MCR-ALS decomposition. The compounds were selected to create separation regions of overlap that required chemometric decomposition.

the rest of the analytes. For the quantification study, a second test mixture with the same compounds was prepared varying the concentrations of 1-hexene (4), and 2-pentanone (13). The concentration of 1-hexene (4) injected for one test mixture was 34 parts-per-thousand by volume (µl/ml) and 39 µl/ml for the other mixture, and concentrations for 2-pentanone (13) were 48 µl/ml and 81 µl/ml, respectively. The studies used a “normal” column configuration: a non-polar ^{1}D column coated with DB-5 stationary phase (3.0 m length × 100 µm $^{1}d_{c}$ × 0.10 µm $^{1}d_{f}$), followed

by a polar ^{2}D column coated with DB-WAX stationary phase (1.0 m length × 100 μm ^2d_c × 0.10 μm ^2d_f). The inlet flow rate was set to 1.5 ml/min, equating to a P_{inlet} of 384.7 kPa (55.8 psig) at the inlet. The auxiliary flow to the pulse flow valve was set to a P_{aux} of 393.7 kPa (57.1 psig) with a p_w of 6 ms and a P_M of 250 ms. A sample volume of 1 μl was injected with a split of 150:1 at the inlet. The TOFMS was set to collect *m/z* 15-150 at a collection frequency of 500 Hz. The heaviest component of the test mixture was octane, with a molar mass of 114 g/mol, allowing for use of the narrow *m/z* range. A relatively narrow *m/z* range was also beneficial to reduce the size of the data obtained with this high collection frequency. An electron impact ionization voltage of -70 eV was used with a detector voltage of 1562 V.

3.3 RESULTS AND DISCUSSION

The compounds in the 15-component mixture were chosen to create a heavily overlapped GC×GC chromatogram to evaluate the ability to analyze the data using MCR-ALS. The raw total ion current (TIC) chromatographic data obtained from a 20 s window of the separation of the 15-component mixture is shown in Fig. 3.2A, while an overlay of the individual *m/z* raw chromatographic data are shown in Fig. 3.2B. In order to provide an *approximate* GC×GC chromatogram, the raw TIC chromatographic data in Fig. 3.2A was baseline corrected using a rolling ball minimum algorithm,[26,29] with the result provided in Fig. 3.2C. The baseline correction effectively subtracted the underlying ^{1}D chromatogram from the raw TIC data to isolate the ^{2}D data (albeit with some artifacts at this stage due to peak overlaps). Analogous to full modulation methods, the data in Fig. 3.2C was then cut-and-folded into a 2D contour plot (Fig. 3.2D), which has the appearance of a typical GC×GC chromatogram. Although the image in Fig. 3.2D contains artifacts due to the peak overlaps that have not been properly handled via chemometric decomposition, and hence is an *approximate* GC×GC chromatogram, the image

provides a suitable starting point to initiate the chemometric analysis. One can see that the 15 analytes are heavily overlapped along the ^{1}D separation, with only one analyte, 1-heptyne, having any substantial amount of its ^{1}D peak elute alone ($^{1}t_{R}$ = 98.75 s). Due to this heavy overlap, and in order to apply MCR-ALS with a suitable rank for any given decomposition analysis, the data was divided into five "time windows" along the ^{1}D axis. The accuracy of the decomposition was increased along with a reduction of the computational load. The five time windows were: 80.0-87.5 s (pentane, acetone, isopropyl alcohol), 86.5-92.0 s (1-hexene, 1-hexyne, 2-butanone, and 2-butanol), 89.0-97.5 s (methylcyclopentane and 1,2-dichlororethane), 92.0-101.0 s (heptane, cyclohexene, benzene, 2-pentanone, and thiophene), and 96.0-102.0 s (1-heptyne). The five time windows overlap such that each analyte is completely decomposed in the window indicated, although some analytes are also partially observed in the decomposition of an adjacent window.

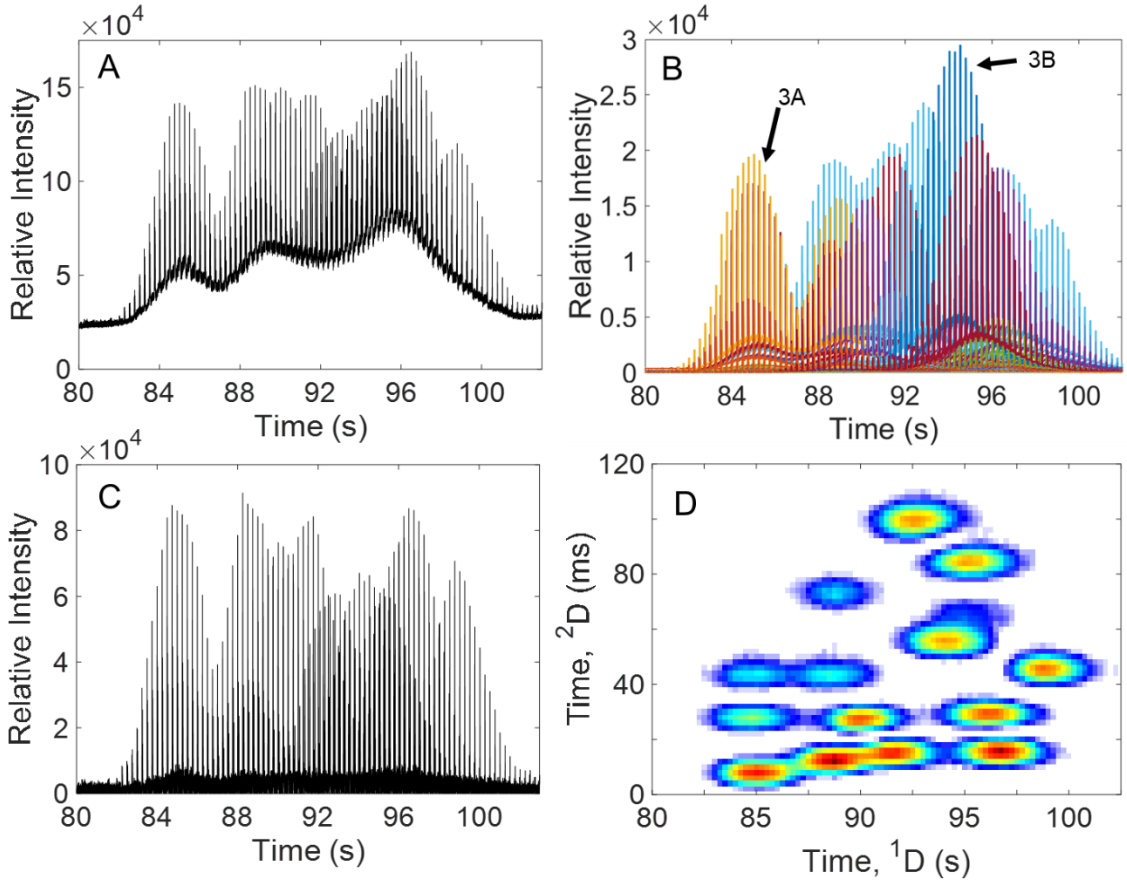

Figure 3.2. (A) The total ion current (TIC) raw data for the separation of the 15-component mixture by GC×GC-TOFMS using partial modulation in the negative pulse mode. (B) The raw data in (A) showing mass channels (*m/z*) 15-150 with the regions 3.3A and 3.3B corresponding to heavily overlapped regions selected for demonstrating decomposition by MCR-ALS. (C) Baseline corrected TIC obtained by subtracting the underlying ^{1}D profile from (A) prior to decomposition. (D) Two-dimensional contour plot for visualization purposes, obtained by treating the baseline corrected data in (C) as raw GC×GC data, and cutting and folding on the P_M = 250 ms intervals (only 120 of 250 ms on ^{2}D is shown).

In order to better visualize the ^{2}D separations in Fig. 3.2B, the signals for all *m/z* for specific modulations along the ^{1}D separation for two of the time windows are provided in Fig.

3.3A for pentane (1), acetone (2), and isopropyl alcohol (3) nominally centered at a ^1t_R = 84.75 s, and in Fig. 3.3B for heptane (10), cyclohexene (11), benzene (12), 2-pentanone (13), and thiophene (14) centered at a ^1t_R = 94.25 s. In Fig. 3.3A, pentane (1), acetone (2), and isopropyl alcohol (3) appear within a 60 ms window on the ^{2}D separation. Due to the narrow ^2W_b achieved by the partial modulation in the NPM, the peaks in this window should be readily decomposed by MCR-ALS. A more challenging region for MCR-ALS decomposition is shown in Fig. 3.3B, where there is less resolution on the ^{2}D separation and apparently fewer selective *m/z*. Both of these time windows will serve to illustrate the chemometric data analysis workflow.

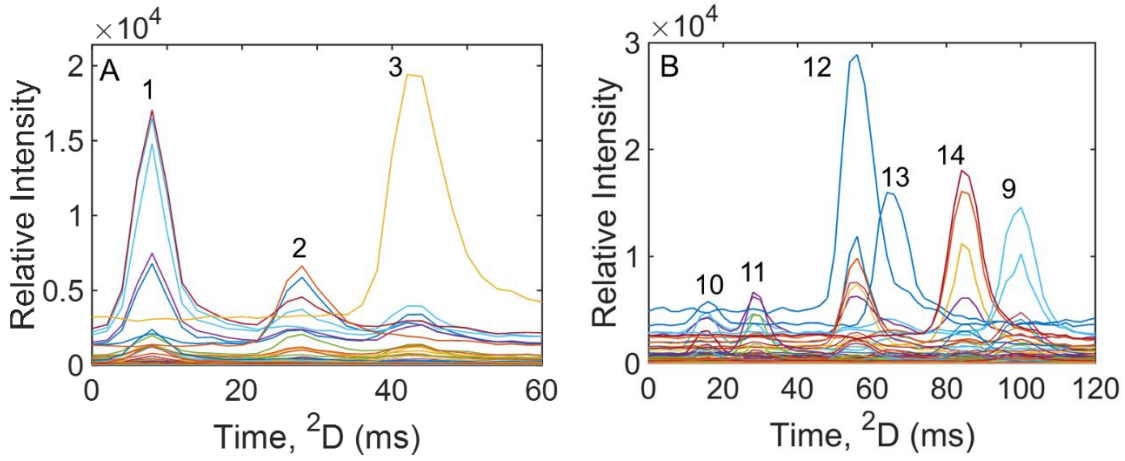

Figure 3.3. Sections highlighted in Fig. 3.2B for demonstration of decomposition by MCR-ALS. (A) Plot of *m/z* the first 60 ms in a single ^{2}D modulation at ^1t_R = 84.75 s in the first time window (80.0-87.5 s). From left to right: pentane (1), acetone (2), and isopropyl alcohol (3). (B) Plot of *m/z* the first 120 ms in a single ^{2}D modulation at ^1t_R = 94.25 s in the fourth time window (92.0-101.0 s). From left to right: heptane (10), cyclohexene (11), benzene (12), 2-pentanone (13), thiophene (14), and 1,2-dichloroethane (9).

The raw, three-dimensional (3D) data (^1t_R, ^2t_R, *m/z*), as illustrated in Figs. 3.2 and 3.3A, is fed into MCR-ALS in a series of the defined ^{1}D time windows. The first time window, from 80.0

to 87.5 s, covering the first three analytes (pentane, acetone, isopropyl alcohol) is shown in Fig. 3.4A. The data was entered into MCR-ALS as a 2-column array for decomposition after *m/z* 18, 28, and 32, that are affected by atmospheric contamination, were set to zero. To avoid negative elution profiles and spectra, the algorithm was initialized by applying non-negativity constraints. All MCR-ALS analyses were non-targeted with no additional filters or thresholds applied using the functions available in MATLAB R2017b. The MCR-ALS algorithm returns the decomposed analyte peak profiles i.e., loadings (Fig. 3.4B), yet still in the form provided by partial modulation in the NPM with the ^{2}D peaks superimposed on the ^{1}D peak background (which is relatively small). Not shown are the noise loadings, or the sum of all *m/z* with essentially zero analyte signal. MCR-ALS also returns the mass spectral profiles for each of the decomposed analytes (Fig. 3.4C). The mass spectral profiles can be directly compared with NIST library standards (or in-house collected mass spectral standards) for match value (MV) calculations to assist analyte identification. This MV was calculated by the match spectral matching algorithm defined by

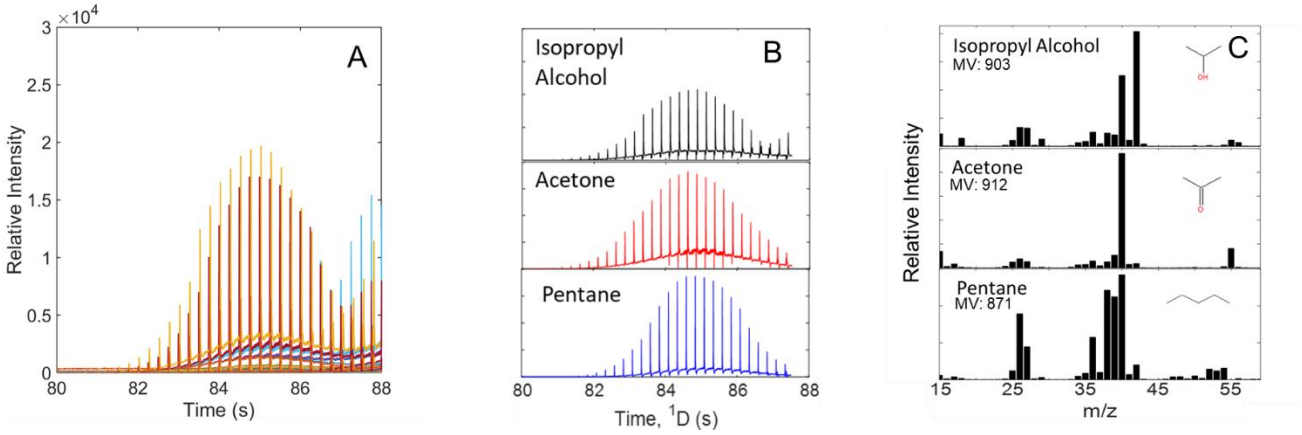

Figure 3.4. (A) The raw data (all *m/z*) of the first time window (80.0-87.5 s), input into MCR-ALS for decomposition. (B) Loadings obtained, providing concurrent ^{1}D and ^{2}D separation information for each individual analyte: pentane (1), acetone (2), and isopropyl alcohol (3). (C)

Mass spectral profiles obtained. These were compared against the NIST library for match value (MV) comparisons. The average MV obtained with excellent accuracy (RSD ≤ 1.35 %) are included in the scores plot for the respective analyte.

Stein[49] using MS Search 2.0 (NIST, Gaithersburg, MD, U.S.A.) applying no limits to the mass range of NIST that was searched. A forward match value of 800 was accepted for identification. To address the issue of rotational ambiguity when using MCR-ALS for a single data matrix, augmented data matrices were created containing each replicate for each time window. MCR-ALS analysis of the augmented data matrices was performed four times, providing a unique solution that was essentially the same as each single data matrix solution. This included the explained variance (R^2), with values 99.93% or higher for each, and the percent fit for each component that was modeled in the given time window.

The individual analyte peak loadings in Fig. 3.4B contain both the naturally coupled ^{1}D and ^{2}D peak profiles, which must be uncoupled for further analysis. Application of a rolling minimum baseline subtraction algorithm as previously described (written in-house),[26,29] and Savitsky-Golay smoothing readily provides the uncoupling, producing two "sub-loadings," referred to as loading 1.1 (^{2}D peak profiles) in Fig. 3.5A, and loading 1.2 (^{1}D peak profile) in Fig. 3.5B. A zoom in of one modulation from each individual analyte in Fig. 3.5A (loading 1.1) is provided in Fig. 3.5C to assist in visualizing the narrow ^{2}D peaks. All peaks in Fig. 3.5C are taken at 84 s in Fig. 3.5A. From here, pertinent figures-of-merit for both dimensions, such as t_R and W_b, can be readily obtained without any mathematical peak reconstruction. After uncoupling the elution time modes by baseline subtraction, the loading 1.1 (Fig. 3.5A) can be treated analogous to traditional GC×GC data, and can be cut-and-folded into a contour plot (Fig. 3.5D)

for visual interpretation.[28,29] Note that Fig. 3.5D is an overlay of the individual contour plots for each analyte from Fig. 3.5A.

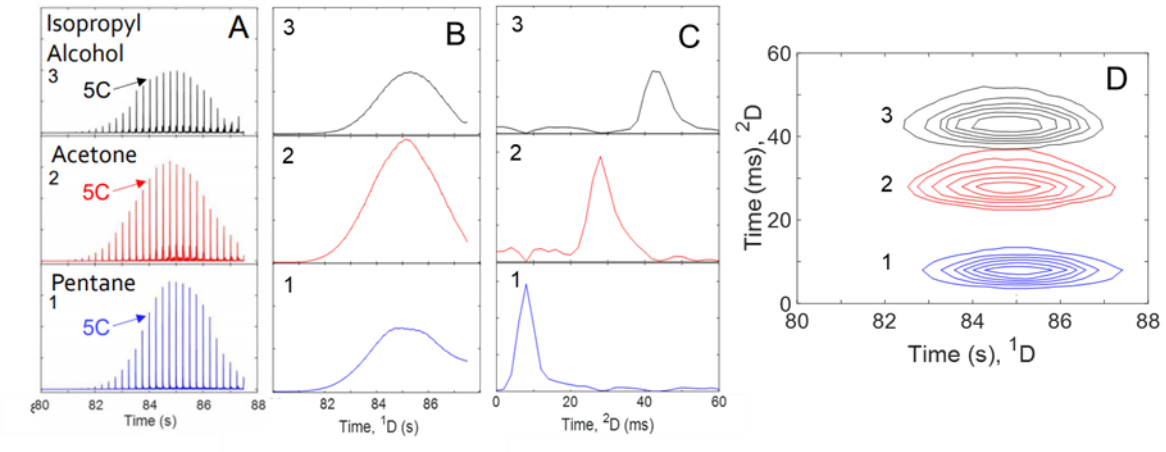

Figure 3.5. Presentation of data processing steps, starting with the MCR-ALS loadings from Fig. 3.4B. (A) Stacked baseline-corrected response profiles (loading 1.1) for pentane (1, blue), acetone (2, red), and isopropyl alcohol (3, black) achieved by baseline correcting the loadings in Fig. 3.4B. (B) The ^{1}D analyte profiles (loading 1.2) are obtained for each analyte by Savitsky-Golay smoothing the baseline subtracted data from (A), or (3.4B)-(3.5A). These plots were used to determine ^1t_R and ^1W_b (4σ), presented in Table 3.2. (C) The first 60 ms of a single ^{2}D modulation, showing the differences in ^2t_R and narrow ^2W_b obtained, obtained by zooming in on a single modulation at 84 s in (A) as indicated by the arrows. These plots were used to determine ^2t_R and ^2W_b (4σ) in Table 3.2. (D) Overlay of individual analyte 2D contour plots created by cutting and folding the loading 1.1 profiles in (A).

The first three analytes, pentane (1), acetone (2), and isopropyl alcohol (3), are severely overlapped in the ^{1}D separation, as can be seen in Fig. 3.5B. The difference in ^1t_R is 0.25 s between analytes, and with a ^1W_b of 5 s, these analytes would normally remain inseparable to chemometric decomposition due to their low ^{1}D resolution (^1R_s) of 0.05. Due to the short, 1.0 m

^{2}D column, the difference in ^2t_R between each of these three analytes is never greater than 20 ms. However, due to the high ^{2}D separating power facilitated by partial modulation in the NPM, an average ^2W_b of 15 ms was produced. The resulting ^2R_s for pentane (1) and acetone (2) is 1.6 and for acetone (2) and isopropyl alcohol (3) the ^2R_s is 1.1, i.e., there is near baseline separation on ^{2}D between adjacent analyte pairs. The ^2R_s was sufficiently high that it compensated for the low ^1R_s, of 0.05, for the two analyte pairs, resulting in a 2D resolution ($R_{s,2D}$) of 1.6 between pentane (1) and acetone (2), and $R_{s,2D}$ of 1.1 between acetone (2) and isopropyl alcohol (3). Here, the 2D resolution, $R_{s,2D}$, is defined as the Euclidean norm of the resolution in each dimension.[50] The significantly higher ^2R_s enabled a successful MCR-ALS decomposition, albeit with some noise, of the individual analyte peak profiles, observed in Fig. 3.5C.

Next, the MCR-ALS analysis of the most complicated ^{1}D time window (92.0-101.0 s) that fully contained heptane (10), cyclohexene (11), benzene (12), 2-pentanone (13), and thiophene (14), and partially contained 1,2-dichloroethane (9) is presented. The most challenging analytes to separate in this time window were benzene (12) and 2-pentanone (13) due the severe overlap on both dimensions. The ^1R_s was determined to be 0.19 and the ^2R_s is 0.56, resulting in a $R_{s,2D}$ of 0.6. The lack of ^{1}D resolution was overcome by a sufficiently high ^{2}D resolution, facilitating decomposition by MCR-ALS. The raw, 3D data (^1t_R, ^2t_R, *m/z*) for this section was illustrated in Figs. 3.2 and 3.3B. The MCR-ALS results are summarized in Fig. 3.6 at the same level of processing as in Fig. 3.5 for the first ^{1}D time window. In Fig. 3.6A are ^{2}D peak profiles (loading 1.1) following the baseline correction of the full peak loadings, and in Fig. 3.6B are the ^{1}D peak profiles (loading 1.2). A zoom in of one of the ^{2}D peak profiles from Fig. 3.6A is provided in Fig. 3.6C to better judge the performance of the decomposition and to assess ^{2}D peak widths. Once again, the ^{2}D peak profiles in Fig. 3.6A (loading 1.1) were cut-and-folded into

individual contour plots and added together to produce a traditional appearing GC×GC plot for this time window, presented in Fig. 3.6D. Although 1,2-dichloroethane (9) appears in Fig. 3.6D, note that part of the peak is missing in this time window. For the purpose of providing an accurate analysis for 1,2-dichloroethane (9), it is fully analyzed in the ^{1}D time window of 89.0-97.5 s that fully contains methylcyclopentane (8) and 1,2-dichlororethane (9).

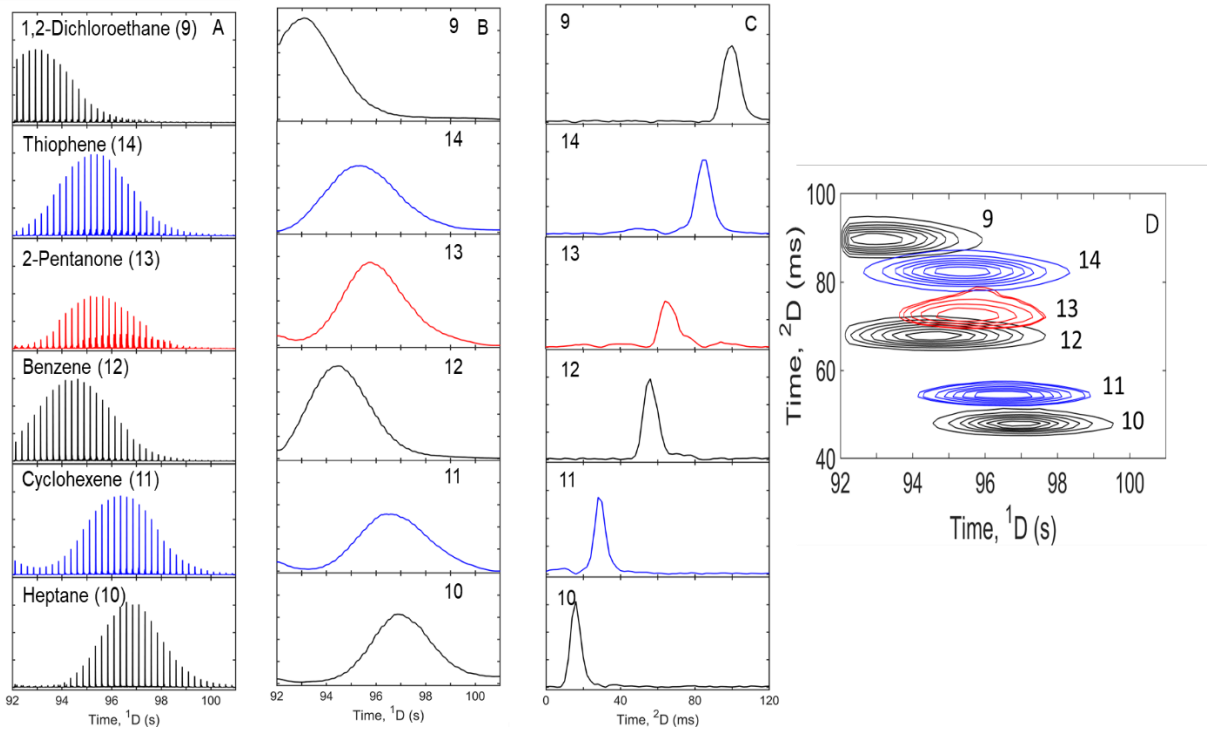

Figure 3.6. MCR-ALS decomposition of the fourth time window (Fig. 3.3B), illustrating a more complex separation region. The same processing approach applied in Figs. 3.4 and 3.5 was used. (A) Stacked plots of each baseline corrected loading 1.1 of heptane (10), cyclohexene (11), benzene (12), 2-pentanone (13), thiophene (14), and 1,2-dichloroethane (9). (B) The ^{1}D analyte profiles (loading 1.2) are obtained for each analyte by Savitsky-Golay smoothing the baseline subtracted data from (A). The $^{1}R_{s}$ between adjacent peaks is never greater than 0.35 (1,2-dichloroethane and benzene). (C) Stacked plots of the first 120 ms of a single ^{2}D modulation. The ^{1}D and ^{2}D overlap between 2-pentanone (13) and benzene (12) is evident in (B) and (C). (D)

Overlay of the 2D contour plots for each analyte obtained by cutting and folding each loading 1.1 in (A).

The same analytical workflow was applied to the three remaining ^{1}D time windows. Using the isolated loadings for each analyte, each analyte was individually processed to form an overlay 2D contour plot presented in Fig. 3.7, providing clear detail regarding the extent of overlap in both separation dimensions. As previously mentioned, the only analyte to have any significant amount of its peak profile elute alone is 1-heptyne (15). The most challenging analyte to fully resolve was 1-hexene (4) due to ^{2}D overlap with two other analytes, pentane (1) and

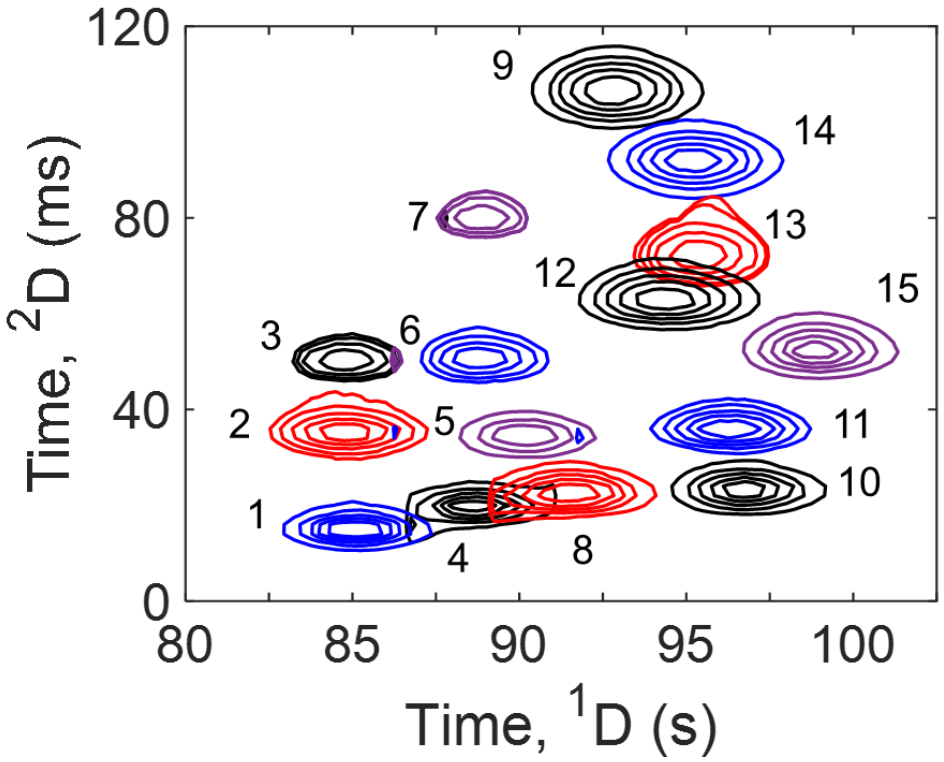

Figure 3.7. Overlay of the 2D contour plots for each analyte of the 15-component mixture obtained by MCR-ALS decomposition. All components were decomposed in a 20 s ^{1}D window

with the analytes ordered according to Table 3.2. The 2D contour plot clearly shows the severe overlap on both dimensions.

methylcyclopentane (8), with both adjacent pairs producing a ${}^{2}R_s$ of 0.36. Similar to previous examples, the analytes were resolved due to the relatively higher ${}^{1}R_s$ of 0.8 resulting in a $R_{s,2D}$ of 0.85 for both adjacent analyte pairs. Despite this high degree of overlap, all 15 analytes were successfully decomposed by MCR-ALS, with each mass spectral profile subsequently compared to the NIST library for MV comparison, as provided in Table 3.2. The average MVs obtained from the mass spectral profiles of the decomposed analytes matched to the NIST library are remarkably all ≥ 800, with average values for four analytes above 900. These high MVs obtained from MCR-ALS decomposition prove to be excellent for accurate identification. Table 3.2 shows the calculated ${}^{1}t_R$, ${}^{1}W_b$, ${}^{2}t_R$, and ${}^{2}W_b$ values, obtained by using sub-loadings 1.1 and 1.2 for each individual analyte, reported for a single representative run. We found the average ${}^{1}W_b$ of all analytes is 5 s (± 0.5 s), and the average ${}^{2}W_b$ is 15 ms (± 3 ms). Fully resolving all 15 compounds with such narrow ${}^{2}W_b$, despite low R_s values, produced by the partially modulated data in the NPM highlights the quality of the response profiles obtained by MCR-ALS.

Peak Number	Analyte Name	MV average (± sd)	${}^{1}t_R$ (s)	${}^{1}W_b$ (s)	${}^{2}t_R$ (ms)	${}^{2}W_b$ (ms)
1	Pentane	871 (± 5)	84.50	4.7	8	10
2	Acetone	912 (± 7)	84.75	5.0	28	15
3	Isopropyl Alcohol	903 (± 12)	85.00	4.7	44	15
4	1-Hexene	800 (± 27)	88.00	4.5	12	10
5	1-Hexyne	874 (± 9)	90.00	4.5	28	12
6	2-Butanone	876 (± 16)	88.50	4.8	44	18
7	2-Butanol	813 (± 45)	88.75	5.0	74	18
8	Methylcyclopentane	910 (± 5)	91.75	5.0	16	12

9	1,2-Dichloroethane	885 (± 14)	92.50	5.9	100	17
10	Heptane	827 (± 11)	96.75	5.5	16	12
11	Cyclohexene	882 (± 27)	96.25	5.6	28	14
12	Benzene	906 (± 6)	94.25	5.5	56	16
13	2-Pentanone	837 (± 24)	95.25	5.0	66	20
14	Thiophene	884 (± 6)	95.00	5.8	86	18
15	1-Heptyne	863 (± 11)	98.75	4.9	46	15

Table 3.2. All 15 components in the mixture are listed in order by $^{2}t_{R}$ within the time window used for MCR-ALS decomposition. Average MV from comparison of mass spectral profiles to NIST library spectra and corresponding figures-of-merit are listed, with standard deviation (sd). All MVs are for six runs and are ≥ 800. All t_{R} and W_{b} values reported are for a representative replicate. The average $^{1}W_{b}$ is 5 s (± 0.5 s) and the average $^{2}W_{b}$ is 15 ms (± 3 ms).

Last, we report on the ability to use the isolated ^{2}D peaks (i.e. loadings 1.1) to demonstrate how quantitative analysis is performed. Two test mixtures composed of the analytes in Table 1 were prepared for the quantification study with two different concentrations of 1-hexene (4) and 2-pentanone (13) injected. Peak areas were calculated for a given analyte by the "two-step method" for GC×GC, where the ^{2}D peaks were uncoupled from the ^{1}D profile and the peak area for the analyte was calculated as the sum of the area of all ^{2}D peaks [25,26,48]. The average peak areas (n=3 replicates) calculated for the highest concentration for each analyte were fitted to the origin, generating a calibration line used to predict their lower concentration. As can be seen in Fig. 3.7, 1-hexene is severely overlapped on ^{2}D between pentane (1) and methylcyclopentane (8), and all of these analytes share several *m/z* with high signal. The predicted versus prepared concentration for 1-hexene was found to be in relatively good

agreement, albeit with a slight negative bias quantified by the percent deviation of -5.6% (± 2.2%). The challenge in resolving the 1-hexene peak on ^{2}D and many shared *m/z* may have contributed to the slight negative bias observed. Meanwhile, the percent deviation for the prediction of the concentration of 2-pentanone was 1.8% (± 3.4%), possibly due to the ^{1}D and ^{2}D overlap with benzene (12) as seen in the decomposition of the time window in Fig. 3.6. Overall, the predicted and prepared concentration values are in good agreement with percent deviation values of -5.6% (± 2.2%) for 1-hexene and 1.8% (± 3.4%) for 2-pentanone, providing promising results supporting the notion that NPM produces quantifiable data.

3.4 CONCLUSION

Partial modulation in the NPM is demonstrated to be a powerful form of modulation for GC×GC-TOFMS. The method is amenable to commercial chemometric tools, demonstrated with MCR-ALS, for analyte decomposition, identification, and quantification. This fast modulation technique readily separated similar, volatile organic compounds over two short separation columns and provided sufficient R_s in the 2D separation space. The 15-component mixture eluted within a 20 s time window with no R_s in the ^{1}D separation being greater than 0.38 (1-heptyne to heptane). Despite the severe overlap in the ^{1}D, the excellent separation efficiency on the ^{2}D separation produced narrow ^{2}D peaks (average ^2W_b = 15 ms) with TOFMS detection, facilitating successful MCR-ALS decomposition of the peak profiles. Further, we demonstrated how the loadings produced by MCR-ALS can be further analyzed to extract the ^{1}D and ^{2}D peak profiles in order to obtain pertinent chemical measurements (retention times and peak widths) without the typical mathematical reconstruction of the ^{1}D peak profile from modulated data. Last, the ^{2}D peak profiles isolated from the MCR-ALS data were shown to be quantifiable and

accurate with excellent mass spectral match values. This study provides further impetus into fast GC research for high throughput analysis as modulation techniques are beginning to easily achieve sub-second separations and push the limit of detector collection frequencies.

3.5 REFERENCES

(1) Liu, Z.; Phillips, J. B. Comprehensive Two-Dimensional Gas Chromatography Using an On-Column Thermal Modulator Interface. *J. Chromatogr. Sci.* **1991**, *29* (6), 227–231. https://doi.org/10.1093/chromsci/29.6.227.

(2) Klee, M. S.; Cochran, J.; Merrick, M.; Blumberg, L. M. Evaluation of Conditions of Comprehensive Two-Dimensional Gas Chromatography That Yield a near-Theoretical Maximum in Peak Capacity Gain. *J. Chromatogr. A* **2015**, *1383*, 151–159. https://doi.org/10.1016/j.chroma.2015.01.031.

(3) Blumberg, L. M.; David, F.; Klee, M. S.; Sandra, P. Comparison of One-Dimensional and Comprehensive Two-Dimensional Separations by Gas Chromatography. *J. Chromatogr. A* **2008**, *1188* (1), 2–16. https://doi.org/10.1016/j.chroma.2008.02.044.

(4) Murray, J. A. Qualitative and Quantitative Approaches in Comprehensive Two-Dimensional Gas Chromatography. *J. Chromatogr. A* **2012**, *1261*, 58–68. https://doi.org/10.1016/j.chroma.2012.05.012.

(5) Marriott, P. J.; Chin, S. T.; Maikhunthod, B.; Schmarr, H. G.; Bieri, S. Multidimensional Gas Chromatography. *TrAC, Trends Anal. Chem.* **2012**, *34*, 1–21. https://doi.org/10.1016/j.trac.2011.10.013.

(6) Seeley, J. V. Recent Advances in Flow-Controlled Multidimensional Gas Chromatography. *J. Chromatogr. A* **2012**, *1255*, 24–37. https://doi.org/10.1016/j.chroma.2012.01.027.

(7) Tranchida, P. Q.; Purcaro, G.; Dugo, P.; Mondello, L. Modulators for Comprehensive Two-Dimensional Gas Chromatography. *TrAC, Trends Anal. Chem.* **2011**, *30* (9), 1437–1461. https://doi.org/10.1016/j.trac.2011.06.010.

(8) Bahaghighat, H. D.; Freye, C. E.; Synovec, R. E. Recent Advances in Modulator Technology for Comprehensive Two Dimensional Gas Chromatography. *TrAC, Trends Anal. Chem.* **2018**, *113*, 379–391. https://doi.org/10.1016/j.trac.2018.04.016.

(9) Seeley, J. V.; Seeley, S. K. Multidimensional Gas Chromatography: Fundamental Advances and New Applications. *Anal. Chem.* **2013**, *85* (2), 557–578. https://doi.org/10.1021/ac303195u.

(10) Pierce, K. M.; Kehimkar, B.; Marney, L. C.; Hoggard, J. C.; Synovec, R. E. Review of Chemometric Analysis Techniques for Comprehensive Two Dimensional Separations Data. *J. Chromatogr. A* **2012**, *1255*, 3–11. https://doi.org/10.1016/j.chroma.2012.05.050.

(11) Edwards, M.; Boswell, H.; Górecki, T. Comprehensive Multidimensional Chromatography. *Curr. Chromatogr.* **2015**, *2* (2), 80–109. https://doi.org/10.2174/2213240602666150722232236.

(12) Prebihalo, S. E.; Berrier, K. L.; Freye, C. E.; Bahaghighat, H. D.; Moore, N. R.; Pinkerton, D. K.; Synovec, R. E. Multidimensional Gas Chromatography: Advances in

Instrumentation, Chemometrics, and Applications. *Anal. Chem.* **2018**, *90* (1), 505–532. https://doi.org/10.1021/acs.analchem.7b04226.
(13) Adahchour, M.; Beens, J.; Vreuls, R. J. J.; Brinkman, U. A. T. Recent Developments in Comprehensive Two-Dimensional Gas Chromatography (GC × GC). I. Introduction and Instrumental Set-Up. *TrAC, Trends Anal. Chem.* **2006**, *25* (5), 438–454. https://doi.org/10.1016/j.trac.2006.03.002.
(14) Zeng, Z.; Li, J.; Hugel, H. M.; Xu, G.; Marriott, P. J. Interpretation of Comprehensive Two-Dimensional Gas Chromatography Data Using Advanced Chemometrics. *TrAC, Trends Anal. Chem.* **2014**, *53*, 150–166. https://doi.org/10.1016/j.trac.2013.08.009.
(15) Tranchida, P. Q.; Salivo, S.; Franchina, F. A.; Mondello, L. Flow-Modulated Comprehensive Two-Dimensional Gas Chromatography Combined with a High-Resolution Time-of-Flight Mass Spectrometer: A Proof-of-Principle Study. *Anal. Chem.* **2015**, *87* (5), 2925–2930. https://doi.org/10.1021/ac5044175.
(16) Tessarolo, N. S.; dos Santos, L. R. M.; Silva, R. S. F.; Azevedo, D. A. Chemical Characterization of Bio-Oils Using Comprehensive Two-Dimensional Gas Chromatography with Time-of-Flight Mass Spectrometry. *J. Chromatogr. A* **2013**, *1279* (2013), 68–75. https://doi.org/10.1016/j.chroma.2012.12.052.
(17) Cai, H.; Stearns, S. D. Partial Modulation Method via Pulsed Flow Modulator for Comprehensive Two-Dimensional Gas Chromatography. *Anal. Chem.* **2004**, *76* (20), 6064–6076. https://doi.org/10.1021/ac0492463.
(18) Harynuk, J.; Górecki, T. New Liquid Nitrogen Cryogenic Modulator for Comprehensive Two-Dimensional Gas Chromatography. *J. Chromatogr. A* **2003**, *1019* (1–2), 53–63. https://doi.org/10.1016/j.chroma.2003.08.097.
(19) Seeley, J. V.; Micyus, N. J.; Bandurski, S. V.; Seeley, S. K.; McCurry, J. D. Microfluidic Deans Switch for Comprehensive Two-Dimensional Gas Chromatography. *Anal. Chem.* **2007**, *79* (5), 1840–1847. https://doi.org/10.1021/ac061881g.
(20) Krupčík, J.; Gorovenko, R.; Špánik, I.; Sandra, P.; Armstrong, D. W. Flow-Modulated Comprehensive Two-Dimensional Gas Chromatography with Simultaneous Flame Ionization and Quadrupole Mass Spectrometric Detection. *J. Chromatogr. A* **2013**, *1280*, 104–111. https://doi.org/10.1016/j.chroma.2013.01.015.
(21) De Geus, H. J.; De Boer, J.; Brinkman, U. A. T. Development of a Thermal Desorption Modulator for Gas Chromatography. *J. Chromatogr. A* **1997**, *767* (1–2), 137–151. https://doi.org/10.1016/S0021-9673(97)00038-1.
(22) Khummueng, W.; Harynuk, J.; Marriott, P. J. Modulation Ratio in Comprehensive Two-Dimensional Gas Chromatography. *Anal. Chem.* **2006**, *78* (13), 4578–4587. https://doi.org/10.1021/ac052270b.
(23) Blumberg, L. M. Accumulating Resampling (Modulation) in Comprehensive Two-Dimensional Capillary GC (GC×GC). *J. Sep. Sci.* **2008**, *31* (19), 3358–3365. https://doi.org/10.1002/jssc.200800424.
(24) Freye, C. E.; Synovec, R. E. High Temperature Diaphragm Valve-Based Comprehensive Two-Dimensional Gas Chromatography with Time-of-Flight Mass Spectrometry. *Talanta* **2016**, *161*, 675–680. https://doi.org/10.1016/j.talanta.2016.09.002.
(25) Freye, C. E.; Mu, L.; Synovec, R. E. High Temperature Diaphragm Valve-Based Comprehensive Two-Dimensional Gas Chromatography. *J. Chromatogr. A* **2015**, *1424*, 127–133. https://doi.org/10.1016/j.chroma.2015.10.098.

(26) Freye, C. E.; Bahaghighat, H. D.; Synovec, R. E. Comprehensive Two-Dimensional Gas Chromatography Using Partial Modulation via a Pulsed Flow Valve with a Short Modulation Period. *Talanta* **2018**, *177* (September 2017), 142–149. https://doi.org/10.1016/j.talanta.2017.08.095.
(27) Bahaghighat, H. D.; Freye, C. E.; Gough, D. V.; Sudol, P. E.; Synovec, R. E. Ultrafast Separations via Pulse Flow Valve Modulation to Enable High Peak Capacity Multidimensional Gas Chromatography. *J. Chromatogr. A* **2018**, *1573*. https://doi.org/10.1016/j.chroma.2018.08.001.
(28) Bahaghighat, H. D.; Freye, C. E.; Gough, D. V.; Synovec, R. E. Comprehensive Two-Dimensional Gas Chromatography and Time-of-Flight Mass Spectrometry Detection with a 50 Ms Modulation Period. *J. Chromatogr. A* **2019**, *1583*, 117–123. https://doi.org/10.1016/j.chroma.2018.11.027.
(29) Gough, D. V.; Song, D. H.; Schöneich, S.; Prebihalo, S. E.; Synovec, R. E. Development of Ultrafast Separations Using Negative Pulse Partial Modulation to Enable New Directions in Gas Chromatography. *Anal. Chem.* **2019**, *91* (11), 7328–7335. https://doi.org/10.1021/acs.analchem.9b01085.
(30) Rajalahti, T.; Kvalheim, O. M. Multivariate Data Analysis in Pharmaceutics: A Tutorial Review. *Internat. J. Pharm.* **2011**, *417* (1–2), 280–290. https://doi.org/10.1016/j.ijpharm.2011.02.019.
(31) Tauler, R. Chemometrics and Intelligent Laboratory Systems Multivariate Curve Resolution Applied to Second Order Data. *Chemom. Intell. Lab. Syst.* **1995**, *30* (95), 133–146.
(32) Tauler, R.; Smilde, A.; Kowalski, B. Selectivity, Local Rank, Three-Way Data Analysis and Ambiguity in Multivariate Curve Resolution. *J. Chemom.* **1995**, *9* (1), 31–58. https://doi.org/10.1002/cem.1180090105.
(33) Bro, R. PARAFAC. Tutorial and Applications. *Chemom. Intell. Lab. Syst.* **1997**, *38* (2), 149–171. https://doi.org/10.1016/S0169-7439(97)00032-4.
(34) Sinha, A. E.; Hope, J. L.; Prazen, B. J.; Fraga, C. G.; Nilsson, E. J.; Synovec, R. E. Multivariate Selectivity as a Metric for Evaluating Comprehensive Two-Dimensional Gas Chromatography-Time-of-Flight Mass Spectrometry Subjected to Chemometric Peak Deconvolution. *J. Chromatogr. A* **2004**, *1056* (1-2 SPEC.ISS.), 145–154. https://doi.org/10.1016/j.chroma.2004.06.110.
(35) Sinha, A. E.; Fraga, C. G.; Prazen, B. J.; Synovec, R. E. Trilinear Chemometric Analysis of Two-Dimensional Comprehensive Gas Chromatography-Time-of-Flight Mass Spectrometry Data. *J. Chromatogr. A* **2004**, *1027* (1–2), 269–277. https://doi.org/10.1016/j.chroma.2003.08.081.
(36) Amigo, J. M.; Skov, T.; Bro, R.; Coello, J.; Maspoch, S. Solving GC-MS Problems with PARAFAC2. *TrAC, Trends Anal. Chem.* **2008**, *27* (8), 714–725. https://doi.org/10.1016/j.trac.2008.05.011.
(37) Kiers, H. A. L.; ten Berge, J. M. F.; Bro, R. PARAFAC2 - Part I. A Direct Fitting Algorithm for the PARAFAC2 Model. *J. Chemom.* **1999**, *13* (3–4), 275–294. https://doi.org/10.1002/(sici)1099-128x(199905/08)13:3/4<275::aid-cem543>3.3.co;2-2.
(38) Izadmanesh, Y.; Garreta-Lara, E.; Ghasemi, J. B.; Lacorte, S.; Matamoros, V.; Tauler, R. Chemometric Analysis of Comprehensive Two Dimensional Gas Chromatography–Mass Spectrometry Metabolomics Data. *J. Chromatogr. A* **2017**, *1488*, 113–125. https://doi.org/10.1016/j.chroma.2017.01.052.

(39) Parastar, H.; Tauler, R. Multivariate Curve Resolution of Hyphenated and Multidimensional Chromatographic Measurements: A New Insight to Address Current Chromatographic Challenges. *Anal. Chem.* **2014**, *86* (1), 286–297. https://doi.org/10.1021/ac402377d.

(40) Mogollon, N. G. S.; Ribeiro, F. A. de L.; Lopez, M. M.; Hantao, L. W.; Poppi, R. J.; Augusto, F. Quantitative Analysis of Biodiesel in Blends of Biodiesel and Conventional Diesel by Comprehensive Two-Dimensional Gas Chromatography and Multivariate Curve Resolution. *Anal. Chim. Acta* **2013**, *796*, 130–136. https://doi.org/10.1016/j.aca.2013.07.071.

(41) Omar, J.; Vallejo, A.; Olivares, M.; Usobiaga, A.; Zuloaga, O.; Etxebarria, N. Resolution and Identification of Co-Eluting Alkylphenols in Comprehensive Two-Dimensional Gas Chromatography-Mass Spectrometry by Multivariate Curve Resolution-Alternating Least Squares. *J. Chemom.* **2015**, *29* (4), 237–244. https://doi.org/10.1002/cem.2701.

(42) De Juan, A.; Tauler, R. Chemometrics Applied to Unravel Multicomponent Processes and Mixtures: Revisiting Latest Trends in Multivariate Resolution. *Anal. Chim. Acta* **2003**, *500* (1–2), 195–210. https://doi.org/10.1016/S0003-2670(03)00724-4.

(43) Omar, J.; Olivares, M.; Amigo, J. M.; Etxebarria, N. Resolution of Co-Eluting Compounds of Cannabis Sativa in Comprehensive Two-Dimensional Gas Chromatography/Mass Spectrometry Detection with Multivariate Curve Resolution-Alternating Least Squares. *Talanta* **2014**, *121*, 273–280. https://doi.org/10.1016/j.talanta.2013.12.044.

(44) de Godoy, L. A. F.; Hantao, L. W.; Pedroso, M. P.; Poppi, R. J.; Augusto, F. Quantitative Analysis of Essential Oils in Perfume Using Multivariate Curve Resolution Combined with Comprehensive Two-Dimensional Gas Chromatography. *Anal. Chim. Acta* **2011**, *699* (1), 120–125. https://doi.org/10.1016/j.aca.2011.05.003.

(45) Jaumot, J.; Tauler, R. MCR-BANDS: A User Friendly MATLAB Program for the Evaluation of Rotation Ambiguities in Multivariate Curve Resolution. *Chemom. Intell. Lab. Syst.* **2010**, *103* (2), 96–107. https://doi.org/10.1016/j.chemolab.2010.05.020.

(46) Golshan, A.; Abdollahi, H.; Beyramysoltan, S.; Maeder, M.; Neymeyr, K.; Rajkó, R.; Sawall, M.; Tauler, R. A Review of Recent Methods for the Determination of Ranges of Feasible Solutions Resulting from Soft Modelling Analyses of Multivariate Data. *Anal. Chim. Acta* **2016**, *911*, 1–13. https://doi.org/10.1016/j.aca.2016.01.011.

(47) Carabajal, M. D.; Arancibia, J. A.; Escandar, G. M. Multivariate Curve Resolution Strategy for Non-Quadrilinear Type 4 Third-Order/Four Way Liquid Chromatography–Excitation-Emission Fluorescence Matrix Data. *Talanta* **2018**, *189*, 509–516. https://doi.org/10.1016/j.talanta.2018.07.017.

(48) Amador-Muñoz, O.; Marriott, P. J. Quantification in Comprehensive Two-Dimensional Gas Chromatography and a Model of Quantification Based on Selected Summed Modulated Peaks. *J. Chromatogr. A* **2008**, *1184* (1), 323–340. https://doi.org/10.1016/j.chroma.2007.10.041.

(49) Stein, S. E.; Scott, D. R. Optimization and Testing of Mass Spectral Library Search Algorithms for Compound Identification. *J. Am. Soc. Mass Spectrom.* **1994**, *5* (9), 859–866. https://doi.org/10.1016/1044-0305(94)87009-8.

(50) Murphy, R. E.; Schure, M. R.; Foley, J. P. Effect of Sampling Rate on Resolution in Comprehensive Two-Dimensional Liquid Chromatography. *Anal. Chem.* **1998**, *70* (8), 1585–1594. https://doi.org/10.1021/ac971184b.

Chapter 4. Developments in Comprehensive Three-Dimensional Gas Chromatography (GC^3) Using the Pulse Valve in the Full Modulation Mode

4.1 INTRODUCTION

The field of multidimensional gas chromatography (MDGC), principally the techniques of GC×GC and GC^3, has experienced a large evolution of technologies and methodologies, enabling a significantly higher fraction of the analytes in extremely complex and challenging samples to be separated for detection.[1–7] Gains discovered in the instrumentation advancements, such as through the injector and modulator innovations,[8–12] have enabled a wider and more diverse array of analytes to be chromatographically separated. Specifically, the modulator has undergone the most significant series of evolutions and upgrades, as the modulator(s) can be viewed as the heart of the MDGC instrument. The modulator is the single piece of equipment that bridges the gap between a one-dimensional and a multidimensional GC instrument.

The modulator can be viewed as a second (or third) injector within an GC-based instrument, connecting two (or three) successive separation columns. There are numerous types of modulators, such as thermal[9,13–15] and flow-based modulators,[8,16–19] but they generally operate by the same principles. For example, with GC×GC, the analyte compounds in the eluate departing the first-dimension column (^{1}D) are trapped and often focused by the modulator. Next, the modulator re-injects the trapped analytes on to the second-dimension column (^{2}D). This modulation process nominally breaks up the analyte Gaussian-like ^{1}D peak profile into a series of successive, significantly narrower ^{2}D peaks; the peak maximum of the ^{2}D peaks follow the same overall shape as the original ^{1}D peak profile but at higher signal intensities due to the trapping and focusing

effect. An important factor in multidimensional separation performance is the number of times that a modulator samples an analyte peak, termed the sampling density (ρ_s). Again, using GC×GC as the example, the sampling density is calculated by dividing the width-at-base (w_b) of the analyte ^{1}D profile (^1w_b) by the time interval between modulations, termed the modulation period (P_M). Previous work has shown that a minimum ρ_s of at least 2 will yield a comprehensive multidimensional separation, i.e., the envelope of ^{2}D profile maxima sufficiently retain the analyte characteristics within a sample (^{1}D figures-of-merit such as peak width, height and area) while providing a quantitative signal for accurate and precise analysis.

Recent improvements to modulation frequency, i.e., how quickly a modulator can actuate defined as the inverse of the modulation period ($1/P_M$), have continued to emerge at a rapid pace. Commercial modulators are designed for typical use with P_M in the 1-10 s range,[6,20–22] with fast modulators able to actuate as quickly as every ~ 250 ms, although these reports were not using the modulator in the specified operation range.[12,19,23] Introduction of the pulse valve modulator for partial modulation was pioneered by Cai and Stearns.[24] More recently, partial modulation was advanced by our group,[25–29] facilitated by a new modulator that could mechanically actuate as quickly as every 50 ms. Initially, this new high frequency modulator gave very promising GC×GC results, although modulation at the higher frequencies was unnecessary due to the excessive ρ_s achieved for typical timescale GC×GC. If the ρ_s is excessive, additional chemical information for an analyte is not provided and the ^{2}D peak capacity, ^2n_c, is restricted.[30–32] The exorbitantly high ρ_s possible (in excess of 10-20) for ^1w_b in the 1-2 s range, meant that the modulator performance was not fully utilized for GC×GC. Indeed, the pulse valve modulator could not be used to its utmost potential due to the peak widths provided by the ^{1}D separations.

While research can, and should, go into improving ^{1}D separations with new advancements to injectors and ^{1}D column performance to reduce $^{1}w_b$ to approximately 200-500 ms wide. This would ensure a ρ_s in the range of 2-5 (with a P_M of 100 ms or so), providing a comprehensive separation with maximum peak capacity. However, a more direct path to more fully utilize pulse valve modulation is to add it to the end of a traditional comprehensive GC×GC instrument, creating a multidimensional GC instrument with three separation dimensions (^{3}D). Current GC×GC instruments already produce analyte ^{2}D peak widths ($^{2}w_b$) in the range of 200-500 ms wide,[5,10,21,23,33] which is suitable for further modulation, and separation, by the pulse valve, between the ^{2}D and ^{3}D columns to produce a comprehensive three-dimensional GC instrument (GC×GC×GC or GC^{3}). Indeed, we have reported on this topic with partial modulation in the positive pulse mode (PPM) and negative pulse mode (NPM).[25–29] One-dimensional gas chromatography (1D-GC) instruments produce a single vector of data, relating time and signal intensity. Two-dimensional GC instruments produce the same single vector of data from the detector, but the raw data can be "cut-and-folded" along the P_M into a 2D contour plot. The raw data from three-dimensional GC instruments (GC^{3}) (Figure 4.1A), can be cut-and-folded along both $^{1}P_M$ and $^{2}P_M$ to create a data cube (Figure 4.1B), with the signal from the detector being a fourth dimension of data. The third separation column allows analytes to undergo an additional column of separation to further differentiate between similar species. Additionally, this provides another axis in time to physically separate closely eluting analytes, increasing the resolution (R_S) between any two analytes and the total peak capacity of the run.

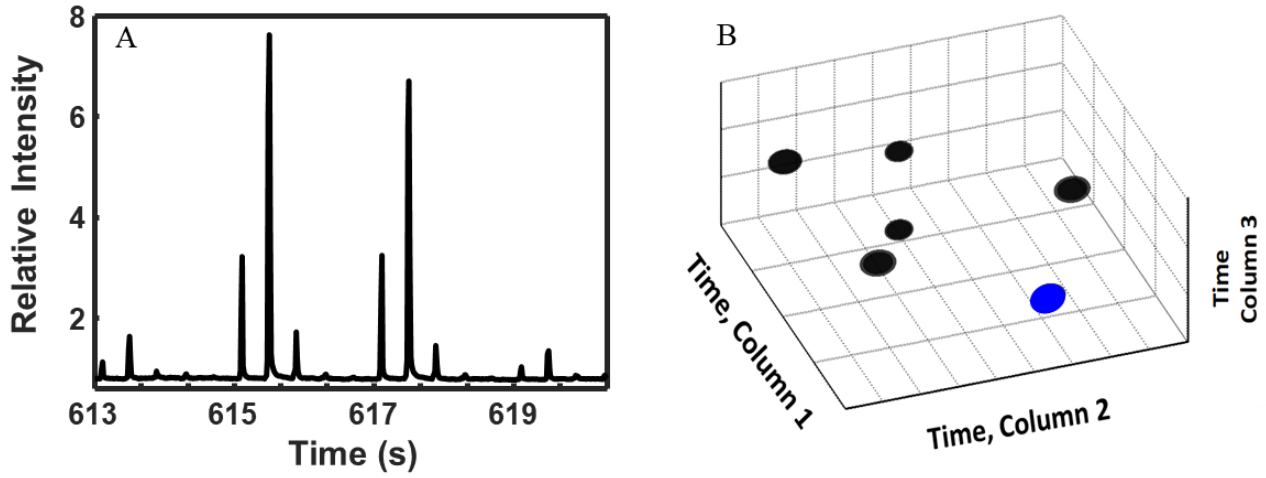

Figure 4.1. A) Raw, GC^3 data as it appears at a detector. In this example, a single analyte was chosen from a larger separation and the total ion chromatogram (TIC) is displayed. B) Fully analyzed, i.e. cut-and-folded, data for a GC^3 instrument appears as a "data cube" with each axis being a time dimension. The analyte from A, being alone on the ^{1}D time axis, would appear as the ellipsoid highlighted in blue, with later eluting analytes (on the ^{1}D) being shown as the black ellipsoids. This figure is a representation of what a 3D plot can look like and is not actual data.

One of the primary reasons for this research into a GC^3 instrument is to greatly increase the total separation peak capacity to handle the ever-increasing complexity of samples presented to GC analysts. The ideal peak capacity (n_c) can be defined as the run time in the x^{th} dimension divided by the average w_b in the x^{th} dimension (Equation 4.1).

$$ {}^{x}n_c = \frac{{}^{x}t}{{}^{x}w} \tag{4.1} $$

To find the total "ideal" peak capacity of a GC^3 instrument ($n_{c,3D}$), one multiplies each of the individual ${}^{x}n_c$ together (Equation 4.2).

$$ n_{c,3D} = {}^{1}n_c \times {}^{2}n_c \times {}^{3}n_c \tag{4.2} $$

Equation 2 can be modified to provide a more useful version to aid in planning experimental parameters before an experiment. The ^{2}D separation time is the same as the P_M for that dimension, i.e., $^2t = {}^1P_M$. Likewise, the ^{3}D separation time is the same as the ^2P_M for that dimension, i.e., $^3t = {}^2P_M$. Substituting in ^1P_M and ^2P_M for ^2t and ^3t, respectively, yields Equation 4.3.

$$n_{c,3D} = \frac{{}^1t}{{}^1w} \times \frac{{}^1P_M}{{}^2w} \times \frac{{}^2P_M}{{}^3w} \tag{4.3}$$

Equation 4.3 provides a framework for planning how to maximize the peak capacity for GC^3. Ideally, the goal is to maximize the peak capacity production (peaks/min) over a suitably long ^{1}D separation. This thinking process begins (and is limited by) the average peak width produced on the ^{3}D separations, ^3w_b. Previous work with the pulse valve in the NPM has shown that ^3w_b between 7-15 ms can be readily produced. Thus, for an average ^3w_b of 10 ms with a ^2P_M of 100 ms, a ^3n_c of 10 is produced. The average ^2w_b for the ^{2}D separations, modulated with a ρ_s of 2, would then be 200 ms. Accordingly, to achieve a ^2n_c at 10, the ^1P_M would have to be 2 s. Repeating this process, the ^1w_b would have to be at least 4 s to have a ρ_s of at least 2. If the separation run time is 40 min (2,400 s), this would produce a ^1n_c of 600, and an $n_{c,3D}$ of 60,000. This works out to a sustained peak capacity production of 1,500 peaks/min for the 40 min separation. In previous work[28,29] these equations have been used to attempt to achieve this lofty goal, and thus far (for 40 min separations), the GC^3 instrument has been able to produce a peak capacity of ~880 peaks/min with TOFMS detection.

While previous work has focused on the potential gains in $n_{c,3D}$ possible due to the third dimension in GC^3, more recent research into GC^3 instrumentation has been aimed at improving the gains in signal intensity (*S/N*). The pulse valve is a truly powerful modulator that can be used in both partial and full modulation modes.[34] In the full modulation mode, the pulse valve in the T-union configuration using a suitably matched auxiliary pressure, p_w and P_M, behaves much like

a thermal modulator, since it can focus the entire ^{1}D eluate (in time) for modulation, at a much higher frequency than any thermal modulator, and retains a duty cycle of 1.0 (100% analyte mass transfer). Additionally, pulse valve modulation can do so without the same limitations that are inherent to a thermal modulator (such as analyte volatility ranges). Second, GC^3 instruments provide a plethora of unstudied ways to view and analyze data, before we even consider the kinds of chemometric analyses tools that can be applied to the data. The complete utility of three time dimensions of separation is truly unknown, but there are a multitude of unique ways to simplify this data, take it out of a cube, and display it in more "bite-sized" chunks of manageable information. This chapter will primarily focus on the *S/N* enhancement of a 100% duty cycle GC^3 instrument, which has not been previously reported with a GC^3-TOFMS instrument, and to do so using various approaches to visualize the GC^3 data set.

4.2 EXPERIMENTAL

The GC^3-TOFMS instrumental platform (Figure 4.2) consisted of an Agilent 6890N GC (Agilent Technologies, Palo Alto, CA, USA) connected to a LECO Pegasus III TOFMS (LECO Corporation, St. Joseph, MI, USA). The stock, 4D thermal modulator within the Pegasus III was used. The electron impact energy for the TOFMS was set to -70 eV with a detector voltage of 1600 V. The TOFMS detector scan rate was operated at 500 *Hz*. The pulse valve (Model 009-0347-900, Parker Hannifin, Hollis, NH, USA) was mounted outside of the GC oven with a custom-built fitting to connect a 125 µm inner diameter (ID) stainless steel tubing (VICI model T5C5D, Valco Instruments Company Inc., Houston, TX, USA) to a 3-way T-union (model MT.5CXS6, Valco Instruments Company Inc., Houston, TX, USA).

The T-union was mounted inside the oven and served as the point of modulation for the pulse valve. The pulse valve was controlled by an Iota One Microfluidic Driver (Model 060-

0010-900, Parker Hannifin, Hollis, NH, USA). All pressures and flow rates were controlled by the stock gauges on the GC instrument platform. Post-run data processing was completed by transferring the data to MATLAB 2018a (The Mathworks Inc., Natick, MA, USA) using an in-house written script. All experiments covered in this chapter utilized this same experimental setup with a $^{1}P_{M}$ of 1.5 s and a $^{2}P_{M}$ of 300 ms, with an oven temperature ramp of 10 °C/min from 40 °C to 250 °C with a temperature hold of 2 min at the start and end of the separation.

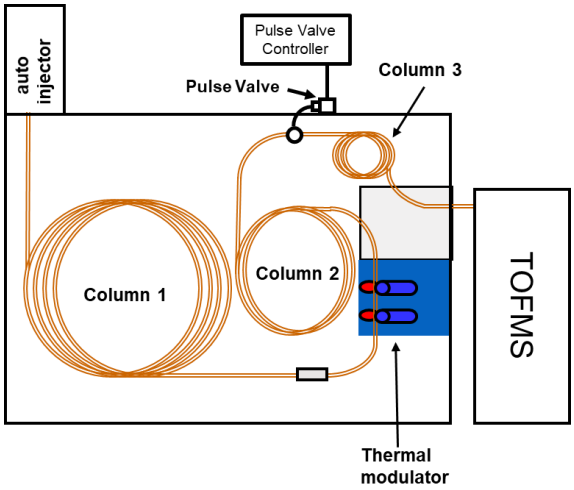

Figure 4.2. GC^{3}-TOFMS instrument schematic. The first modulator is the stock thermal modulator provided by LECO within the Agilent 6890N. The second modulator is the pulse valve modulator.

4.3 Results and Discussion

The raw 3D data that comes from the TOFMS detector is a single row vector per mass channel (*m/z*). For a single, chromatographically isolated analyte, this data appears as a series of sets of small peaks, where the maxima of the ^{3}D peak profiles each follow an overall ^{2}D peak profile, and all of the maxima of the ^{2}D peak profiles follow the larger ^{1}D peak profile (Figure 4.3A).

One can imagine (or calculate mathematically) connecting the maxima of each ^{3}D peak together to form a larger ^{2}D peak. Taking this one more step, connecting the maxima of each of these ^{2}D peaks would then mathematically recreate the ^{1}D peak. The instrumental design and implementation for the data presented in this first study was planned using Eq. 4.3. For the data in Fig. 4.3, the pulse valve in full modulation mode created data with $^{3}w_{b} \approx 25$ ms. With a $^{2}P_{M}$ of 300 ms, this resulted in a $^{3}n_{c}$ of 12 (Figure 4.3B). Concurrently, the $^{2}w_{b}$ of ~600 ms using the $^{2}P_{M}$ of 300 ms enabled a $^{2}\rho_{s} \approx 2$ for a comprehensive GC×GC separation from the ^{2}D separation to the ^{3}D separation. The $^{1}w_{b}$ of ~4 s enabled a $^{1}\rho_{s} \approx 2$, using the $^{1}P_{M}$ of 2 s, again providing a comprehensive GC×GC separation from the ^{1}D separation to the ^{2}D separation. Using Equation 4.3, we find an $n_{c,3D}$ of ≈ 10,350 for this 25 min separation, or ~415 peaks/min. Previously, in

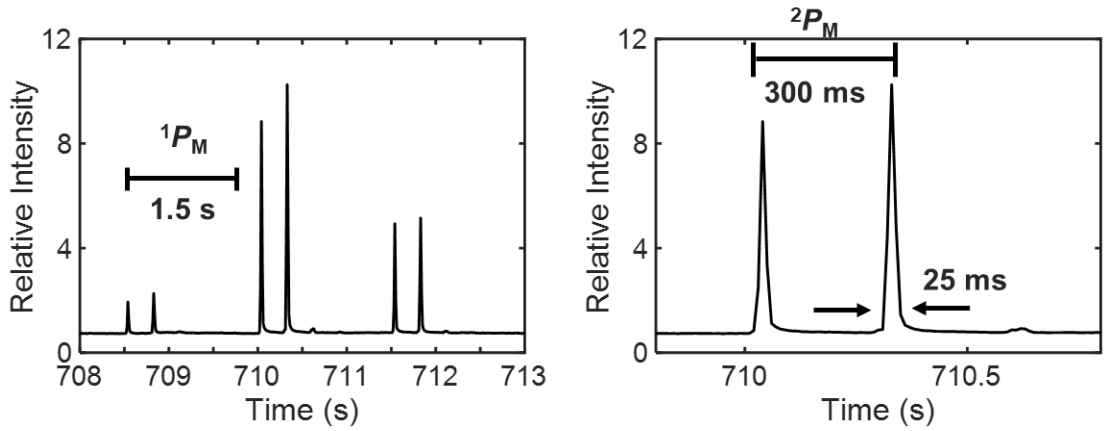

Figure 4.3. Raw, unfolded GC^{3} data from a GC^{3}-TOFMS. A) The full profile (one-, two-, and three-dimensions) of 1-chlorohexane. The analyte $^{1}w_{b}$ is ~ 4 s wide and was modulated ~2-3 times by the thermal modulator ($^{1}\rho_{s} \approx 2$). B) A zoom in of ~750 ms of the separation. The analyte $^{2}w_{b}$ is ~600 ms wide and was modulated ~2 times by the pulse valve ($^{2}\rho_{s} \approx 2$). One can visualize connecting the maxima of these ^{3}D peaks to mathematically reconstruct a single ^{2}D peak. This process could be repeated to reconstruct the ^{1}D peak from ^{2}D peaks in (A).

Chpt 2, when using the NPM with a GC^3-TOFMS an $n_{c,3D}$ (Equation 4.3) of ~35,000 was produced in a 45 min separation, or ~780 peaks/min. The w_b produced by the pulse valve in the full modulation mode are generally wider than the w_b's provided by the NPM. This currently presents some difficulty in the optimization of peak capacity with a GC^3-TOFMS, as optimizing ${}^3n_c$ can detract from either the ${}^1n_c$ or ${}^2n_c$ and further research is needed to address this shortcoming. However, this shortcoming is overshadowed by other gains realized with the full modulation method.

Mathematical reconstruction of peaks (as just described) to compare figures-of-merit does not sufficiently convey the gains in focusing achieved by GC^3 compared to GC×GC and 1D-GC, as connecting the dots between peak maxima does not display the actual gains in signal enhancement realized. In order to clearly evaluate the gains obtained by GC^3 in full modulation mode for both modulation processes, the GC^3 instrument was operated as a 1D-GC instrument (with both the thermal and pulse valve modulators turned off), then as a GC×GC instrument (thermal modulator on, pulse valve off), and then as a full GC^3 instrument. By running these three instrumental conditions, the full set of benefits provided by sequential focusing by in-series, high frequency modulators with 100% duty cycle is apparent. Figure 4.4 demonstrates the results of this experimental comparison. Two analytes (dodecene and tridecane) from a 90-analyte mixture are shown eluting from the three GC-based conditions previously described. In this experiment, the ${}^1P_M$ (modulation period for the thermal modulator from the ^{1}D column to ^{2}D column) was 1.5 s and the ${}^2P_M$ (modulation period for the pulse valve from the ^{2}D column to the ^{3}D column) was 300 ms. The raw data in Figure 4.4 is overlaid without any retention time correction. The analyte peak heights (one for each analyte) from the platform operating as a 1D-

GC instrument (black trace), obtained with both the thermal and pulse valve modulators are turned off, were lower than the maximum peak heights obtained in either the GC×GC (red trace) and GC^3 (blue trace) modes. In GC×GC mode the thermal modulator is on while the pulse valve is turned off; there is only modulation from the ^{1}D column to the ^{2}D column (with additional retention of the ^{3}D column occurring along with the ^{2}D separation). In the GC^3 mode, all the modulators are operating.

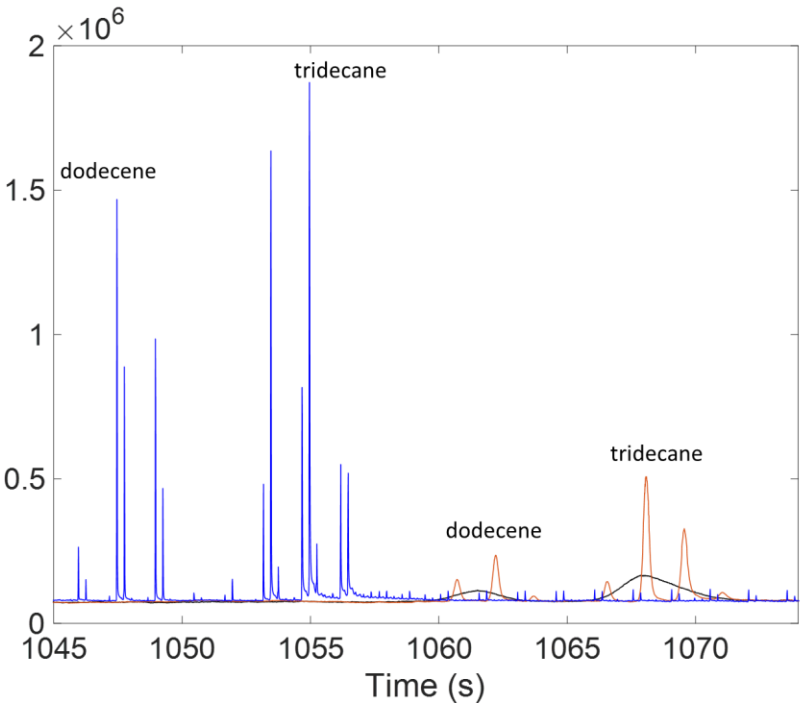

Figure 4.4. Comparison of raw, TIC data for dodecene and tridecane eluting on 1D-GC (black trace), GC×GC (red trace), and GC^3 (blue trace) with TOFMS detection. Note that the pulse valve modulator slightly shifted the retention time of peaks in the GC^3 mode.

Using the data in Fig. 4.4, the detector response enhancement factors (*DREF*) were calculated for both modulation stages for both of these representative analytes.[35] The *DREF* is

defined as the height of the tallest modulated peak (^2h) divided by the height of the unmodulated peak (^1h). Here, I expand upon this concept to factor the height of the tallest second-modulated peak (^3h) to account for the second modulator. Thus, the following three equations were used to determine signal enhancement.

$$^1DREF = \frac{^2h}{^1h} \quad (4.4)$$

$$^2DREF = \frac{^3h}{^2h} \quad (4.5)$$

$$^3DREF = \frac{^3h}{^1h} \quad (4.6)$$

The baseline level was steady for all three experimental conditions at ~ 78,000 (arbitrary units). The 1D-GC peak height (black trace) for dodecene was ~115,000 and for tridecane was ~163,000, prior to baseline correction. For GC×GC, the peak height of the largest ^{2}D peak (red trace) for dodecene was ~240,000 and for tridecane was ~510,000. Likewise, for GC^3, the peak height of the largest ^{3}D peak height (blue trace) for dodecene was ~1,470,000 and for tridecane was ~1,870,000. After subtracting the baseline from the peak heights, level the gains in detection sensitivity enhancement due to the 100% duty cycle for both modulation stages were determined as the *DREF* for each modulation stage and compared for 1D-GC, GC×GC, and GC^3.

As expected of the gains in signal intensity from 1D-GC to GC×GC with thermal modulation,[22,36–38] ^{1}*DREF* of 4.4 and 5.1 were obtained for dodecene and tridecane, respectively. Going from GC×GC to GC^3 using the pulse valve modulation with a 100% duty cycle in full modulation mode produced ^{2}*DREF* of 8.6 and 4.1 for dodecene and tridecane, respectively. Thus, the addition of the second modulator produced overall ^{3}*DREF* values of 37.6 and 21.1 for dodecene and tridecane, respectively, going from 1D-GC to GC^3. While these overall *DREF* for

GC^3 are in the same range as those obtained for GC×GC,[34] the current study with GC^3 is very promising for future improvements, most notably separation condition improvements to reduce the ^2D and ^3D band broadening will result in higher overall *DREF*.

Correcting for retention time shifting for dodecene, we can more easily compare the improvements in signal intensity between 1D-GC, GC×GC, and GC^3 in Figure 4.5, as they relate to the issue of peak widths on the three separation dimensions. The previously noted gains in signal intensity going to successively higher dimensions are even more apparent. These gains are possible by the focusing of the analytes as they pass through each modulator, which is manifested by the decreasing w_b of each analyte peak for each successive dimension. For dodecene, the ^1w_b was ~ 4 s, the ^2w_b was ~600 ms, and the ^3w_b was ~25-30 ms. Using Equation 4.1, the ^1P_M of 1.5 s and ^2P_M of 300 ms, we calculate an ^2n_c of ~2.5 and ^3n_c of ~12, or a $^2D\times^3D$ peak capacity of ~30 for every 1.5 s of separation. Using Equation 4.3, factoring a run time of 25 min, the $n_{c,3D}$ is calculated as 10,350, or 415 peaks/min. Furthermore, to ensure that quantitative accuracy is retained, the sum of the peak areas obtained from one separation dimension to the next were compared. Doing so, we found that 97.7% of the peak area was retained going from the 1D-GC separation (area of the single 1D peak) to the GC^3 separation (sum of the areas of all the ^3D peaks). This supports the use of the GC^3 instrument for quantification.

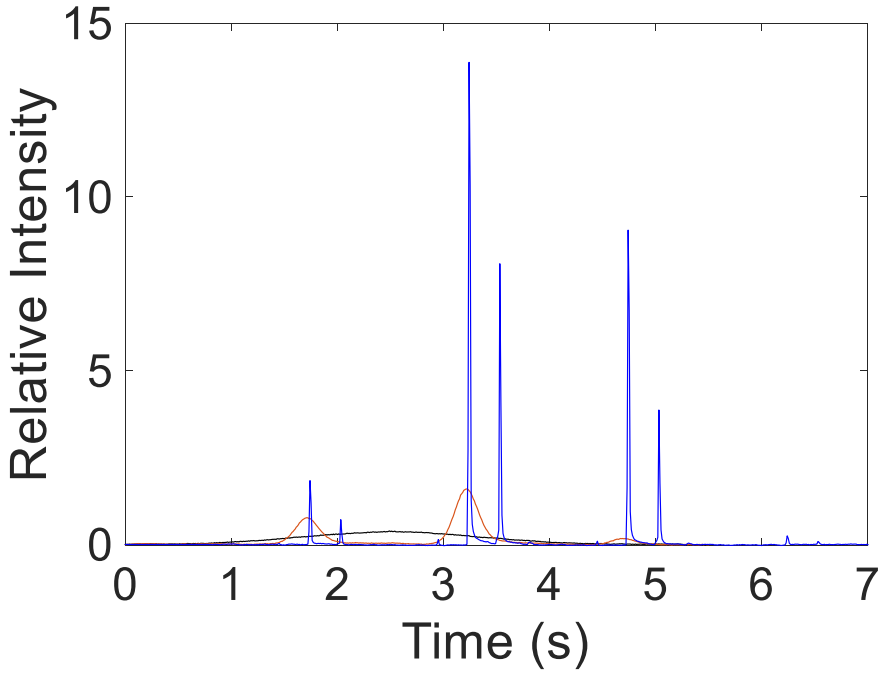

Figure 4.5. Overlay of 1D-GC (black trace), GC×GC (red trace), and GC^3 (blue trace) data for dodecene from Figure 4.4, corrected for retention time shifting.

In addition to the improved detection *S/N*, ^{3}D data provides a plethora of novel ways to look at the three dimensions of GC separations. In its raw form, GC^3 data is very informative, but can be challenging to interpret without training and experience. Hence, the raw data are cut-and-folded based on the number of modulated dimensions, i.e., at the modulation intervals going from ^{1}D to ^{2}D, and then ^{2}D to ^{3}D. Just as GC×GC data can be cut-and-folded at the P_M intervals to yield a 2D graph (surface plot), GC^3 data can be cut-and-folded twice, at both sets of P_M intervals, to yield a 3D graph (isosurface plot). When the isosurface plot is uncrowded (as in Figure 4.6),

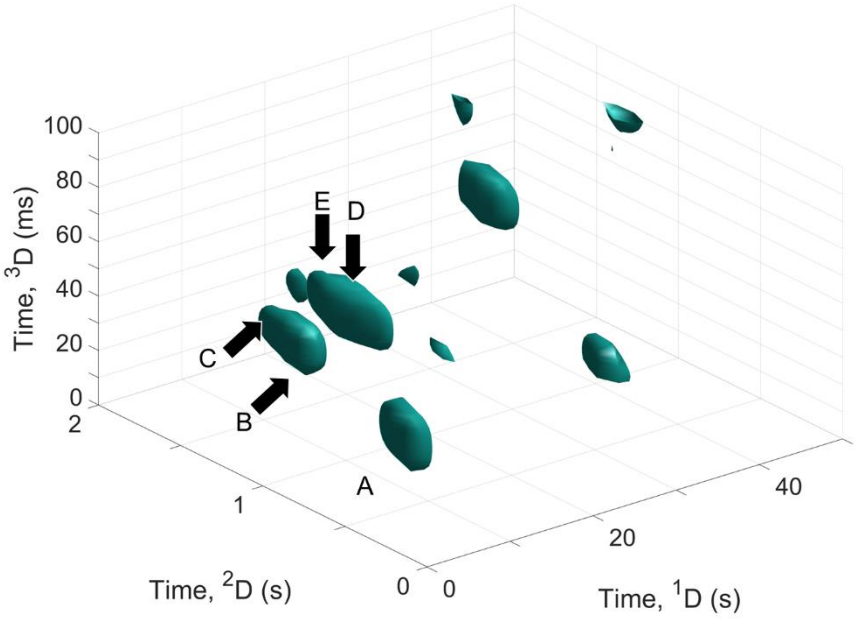

Figure 4.6. A zoom-in of the same GC^3-TOFMS separation as conducted in Figure 4.4, but at a different time point. This experiment utilized a 90-analyte mixture. Shown is a 40 s segment of time (from 490-530 s) along the ^{1}D separation in which several analytes elute at various ^1t_r, ^2t_r, and ^3t_r. Labeled in the figure are (a) cyclohexane, (b) benzene, (c) carbon tetrachloride, (d) 2,2,4-trimethyl pentane, and (e) 2-pentanone.

this plot is straightforward to visualize, and one can imagine to internally rotate and adjust the 3D image about the three separation dimensions. However, even in this uncrowded 3D chromatogram, there are multiple peak overlaps. For example, within the first 20 s of this isosurface plot are what appears to be three main analyte peaks ("blobs"). These three main blobs are actually 5 analytes: A) cyclohexane B) benzene C) carbon tetrachloride D) 2,2,4-trimethyl pentane and E) 2-pentanone. The inability to rotate the image in 3D makes it overly challenging to distinguish these analytes from each other and they appear to be just larger analyte signals. Also, without the ability to manipulate and rotate the 3D image, the viewer cannot determine if

the rest of the small analyte blobs are analytes that wrapped around either the ^{1}D, ^{2}D, or ^{3}D axes, or if they are errant noise in separation. This complication is further compounded when there are dozens to hundreds of analytes, and as this visualization approach becomes much more challenging, alternative visualization approaches can be taken.

Complicated data with many analyte peaks, beyond the data presented in Figure 4.6, can be broken down and visualized with fewer dimensions. As there are three separation dimensions in time, the GC^{3} data can be broken down by sequentially considering each modulation from the ^{1}D column to the ^{2}D column as a 2-s GC×GC separation. To refresh, each $^{1}P_{M}$ is the interval between when the first modulator, in this case a thermal modulator, actuates and "re-injects" analyte from the ^{1}D separation onto the ^{2}D column for separation. By the time the next modulation occurs, analytes will have essentially gone through a very quick GC×GC separation on the ^{2}D and ^{3}D columns. This approach simplifies the visualization process, so the analyst can literally "watch" analyte peaks with rapid GC×GC separations as the analytes emerge from the ^{1}D separation. Doing so, using the GC^{3} data in Figure 4.6 to illustrate the concept, four sequential modulations along ^{1}D at $^{1}P_{M}$ intervals produce a series of four GC×GC chromatograms (Figure 4.7). These four sequential modulations occur from 10-12 s (Figure 4.7A), 12-14 s (Figure 4.7B), 14-16 s (Figure 4.7C), and 16-18 s (Figure 4.7D) in relation to Figure 4.6.

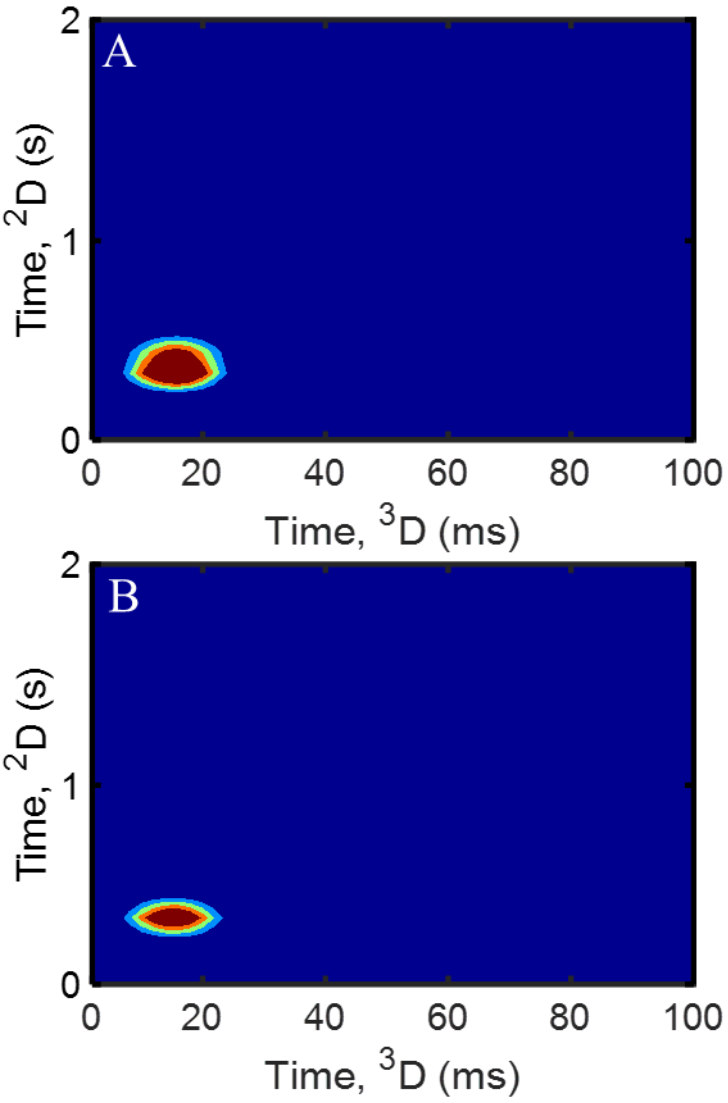
A
B
Time, ^{2}D (s)
Time, ^{3}D (ms)
0
1
2
0
20
40
60
80
100

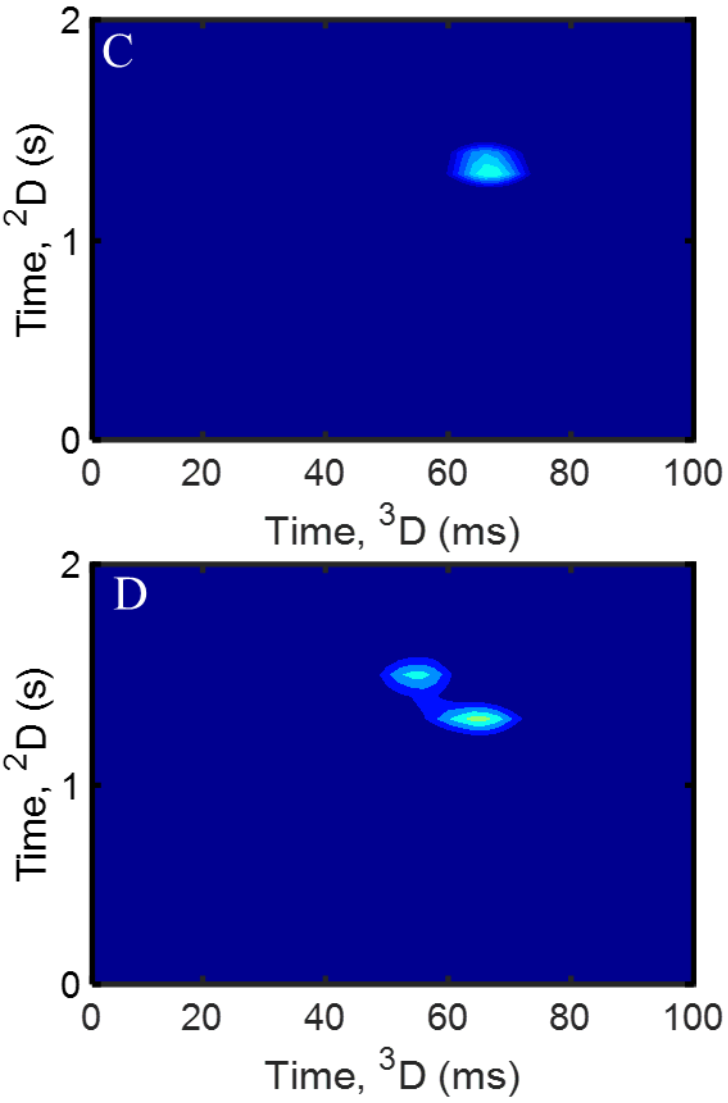

Figure 4.7. A series four sequential ^{1}D from Figure 4.6, going from A) 10-12 s, B) 12-14 s, C) 14-16 s, and D) 16-18 s. One can see how analytes elute from the ^{1}D column, with new analytes appearing in (C) and (D) relative to (A) and (B). Each of these modulations is defined by the specific ^{1}D time that the modulations took place to aid in identification of analytes and placement of these chromatograms in the overall GC^{3} separation.

In this manner, we observe an analyte that is initially of very strong signal intensity and decays away from the detector within 4 s (Figure 4.7A-B), and then a new analyte appears during the 3rd

modulation (Figure 4.7C). Then, that analyte continues to elute from the GC^3 separation into the TOFMS detector as a second eluting analyte begins to appear (Figure 4.7D). This is a relatively simple way to view GC^3 data, and is complementary for complex samples, than the more vigorous task of rotating a mental 3D image (data cube)

4.4 CONCLUSION

The GC^3-TOFMS appears to hold great promise to provide unique attributes and capabilities that may be unmatched by 1D-GC and GC×GC. This proof-of-principle study highlights the gains possible with the addition of a third dimension providing incredibly narrow ${}^3w_b$, on the order of 20 to 30 ms. The pulse valve modulator is able to serve as the second modulator, in the full modulation mode, greatly increasing the potential $n_{c,3D}$ and detection sensitivity. The potential for an $n_{c,3D}$ approaching 60,000 in a 40 min separation was demonstrated. Using the *DREF* as the quantitative metric, the gains in signal intensity between 1D-GC and GC^3 were in the range of 20 to 40. This high degree of signal enhancement is brought about by employing full modulation with 100% duty cycle in both modulation stages. Previous reports on GC^3 focused on only improving the $n_{c,3D}$ possible, with past efforts reaching an $n_{c,3D}$ of ~10,000 in 11 min[26] and ~30,000 in 40 min.[28] This current study is the first report of experimentally achieving this previously achieved high level of peak capacity, but now coupled with much higher signal enhancement, and bodes well for future improvements to concurrently narrowing peak widths in both the ${}^2D$ and ${}^3D$ separation dimensions. This study points toward decreasing the limits of detection and enhancing the identification and quantification for trace analysis of complex samples that are ideally suited for GC^3, along with the added chemical selectivity with the three separation dimensions as previously explored.[39,40] Additionally, by presenting the GC^3 data in a sequential order along the ${}^1D$ separation as a series of ${}^2D\times{}^3D$

separations provide a simple and effective means to analyze and visualize the complex data sets. The analyst can literally watch analyte peaks as they elute from the ^{1}D separation as a series of "mini" GC×GC runs. Moreover, each of these ^{2}D×^{3}D chromatograms had a peak capacity of 30 in a 1.5 s timeframe. However, it should be noted that this capability can only be realized with the selection of a proper modulator. Advent of the pulse valve modulator applied in the full modulation mode with a 100% duty cycle[34] has enabled a third dimension to be added to an optimized GC×GC instrument (using the commercial thermal modulator) enabling more significant studies into the capabilities and applications of GC^{3}.

4.5 REFERENCES

(1) Marriott, P. J. Gas Chromatography | Multidimensional Techniques. In *Encyclopedia of Analytical Science (Second Edition)*; Editors-in-Chief: Paul Worsfold, Alan Townshend, Colin Poole, Eds.; Elsevier: Oxford, **2005**; pp 39–47.

(2) Kulsing, C.; Nolvachai, Y.; Rawson, P.; Evans, D. J.; Marriott, P. J. Continuum in MDGC Technology: From Classical Multidimensional to Comprehensive Two-Dimensional Gas Chromatography. *Anal. Chem.* **2016**, *88* (7), 3529–3538. https://doi.org/10.1021/acs.analchem.5b03839.

(3) Luong, J.; Gras, R.; Yang, G.; Cortes, H.; Mustacich, R. Multidimensional Gas Chromatography with Capillary Flow Technology and LTM-GC. *J. Sep. Sci.* **2008**, *31* (19), 3385–3394. https://doi.org/10.1002/jssc.200800163.

(4) Seeley, J. V.; Seeley, S. K. Multidimensional Gas Chromatography: Fundamental Advances and New Applications. *Anal. Chem.* **2013**, *85* (2), 557–578. https://doi.org/10.1021/ac303195u.

(5) Seeley, J. V. Recent Advances in Flow-Controlled Multidimensional Gas Chromatography. *J. Chromatogr. A* **2012**, *1255*, 24–37. https://doi.org/10.1016/j.chroma.2012.01.027.

(6) Marriott, P. J.; Chin, S.-T.; Maikhunthod, B.; Schmarr, H.-G.; Bieri, S. Multidimensional Gas Chromatography. *TrAC, Trends Anal. Chem.* **2012**, *34*, 1–21. https://doi.org/10.1016/j.trac.2011.10.013.

(7) Prebihalo, S. E.; Berrier, K. L.; Freye, C. E.; Bahaghighat, H. D.; Moore, N. R.; Pinkerton, D. K.; Synovec, R. E. Multidimensional Gas Chromatography: Advances in Instrumentation, Chemometrics, and Applications. *Anal. Chem.* **2018**, *90* (1), 505–532. https://doi.org/10.1021/acs.analchem.7b04226.

(8) Griffith, J. F.; Winniford, W. L.; Sun, K.; Edam, R.; Luong, J. C. A Reversed-Flow Differential Flow Modulator for Comprehensive Two-Dimensional Gas Chromatography. *J. Chromatogr. A* **2012**, *1226*, 116–123. https://doi.org/10.1016/j.chroma.2011.11.036.

(9) de Geus, H.-J.; de Boer, J.; Brinkman, U. A. Th. Development of a Thermal Desorption Modulator for Gas Chromatography. *J. Chromatogr. A* **1997**, *767* (1), 137–151. https://doi.org/10.1016/S0021-9673(97)00038-1.
(10) Duhamel, C.; Cardinael, P.; Peulon-Agasse, V.; Firor, R.; Pascaud, L.; Semard-Jousset, G.; Giusti, P.; Livadaris, V. Comparison of Cryogenic and Differential Flow (Forward and Reverse Fill/Flush) Modulators and Applications to the Analysis of Heavy Petroleum Cuts by High-Temperature Comprehensive Gas Chromatography. *J. Chromatogr. A* **2015**, *1387*, 95–103. https://doi.org/10.1016/j.chroma.2015.01.095.
(11) Edwards, M.; Mostafa, A.; Górecki, T. Modulation in Comprehensive Two-Dimensional Gas Chromatography: 20 Years of Innovation. *Anal. Bioanal. Chem.* **2011**, *401* (8), 2335–2349. https://doi.org/10.1007/s00216-011-5100-6.
(12) Bahaghighat, H. D.; Freye, C. E.; Synovec, R. E. Recent Advances in Modulator Technology for Comprehensive Two Dimensional Gas Chromatography. *TrAC, Trends Anal. Chem.* **2019**, *113*, 379–391. https://doi.org/10.1016/j.trac.2018.04.016.
(13) Phillips, J. B.; Ledford, E. B. Thermal Modulation: A Chemical Instrumentation Component of Potential Value in Improving Portability. *Field Anal. Chem. Technol.* **1996**, *1* (1), 23–29. https://doi.org/10.1002/(SICI)1520-6521(1996)1:1<23::AID-FACT4>3.0.CO;2-F.
(14) Phillips, J. B.; Gaines, R. B.; Blomberg, J.; Wielen, F. W. M. van der; Dimandja, J.-M.; Green, V.; Granger, J.; Patterson, D.; Racovalis, L.; Geus, H.-J. de; et al. A Robust Thermal Modulator for Comprehensive Two-Dimensional Gas Chromatography. *J. High Resolut. Chromatogr.* **1999**, *22* (1), 3–10. https://doi.org/10.1002/(SICI)1521-4168(19990101)22:1<3::AID-JHRC3>3.0.CO;2-U.
(15) Cordero, C.; Rubiolo, P.; Reichenbach, S. E.; Carretta, A.; Cobelli, L.; Giardina, M.; Bicchi, C. Method Translation and Full Metadata Transfer from Thermal to Differential Flow Modulated Comprehensive Two Dimensional Gas Chromatography: Profiling of Suspected Fragrance Allergens. *J. Chromatogr. A* **2017**, *1480*, 70–82. https://doi.org/10.1016/j.chroma.2016.12.011.
(16) Harynuk, J.; Górecki, T. Comprehensive Two-Dimensional Gas Chromatography in Stop-Flow Mode. *J. Sep. Sci.* **2004**, *27* (5–6), 431–441. https://doi.org/10.1002/jssc.200301649.
(17) Seeley, J. V.; Kramp, F.; Hicks, C. J. Comprehensive Two-Dimensional Gas Chromatography via Differential Flow Modulation. *Anal. Chem.* **2000**, *72* (18), 4346–4352. https://doi.org/10.1021/ac000249z.
(18) Bueno, P. A.; Seeley, J. V. Flow-Switching Device for Comprehensive Two-Dimensional Gas Chromatography. *J. Chromatogr. A* **2004**, *1027* (1), 3–10. https://doi.org/10.1016/j.chroma.2003.10.033.
(19) Freye, C. E.; Mu, L.; Synovec, R. E. High Temperature Diaphragm Valve-Based Comprehensive Two-Dimensional Gas Chromatography. *J. Chromatogr. A* **2015**, *1424*, 127–133. https://doi.org/10.1016/j.chroma.2015.10.098.
(20) Fitz, B. D.; Wilson, R. B.; Parsons, B. A.; Hoggard, J. C.; Synovec, R. E. Fast, High Peak Capacity Separations in Comprehensive Two-Dimensional Gas Chromatography with Time-of-Flight Mass Spectrometry. *J. Chromatogr. A* **2012**, *1266*, 116–123. https://doi.org/10.1016/j.chroma.2012.09.096.

(21) Blumberg, L. M. Flow Optimization in One-Dimensional and Comprehensive Two-Dimensional Gas Chromatography. *J. Chromatogr. A* **2018**, *1536*, 27–38. https://doi.org/10.1016/j.chroma.2017.08.040.
(22) Klee, M. S.; Cochran, J.; Merrick, M.; Blumberg, L. M. Evaluation of Conditions of Comprehensive Two-Dimensional Gas Chromatography That Yield a near-Theoretical Maximum in Peak Capacity Gain. *J. Chromatogr. A* **2015**, *1383*, 151–159. https://doi.org/10.1016/j.chroma.2015.01.031.
(23) Freye, C. E.; Synovec, R. E. High Temperature Diaphragm Valve-Based Comprehensive Two-Dimensional Gas Chromatography with Time-of-Flight Mass Spectrometry. *Talanta* **2016**, *161*, 675–680. https://doi.org/10.1016/j.talanta.2016.09.002.
(24) Cai, H.; Stearns, S. D. Partial Modulation Method via Pulsed Flow Modulator for Comprehensive Two-Dimensional Gas Chromatography. *Anal. Chem.* **2004**, *76* (20), 6064–6076. https://doi.org/10.1021/ac0492463.
(25) Freye, C. E.; Bahaghighat, H. D.; Synovec, R. E. Comprehensive Two-Dimensional Gas Chromatography Using Partial Modulation via a Pulsed Flow Valve with a Short Modulation Period. *Talanta* **2018**, *177*, 142–149. https://doi.org/10.1016/j.talanta.2017.08.095.
(26) Bahaghighat, H. D.; Freye, C. E.; Gough, D. V.; Sudol, P. E.; Synovec, R. E. Ultrafast Separations via Pulse Flow Valve Modulation to Enable High Peak Capacity Multidimensional Gas Chromatography. *J. Chromatogr. A* **2018**, *1573*, 115–124. https://doi.org/10.1016/j.chroma.2018.08.001.
(27) Bahaghighat, H. D.; Freye, C. E.; Gough, D. V.; Synovec, R. E. Comprehensive Two-Dimensional Gas Chromatography and Time-of-Flight Mass Spectrometry Detection with a 50 Ms Modulation Period. *J. Chromatogr. A* **2019**, *1583*, 117–123. https://doi.org/10.1016/j.chroma.2018.11.027.
(28) Gough, D. V.; Bahaghighat, H. D.; Synovec, R. E. Column Selection Approach to Achieve a High Peak Capacity in Comprehensive Three-Dimensional Gas Chromatography. *Talanta* **2019**, *195*, 822–829. https://doi.org/10.1016/j.talanta.2018.12.007.
(29) Gough, D. V.; Song, D. H.; Schöneich, S.; Prebihalo, S. E.; Synovec, R. E. Development of Ultrafast Separations Using Negative Pulse Partial Modulation To Enable New Directions in Gas Chromatography. *Anal. Chem.* **2019**, *91* (11), 7328–7335. https://doi.org/10.1021/acs.analchem.9b01085.
(30) Khummueng, W.; Harynuk, J.; Marriott, P. J. Modulation Ratio in Comprehensive Two-Dimensional Gas Chromatography. *Anal. Chem.* **2006**, *78* (13), 4578–4587. https://doi.org/10.1021/ac052270b.
(31) Blumberg, L. M. Accumulating Resampling (Modulation) in Comprehensive Two-Dimensional Capillary GC (GC×GC). *J. Sep. Sci.* **2008**, *31* (19), 3358–3365. https://doi.org/10.1002/jssc.200800424.
(32) Pinkerton, D. K.; Parsons, B. A.; Synovec, R. E. Method to Determine the True Modulation Ratio for Comprehensive Two-Dimensional Gas Chromatography. *J. Chromatogr. A* **2016**, *1476*, 114–123. https://doi.org/10.1016/j.chroma.2016.11.015.
(33) Seeley, J. V.; Schimmel, N. E.; Seeley, S. K. The Multi-Mode Modulator: A Versatile Fluidic Device for Two-Dimensional Gas Chromatography. *J. Chromatogr. A* **2018**, *1536*, 6–15. https://doi.org/10.1016/j.chroma.2017.06.030.

(34) Trinklein, T. J.; Gough, D. V.; Warren, C. G.; Ochoa, G. S.; Synovec, R. E. Dynamic Pressure Gradient Modulation for Comprehensive Two-Dimensional Gas Chromatography. *J. Chromatogr. A* **2019**, 460488. https://doi.org/10.1016/j.chroma.2019.460488.
(35) Krupčík, J.; Májek, P.; Gorovenko, R.; Špánik, I.; Sandra, P.; Armstrong, D. W. On the Determination of a Detector Response Enhancement Factor for Flow Modulated Comprehensive Two-Dimensional Gas Chromatography. *J. Chromatogr. A* **2013**, *1286*, 235–240. https://doi.org/10.1016/j.chroma.2013.02.068.
(36) Davis, J. M. Statistical Theory of Spot Overlap for N-Dimensional Separations. *Anal. Chem.* **1993**, *65* (15), 2014–2023. https://doi.org/10.1021/ac00063a015.
(37) Davis, J. M.; Giddings, J. Calvin. Statistical Theory of Component Overlap in Multicomponent Chromatograms. *Anal. Chem.* **1983**, *55* (3), 418–424. https://doi.org/10.1021/ac00254a003.
(38) Davis, J. M.; Giddings, J. Calvin. Statistical Method for Estimation of Number of Components from Single Complex Chromatograms: Theory, Computer-Based Testing, and Analysis of Errors. *Anal. Chem.* **1985**, *57* (12), 2168–2177. https://doi.org/10.1021/ac00289a002.
(39) Watson, N. E.; Siegler, W. C.; Hoggard, J. C.; Synovec, R. E. Comprehensive Three-Dimensional Gas Chromatography with Parallel Factor Analysis. *Anal. Chem.* **2007**, *79* (21), 8270–8280. https://doi.org/10.1021/ac070829x.
(40) Siegler, W. C.; Crank, J. A.; Armstrong, D. W.; Synovec, R. E. Increasing Selectivity in Comprehensive Three-Dimensional Gas Chromatography via an Ionic Liquid Stationary Phase Column in One Dimension. *J. Chromatogr. A* **2010**, *1217* (18), 3144–3149. https://doi.org/10.1016/j.chroma.2010.02.082.

Chapter 5. Conclusion

5.1 SUMMARY OF PRESENTED WORK

Since the inception of multidimensional GC nearly 30 years ago, there have been great strides to improve the interface, i.e. the modulator, between successive GC columns. That is because modulators are the heart of GC×GC instruments. With this mindset, my work has primarily revolved around advancements to the modulator to improve the performance and applicability of GC instruments. I've worked to introduce new versatility to GC instrumentation and to enable more creative thinking in the application of the GC systems that have already been invested in as opposed to creating a completely brand new system from scratch that would require heavier investment to use.

Chapter 2 focused on the use of the pulse valve modulator in a new form of modulation, partial modulation in the negative pulse mode (NPM). Prior to these studies, my work focused on partial modulation in the positive pulse mode (PPM), which enabled incredibly high peak capacities (~30,000 in 40 min) due to the ability of the pulse valve modulator to produce very narrow peak w_b (as low as 7 ms wide). The NPM improved upon the PPM by reducing the data processing requirements and increasing the *S/N* by creating local concentrations of analytes, while maintaining narrow w_b (as low as 6 ms) and high peak capacities (~35,000 in 45 min), but with a time-of-flight mass spectrometer (TOFMS). Additionally, the pulse valve modulator was used as an injector. We applied the NPM to 1D-GC and continuous monitoring applications, with a steady-state stream of analytes entering the GC instrument and being repeatedly "re-injected" by the pulse valve modulator for fast, successive separations. This demonstrated utility and versatility of the

pulse valve modulator and the NPM bode well for the advancement of GC technologies for quicker analyses and for the novel application of GC instruments for other industrial and commercial uses.

Chapter 3 focused on ability to use commercial chemometric software for the decomposition, separation, identification, and quantification of analytes with TOFMS detection. The high-speed nature of the pulse valve modulator enables it to quickly and efficiently separate very similar analytes in complex mixtures. The actual separation power, and ease-of-use, of the raw data was studied with a mixture of 15 analytes (between pentane and 1-heptyne) in a short (20 sec) separation. This separation produced highly overlapped analytes on the ^{1}D and mass spectral dimensions. However, multivariate curve resolution-alternating least squares (MCR-ALS) analysis was able to decompose the low resolution between analytes (as low as ~0.05 $^{1}R_{s}$), separate and identify each analyte, and show the potential for accurate quantification. Despite the unusual visual representation of NPM data, this study highlighted its utility to potential industrial applications and confirmed that commercial chemometric techniques can utilize the raw data without additional pre-processing steps.

Chapter 4 looked at the application of the pulse valve modulator in the full modulation mode. We had just recently discovered a new application of the pulse valve modulator: the same instrumental setup can yield partial modulation in the PPM or NPM, or it can operate in the full modulation mode. In the full modulation mode, the entire analyte signal is modulated, which can be positively compounded in a GC^{3} instrument. Previous GC^{3} research with the pulse valve modulator used partial modulation techniques, which enabled unprecedented gains in peak capacity without meaningful gains in *S/N* or limits of detection (LOD), thus reducing their value. The pulse valve modulator in the full modulation mode produced comparably narrow peak w_{b} (~10 ms) with demonstrably higher *S/N* than previously possible. Using the detector response

enhancement factor (*DREF*) as a quantitative measurement, we showed a marked gain in *S/N* from a 1D-GC instrument to a GC^3 instrument. An increase between 21 and 40 times the *DREF* was shown between 1D-GC and GC^3, which is well above the theoretical (let alone actual experimental) gains possible in going from 1D-GC to GC×GC. Added utility of the GC^3 instrument was shown through a creative way to view the data. Viewing snippets of ^1D time as successive $^2D \times ^3D$ chromatograms, researchers can observe analytes as they elute at and pass beyond a detector in multiple dimensions. These advancements to the pulse valve modulator and multidimensional GC instrumentation show the potential improvements to the possible speed of separations that can be obtained as well as the continued lowering of detection limits for trace analyte detection in complex samples.

5.2 FUTURE DIRECTION

There are still several unique directions for future research into advancements in the GC field. The pulse valve modulator has been shown to be an incredibly versatile tool for multidimensional GC instruments, and it's potential to improve the field has only just been scratched. Many new proposals have already been started by current graduate students in the Synovec Group. One of the most exciting prospects for continued research is the application of the pulse valve modulator in 1D-GC as a high-speed injector for continuous monitoring applications. For example, reactive analytes can be added to a sample introduction device and the progress of the reaction can be monitored in real time by a detector. Additionally, one can envisage placing a commercial GC in line on an industrial process using modern flow chemistry to provide real time analytics during reagent mixing or product synthesis.

Much of the presented research focused on the high-speed nature of the pulse valve modulator and its capabilities for producing large peak capacity gains for longer (40 min +)

separations. Looking at this another way, a similar separation to what is currently possible is now able to be conducted in much less time. That is, the density of the data has been increased. Future work can expand upon this idea to reliably demonstrate how current methods in use for government regulation and industry quality control can be drastically shortened, increasing efficiency and lowering costs through time savings. Adding in the creative ways presented to view the complex 3D data, a multitude of new avenues open up for future research using techniques such as PLS, PCA, and F-ratio analyses to turn raw data into usable information, faster.

Appendix A

This Appendix is reproduced from the Supporting Information of D.V. Gough, D.H. Song, S. Schoneich, S.E. Prebihalo, R.E. Synovec, "Development of Ultrafast Separations Using Negative Pulse Partial Modulation to Enable New Directions in Gas Chromatography" *Analytical Chemistry* (2019), 91, 11, 7328-7335.

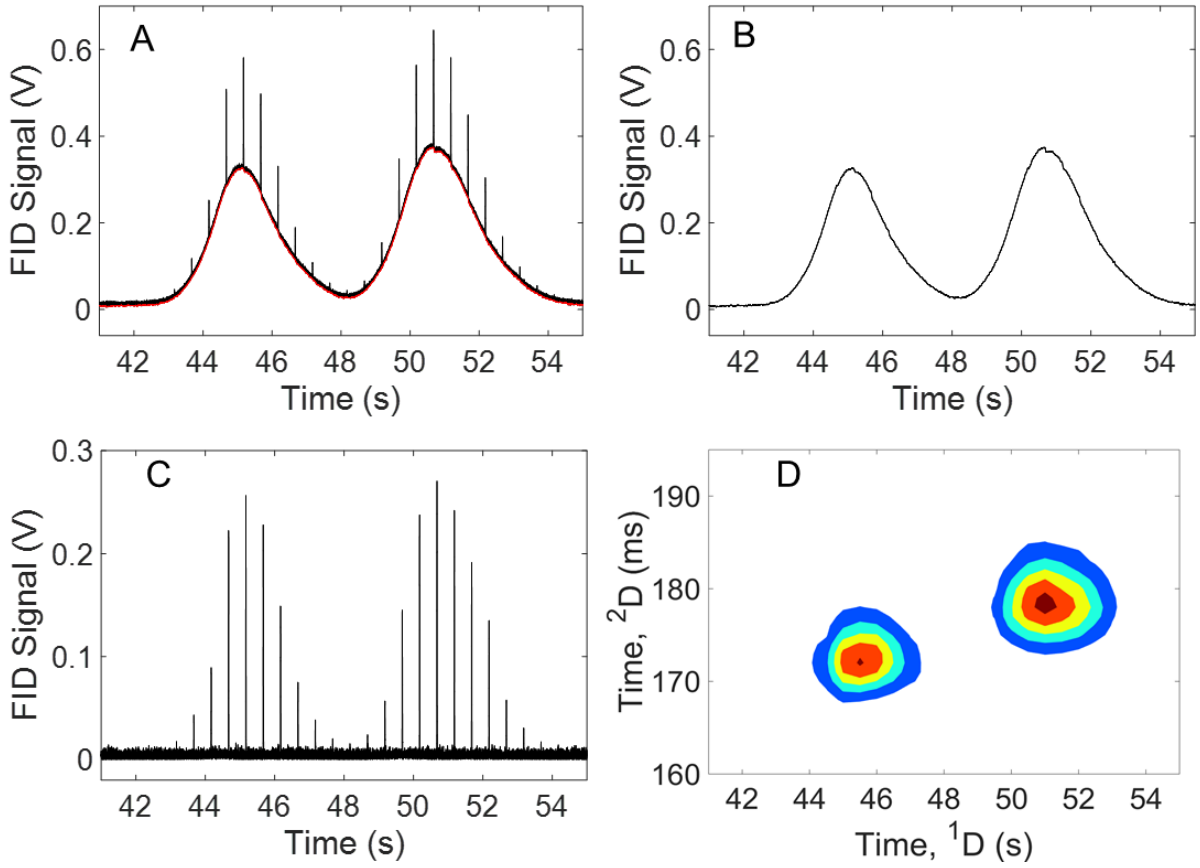

Figure A1. Example of separating the negative pulse mode raw data into its component ^{1}D and ^{2}D chromatographic peak profiles. A GC×GC instrument setup with a DB-5 ^{1}D column (3.0 m ×

180 µm d_c × 0.18 µm d_f) coupled to a DB-WAX ^{2}D column (1.0 m × 180 µm d_c × 0.18 µm d_f) was used to demonstrate this with hexane and heptane. Oven temperature was set to 80 ºC. The ^{1}D column flow was set to 3.0 mL/min, equating to 9.9 psig at the inlet and auxiliary flow was set to 18.6 psig with a p_w of 5 ms. (A) Raw data for hexane and heptane. The red line is the ^{1}D "baseline" that is subtracted, using a rolling-ball baseline correction algorithm. (B) The ^{1}D chromatogram is isolated using a baseline correction algorithm, equivalent to the red line in (A). (C) The resulting ^{2}D peaks that are obtained from the baseline subtraction. (D) The ^{2}D peaks from (C) are cut-and-folded into a traditional GC×GC contour plot chromatogram.

Table A1. (A) Table of the 8 analytes used in the 1D-GC study, shown in their order of elution. (B) Table of the 4 analytes used in the pulse width study. (C) The 20 analytes used in the first GC×GC study. (D) Table of the 90-component mixture, sorted by compound classes, for the GC^3-TOFMS proof-of-concept study. All analytes from S1A-C were obtained from Sigma-Aldrich. Vendors for specific analytes in S1D are provided.

(A) 8 mix	Boiling Point (°C)
Acetone	56
Heptane	98.4
Octane	125
Chloro-benzene	132
Nonane	151
Butyl-benzene	183
Decane	173-174
Benzyl Alcohol	203-205

(B) Pulse Width Study	Boiling Point (°C)
Acetone	56
Octane	125
Nonane	151
Propyl benzene	157-159

(C) 20 mix	Boiling Point (°C)
Acetone	56
Pentane	36.1
Heptane	98.4
Octane	125
1-Propanol	97
2-Butanol	98
Thiophene	84
Pentanol	138
Benzene	80.1
1-Hexene	62-63
1-Hexyne	69-71
1-Heptyne	98-99
Cyclohexene	83
Methyl Cyclopentane	71.8
Isopropyl alcohol	82.6
2-Butanone	79.6
2-Pentanone	101
Toluene	110-111
1,2-Dichloro-ethane	83
Pyridine	115

D) Alkanes	Boiling Point (°C)	Vendor
hexane	69	Sigma-Aldrich
heptane	98	Sigma-Aldrich
octane	126	Sigma-Aldrich
nonane	151	Sigma-Aldrich
decane	174	Sigma-Aldrich
undecane	196	Sigma-Aldrich
dodecane	216	Sigma-Aldrich
tridecane	235	Fluka
tetradecane	254	Fluka
pentadecane	271	Alfa-Aesar
hexadecane	287	Sigma-Aldrich
pristane	296	Sigma-Aldrich
octadecane	316	Fluka
eicosane	343	Sigma-Aldrich
Halogenated Alkanes	**BP (°C)**	**Vendor**
1,5-dichloropentane	179	Sigma-Aldrich
1-chlorohexane	135	Sigma-Aldrich
1-bromohexane	155	Sigma-Aldrich
1-bromoheptane	179	Sigma-Aldrich
1-bromooctane	200	Sigma-Aldrich
1-chlorobutane	78	Sigma-Aldrich
1,1,1-trichloroethane	74	Sigma-Aldrich
1,2-dichloroethane	84	Sigma-Aldrich
carbon tetrachloride	77	Sigma-Aldrich
Cyclics	**BP (°C)**	**Vendor**
methylcyclopentane	72	Fluka
cyclohexane	81	Sigma-Aldrich
cyclooctane	150	Sigma-Aldrich
butylcyclohexane	181	Sigma-Aldrich
bicyclohexyl	227	Sigma-Aldrich
2,2,4-trimethylpentane	99	Sigma-Aldrich
Alkenes	**BP (°C)**	**Vendor**
1-hexene	63	Sigma-Aldrich
cyclohexene	83	Sigma-Aldrich
dodecene	214	Sigma-Aldrich
1-undecene	194	Fluka
Alkynes	**BP (°C)**	**Vendor**
1-hexyne	71	Sigma-Aldrich
1-heptyne	109	Sigma-Aldrich
1-nonyne	151	Sigma-Aldrich
5-decyne	177	Sigma-Aldrich
Alcohols	**BP (°C)**	**Vendor**
1-propanol	97	Sigma-Aldrich
2-butanol	117	Sigma-Aldrich
1-pentanol	137	Sigma-Aldrich
2-pentanol	158	Sigma-Aldrich
hexyl alcohol	158	Sigma-Aldrich
2-heptanol	160	Fluka
1-octanol	194	Sigma-Aldrich
1-nonanol	215	Sigma-Aldrich
1-decanol	229	Sigma-Aldrich
1-tetradecanol	289	Sigma-Aldrich
1-octadecanol	210	Sigma-Aldrich
1-eicosanol	372	Sigma-Aldrich
benzyl alcohol	205	Sigma-Aldrich
2-ethyl-1-hexanol	185	Fluka

Esters	Boiling Point (°C)	Vendor
ethyl formate	54	Sigma-Aldrich
methyl decanoate	224	Eastman Chemicals
methyl caprylate	193	Sigma-Aldrich
methyl salicylate	223	Alfa-Aesar
ethyl salicylate	233	Alfa-Aesar
methyl laurate	262	Sigma-Aldrich
methly caproate	151	Sigma-Aldrich
diethyl phthalate	299	Sigma-Aldrich
Ketones	**BP (°C)**	**Vendor**
2-butanone	80	Sigma-Aldrich
2-pentanone	102	Sigma-Aldrich
3-hexanone	128	Sigma-Aldrich
2-hexanone	128	Sigma-Aldrich
2-heptanone	152	Sigma-Aldrich
3-heptanone	141	Sigma-Aldrich
3-octanone	167	Sigma-Aldrich
2-decanone	209	Sigma-Aldrich
2-undecanone	231	Sigma-Aldrich
2-dodecanone	245	Sigma-Aldrich
Aromatics	**BP (°C)**	**Vendor**
benzene	80	Fischer
toluene	111	Sigma-Aldrich
3-ethyltoluene	161	Sigma-Aldrich
4-ethyltoluene	162	Fluka
mesitylene	165	Sigma-Aldrich
ethylbenzene	136	Sigma-Aldrich
butylbenzene	183	Sigma-Aldrich
isobutylbenzene	170	Sigma-Aldrich
tert-butyl benzene	167	Sigma-Aldrich
propylbenzene	159	Sigma-Aldrich
1-ethylnapthelene	260	Sigma-Aldrich
bromobenzene	155	Sigma-Aldrich
cyclohexylbenzene	239	Sigma-Aldrich
diphenylmethane	265	Sigma-Aldrich
p-xylene	189	Sigma-Aldrich
o-xylene	145	Sigma-Aldrich
m-xylene	128	Sigma-Aldrich
1,2,4-trimethylbenzene	169	Sigma-Aldrich
anisole	154	Sigma-Aldrich
dibutyl phthalate	340	Sigma-Aldrich
a-terpineol (90%)	219	Sigma-Aldrich

Table A2. Full widths at half maximum (FWHM, $w_{1/2}$) were measured for the data collected from the pseudo-steady state analyte stream study (Figure 2.3), and then converted to w_b, with $w_b = 1.7 \times w_{1/2}$. The final analyte, benzyl alcohol, exited the column 164 ms after the first analyte, acetone. All analytes display baseline resolution within this sub-200 ms window. There is a dead time of 108 ms between injection and acetone exiting the column.

	Acetone	**Heptane**	**Octane**	**Chloro-benzene**	**Nonane**	**Butyl Benzene**	**Decane**	**Benzyl Alcohol**
$w_{1/2}$ (ms)	3.81	4.94	6.44	6.81	8.69	11.06	14.81	15.44
$w_{1/2}$ (ms) Standard Deviation	0.26	0.18	0.32	0.26	0.26	0.02	0.59	1.15
w_b (ms)	6.48	8.40	10.95	11.58	14.77	18.80	25.18	26.25
t_r (ms)	108.1	122.9	140.0	158.0	173.6	209.3	237.3	272.1
t_r (ms) Standard Deviation	0.4	0.4	0.0	0.0	0.5	0.7	0.7	0.6
Retention Factor (k')	0.00	0.14	0.29	0.46	0.61	0.94	1.19	1.52

Pulse Width Study

The relationship between the p_w applied and the detected peak width and signal height was studied in more detail, as previously highlighted (Figure 2.1D). Four test analytes were selected (Table A1B) for this purpose. Using the GC×GC mode (Figure 2.1B), each analyte was individually injected, keeping the flow ratio constant while tuning the p_w applied. For each analyte, 1 µL with a split of 300:1 was injected with a P_M of 200 ms, and the data was baseline corrected (Figure A1). The resulting ${}^2w_b$ were measured across 3 replicates and averaged (Table A3). When ${}^2w_b$ was plotted as a function of p_w, a consistent relationship was observed for the three most retained analytes (Figure A2A). Specifically, below a p_w of 8 ms the ${}^2w_b$ remains relatively constant (slope being generally flat), and above a p_w of 8 ms the ${}^2w_b$ increases approximately linearly. For lower p_w than those studied, a similar regime for the least retained analyte, acetone, may also be observed. This was not performed due to the inability to maintain consistent auxiliary pressures at a $p_w < 5$ ms. Meanwhile, the average signal intensity also increases with p_w (Figure A2B), linearly with p_w up to about 8 ms, then increases more slowly above 8 ms due to the concurrent increase in ${}^2w_b$. Accordingly, a p_w of 8-10 ms was selected as the "sweet spot" where the benefits of injecting more as p_w is increased due to the increasing signal intensity is offset by what may be deemed significant additional peak broadening due to the injection process. To create this plot (Figure A2B), the signal intensity for each analyte was normalized to its signal intensity at a p_w of 5 ms to account for within analyte variation. Then, the signal intensity of each analyte was averaged together, by p_w. The increasing size of error bars is due to each analyte increasing in intensity by varying amounts at increasing p_w. For example, at a p_w of 15 ms, the signal intensity for acetone increased only 3-fold while the signal intensity for nonane increased 6-fold.

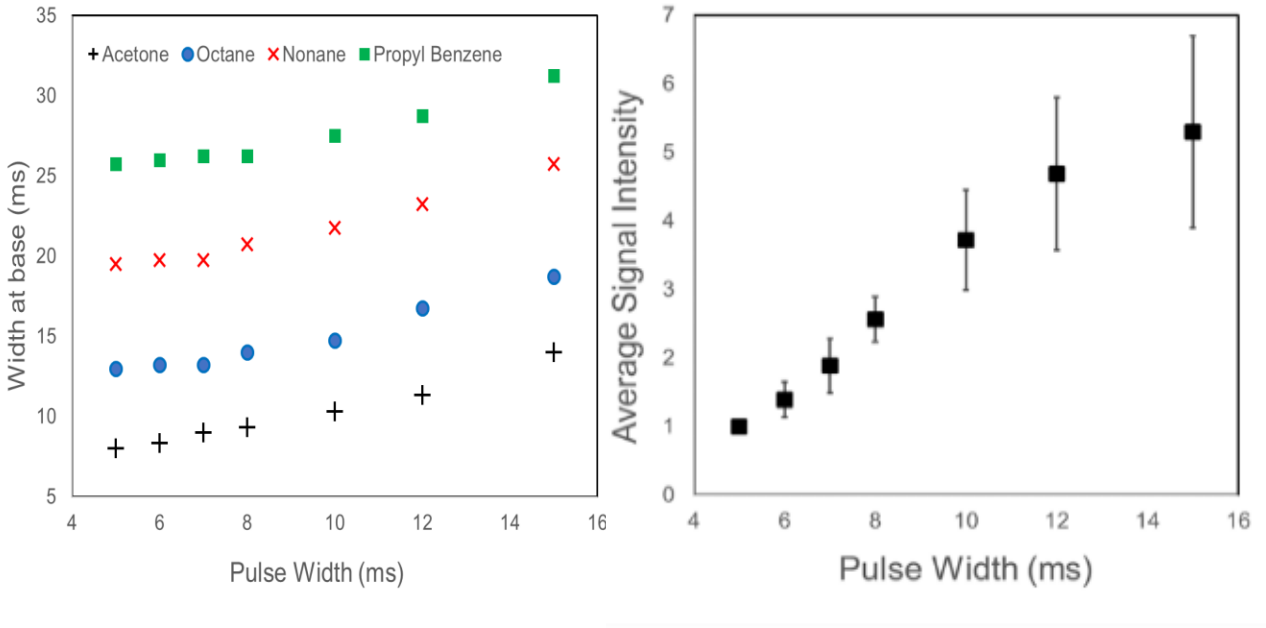

Figure A2. (A) Plot of the ^{2}D width-at-base, $^{2}w_{b,}$ as a function of injected pulse width, p_w, for four test analytes (Table A1B). Shown is the average of 3 replicates, error bars are smaller than each symbol. Octane, nonane, and propyl benzene are relatively constant in $^{2}w_b$ below a p_w of 8 ms and increase in $^{2}w_b$ above a p_w of 8 ms. The data was collected in GC×GC mode (Figure 2.2B). (B) Plot of the average signal intensity (peak height) for all analytes as a function of p_w. The signal intensity for each analyte was normalized to its own signal at p_w = 5 ms, and the four normalized signals were averaged together (standard deviation error bars). An 8-10 ms p_w was determined to be a suitable "sweet spot" for the conditions applied.

Table A3. The measured ^2w_b, in ms, as a function of p_w for all analytes presented (Figure A2). Each analyte was injected 3 times, with no less than 4 modulations per injection used for the calculations.

Pulse Width, p_w (ms)	**^2w_b (ms) Acetone**	**^2w_b (ms) Octane**	**^2w_b (ms) Nonane**	**^2w_b (ms) Propyl Benzene**
5	8.00	13.00	19.50	25.75
6	8.33	13.25	19.75	26.00
7	9.00	13.25	19.75	26.25
8	9.33	14.00	20.75	26.25
10	10.33	14.75	21.75	27.50
12	11.33	16.75	23.25	28.75
15	14.00	18.75	25.75	31.25

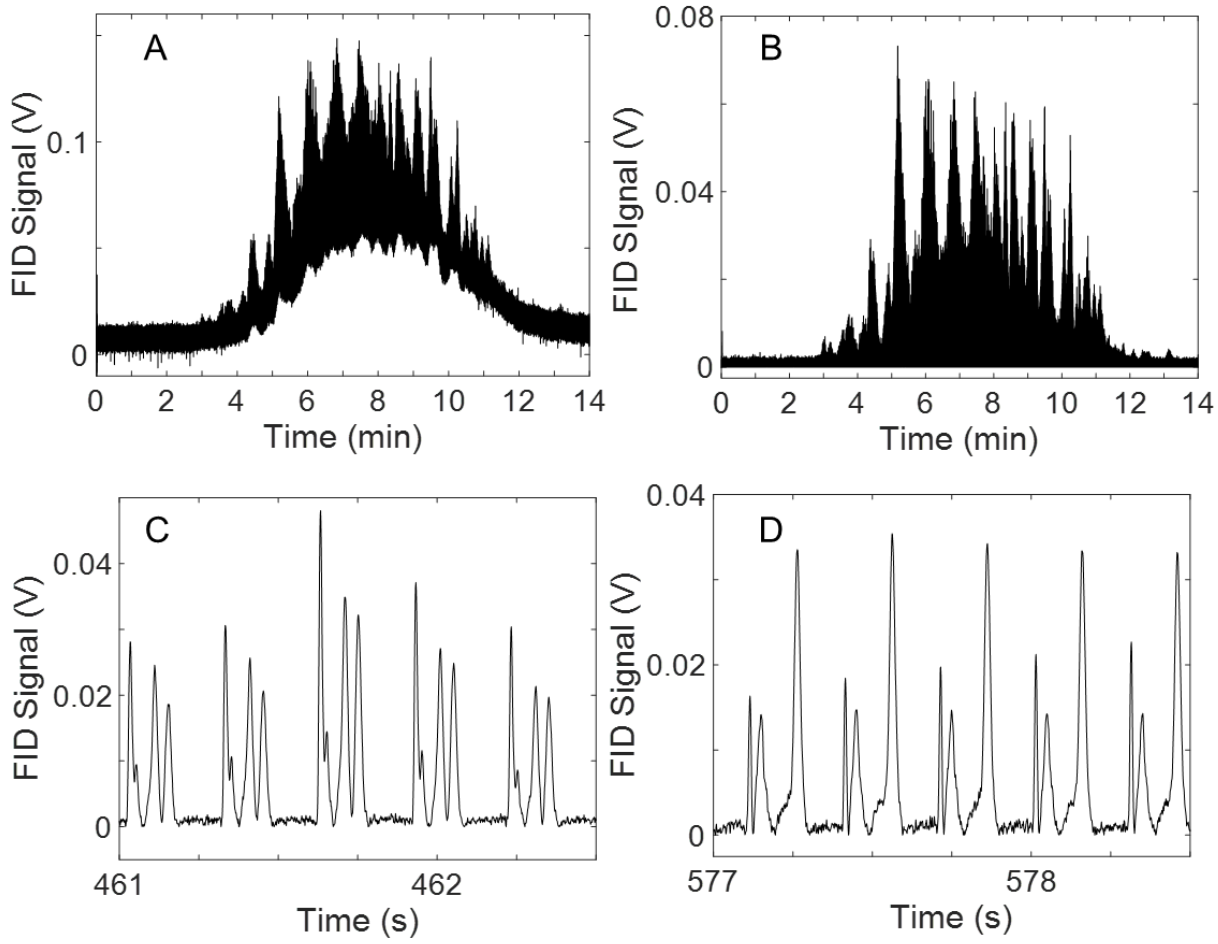

Figure A3. (A) Raw data collected on the diesel (Figure 5). (B) The data is baseline corrected to remove the ^{1}D profile as in Figure A1. (C) A 1.5 s region between 7-8 min is zoomed in to show the performance of the negative pulse method (5 modulations, with P_M = 300 ms. (D) A 1.5 s region between 9-10 min is zoomed in to show three distinct peaks.

Table A4. Chromatographic peak measurements and figures-of-merit for 10 analytes from the 90-component test mixture separated by the GC^3-TOFMS instrument. Analytes were chosen to span the majority of the retention time range on all three dimensions. A total ideal peak capacity, $n_{c,3D}$, of 35,100 was obtained for this separation. The average performance gain, ${}^2n_c \times {}^3n_c$, is 51 peaks per 2 s modulation, when compared to a traditional 1D-GC instrument.

	Ethylbenzene	1-nonyne	1-bromohexane	tert-butyl benzene	1,2,4-trimethyl benzene	5-decyne	1-bromoheptane	1-bromooctane	cyclohexylbenzene	pristane	**AVG**
${}^1t_R$ (s)	719	830	866	988	991	1071	1074	1272	1612	2139	--
${}^1W_b$ (s)	4.1	4	3.75	4.2	3.75	3.75	3.75	4	4.2	4.2	**3.97**
${}^1\rho_s$	2.05	2.00	1.88	2.10	1.88	1.88	1.88	2.00	2.10	2.10	**1.99**
${}^2t_R$ (s)	1.220	0.250	0.566	0.986	1.640	1.766	0.646	0.680	0.410	1.332	--
${}^2W_b$ (ms)	294	238	224	300	300	200	232	236	290	238	**255.20**
${}^2\rho_s$	2.94	2.38	2.24	3	3	2	2.32	2.36	2.9	2.38	**2.55**
${}^2n_c$	6.80	8.40	8.93	6.67	6.67	10.00	8.62	8.47	6.90	8.40	**7.99**
${}^3t_R$ (ms)	54	36	62	54	56	24	62	58	56	36	--
${}^3W_b$ (ms)	16	15	16	16	18	14	14	15	17	16	**15.70**
${}^3n_c$	6.25	6.67	6.25	6.25	5.56	7.14	7.14	6.67	5.88	6.25	**6.41**
${}^2n_c * {}^3n_c$	42.52	56.02	55.80	41.67	37.04	71.43	61.58	56.50	40.57	52.52	**51.56**

BIBLIOGRAPHY

Adahchour, M.; Beens, J.; Vreuls, R. J. J.; Brinkman, U. A. T. Recent Developments in Comprehensive Two-Dimensional Gas Chromatography (GC × GC). I. Introduction and Instrumental Set-Up. TrAC, Trends Anal. Chem. 2006, 25 (5), 438–454. https://doi.org/10.1016/j.trac.2006.03.002.

Amador-Muñoz, O.; Marriott, P. J. Quantification in Comprehensive Two-Dimensional Gas Chromatography and a Model of Quantification Based on Selected Summed Modulated Peaks. J. Chromatogr. A 2008, 1184 (1), 323–340. https://doi.org/10.1016/j.chroma.2007.10.041.

Amigo, J. M.; Skov, T.; Bro, R.; Coello, J.; Maspoch, S. Solving GC-MS Problems with PARAFAC2. TrAC, Trends Anal. Chem. 2008, 27 (8), 714–725. https://doi.org/10.1016/j.trac.2008.05.011.

Bahaghighat, H. D.; Freye, C. E.; Gough, D. V.; Sudol, P. E.; Synovec, R. E. Ultrafast Separations via Pulse Flow Valve Modulation to Enable High Peak Capacity Multidimensional Gas Chromatography. J. Chromatogr. A 2018, 1573, 115–124. https://doi.org/10.1016/j.chroma.2018.08.001.

Bahaghighat, H. D.; Freye, C. E.; Gough, D. V.; Synovec, R. E. Comprehensive Two-Dimensional Gas Chromatography and Time-of-Flight Mass Spectrometry Detection with a 50 ms Modulation Period. J. Chromatogr. A 2019, 1583, 117–123. https://doi.org/10.1016/j.chroma.2018.11.027.

Bahaghighat, H. D.; Freye, C. E.; Synovec, R. E. Recent Advances in Modulator Technology for Comprehensive Two Dimensional Gas Chromatography. TrAC Trends in Anal. Chem. 2019, 113, 379–391. https://doi.org/10.1016/j.trac.2018.04.016.

Blumberg, L. M. Accumulating Resampling (Modulation) in Comprehensive Two-Dimensional Capillary GC (GC×GC). J. Sep. Sci. 2008, 31 (19), 3358–3365. https://doi.org/10.1002/jssc.200800424.

Blumberg, L. M.; David, F.; Klee, M. S.; Sandra, P. Comparison of One-Dimensional and Comprehensive Two-Dimensional Separations by Gas Chromatography. J. Chromatogr. A 2008, 1188 (1), 2–16. https://doi.org/10.1016/j.chroma.2008.02.044.

Blumberg, L. M. Flow Optimization in One-Dimensional and Comprehensive Two-Dimensional Gas Chromatography. J. Chromatogr. A 2018, 1536, 27–38. https://doi.org/10.1016/j.chroma.2017.08.040.

Boeker, P.; Leppert, J. Flow Field Thermal Gradient Gas Chromatography. Anal. Chem. 2015, 87 (17), 9033–9041. https://doi.org/10.1021/acs.analchem.5b02227.

Bro, R. PARAFAC. Tutorial and Applications. Chemom. Intell. Lab. Syst. 1997, 38 (2), 149–171. https://doi.org/10.1016/S0169-7439(97)00032-4.

Bueno, P. A.; Seeley, J. V. Flow-Switching Device for Comprehensive Two-Dimensional Gas Chromatography. J. Chromatogr. A 2004, 1027 (1), 3–10. https://doi.org/10.1016/j.chroma.2003.10.033.

Carabajal, M. D.; Arancibia, J. A.; Escandar, G. M. Multivariate Curve Resolution Strategy for Non-Quadrilinear Type 4 Third-Order/Four Way Liquid Chromatography–Excitation-Emission Fluorescence Matrix Data. Talanta 2018, 189, 509–516. https://doi.org/10.1016/j.talanta.2018.07.017.

Cai, H.; Stearns, S. D. Partial Modulation Method via Pulsed Flow Modulator for Comprehensive Two-Dimensional Gas Chromatography. Anal. Chem. 2004, 76 (20), 6064–6076. https://doi.org/10.1021/ac0492463.

Cordero, C.; Rubiolo, P.; Cobelli, L.; Stani, G.; Miliazza, A.; Giardina, M.; Firor, R.; Bicchi, C. Potential of the Reversed-Inject Differential Flow Modulator for Comprehensive Two-Dimensional Gas Chromatography in the Quantitative Profiling and Fingerprinting of Essential Oils of Different Complexity. J. Chromatogr. A 2015, 1417, 79–95. https://doi.org/10.1016/j.chroma.2015.09.027.

Cordero, C.; Rubiolo, P.; Reichenbach, S. E.; Carretta, A.; Cobelli, L.; Giardina, M.; Bicchi, C. Method Translation and Full Metadata Transfer from Thermal to Differential Flow Modulated Comprehensive Two Dimensional Gas Chromatography: Profiling of Suspected Fragrance Allergens. J. Chromatogr. A 2017, 1480, 70–82. https://doi.org/10.1016/j.chroma.2016.12.011.

Davis, J. M.; Giddings, J. Calvin. Statistical Theory of Component Overlap in Multicomponent Chromatograms. Anal. Chem. 1983, 55 (3), 418–424. https://doi.org/10.1021/ac00254a003.

Davis, J. M.; Giddings, J. C. Statistical Method for Estimation of Number of Components from Single Complex Chromatograms: Theory, Computer-Based Testing, and Analysis of Errors. Anal. Chem. 1985, 57 (12), 2168–2177. https://doi.org/10.1021/ac00289a002.

Davis, J. M. Statistical Theory of Spot Overlap for N-Dimensional Separations. Anal. Chem. 1993, 65 (15), 2014–2023. https://doi.org/10.1021/ac00063a015.

van Deursen, M. M.; Beens, J.; Janssen, H.-G.; Leclercq, P. A.; Cramers, C. A. Evaluation of Time-of-Flight Mass Spectrometric Detection for Fast Gas Chromatography. J. Chromatogr. A 2000, 878 (2), 205–213. https://doi.org/10.1016/S0021-9673(00)00300-9.

Dimitriou-Christidis, P.; Bonvin, A.; Samanipour, S.; Hollender, J.; Rutler, R.; Westphale, J.; Gros, J.; Arey, J. S. GC×GC Quantification of Priority and Emerging Nonpolar Halogenated Micropollutants in All Types of Wastewater Matrices: Analysis Methodology, Chemical

Occurrence, and Partitioning. Enviro. Sci. Technol. 2015, 49 (13), 7914–7925. https://doi.org/10.1021/es5049122.

Dong, H.; Zhang, F. J.; Wang, F. Y.; Wang, Y. Y.; Guo, J.; Kanhar, G. M.; Chen, J.; Liu, J.; Zhou, C.; Yan, M.; et al. Simultaneous On-Line Monitoring of Propofol and Sevoflurane in Balanced Anesthesia by Direct Resistive Heating Gas Chromatography. J. Chromatogr. A 2017, 1506, 93–100. https://doi.org/10.1016/j.chroma.2017.05.001.

Duhamel, C.; Cardinael, P.; Peulon-Agasse, V.; Firor, R.; Pascaud, L.; Semard-Jousset, G.; Giusti, P.; Livadaris, V. Comparison of Cryogenic and Differential Flow (Forward and Reverse Fill/Flush) Modulators and Applications to the Analysis of Heavy Petroleum Cuts by High-Temperature Comprehensive Gas Chromatography. J. Chromatogr. A 2015, 1387, 95–103. https://doi.org/10.1016/j.chroma.2015.01.095.

Edwards, M.; Mostafa, A.; Górecki, T. Modulation in Comprehensive Two-Dimensional Gas Chromatography: 20 Years of Innovation. Anal. Bioanal. Chem. 2011, 401 (8), 2335–2349. https://doi.org/10.1007/s00216-011-5100-6.

Edwards, M.; Boswell, H.; Górecki, T. Comprehensive Multidimensional Chromatography. Curr. Chromatogr. 2015, 2, 80–109. https://doi.org/10.2174/2213240602666150722232236.

Ettre, L. S. Development of Chromatography. Anal. Chem. 1971, 43 (14), 20A – 31a. https://doi.org/10.1021/ac60308a022.

Ettre, L. S. The Development of Gas Chromatography. J. Chromatogr. A 1975, 112, 1–26. https://doi.org/10.1016/S0021-9673(00)99939-4.

Ettre, L. S. Chromatography: The Separation Technique of the 20th Century. Chromatographia 2000, 51 (1), 7. https://doi.org/10.1007/BF02490689.

Fitz, B. D.; Wilson, R. B.; Parsons, B. A.; Hoggard, J. C.; Synovec, R. E. Fast, High Peak Capacity Separations in Comprehensive Two-Dimensional Gas Chromatography with Time-of-Flight Mass Spectrometry. J. Chromatogr. A 2012, 1266, 116–123. https://doi.org/10.1016/j.chroma.2012.09.096.

Fitz, B. D.; Mannion, B. C.; To, K.; Hoac, T.; Synovec, R. E. Evaluation of Injection Methods for Fast, High Peak Capacity Separations with Low Thermal Mass Gas Chromatography. J. Chromatogr. A 2015, 1392, 82–90. https://doi.org/10.1016/j.chroma.2015.03.009.

Focant, J.-F.; Sjödin, A.; Patterson Jr., D. G. Qualitative Evaluation of Thermal Desorption-Programmable Temperature Vaporization-Comprehensive Two-Dimensional Gas Chromatography–Time-of-Flight Mass Spectrometry for the Analysis of Selected Halogenated Contaminants. J. Chromatogr. A 2003, 1019 (1–2), 143–156. https://doi.org/10.1016/j.chroma.2003.07.007.

Freye, C. E.; Mu, L.; Synovec, R. E. High Temperature Diaphragm Valve-Based Comprehensive Two-Dimensional Gas Chromatography. J. Chromatogr. A 2015, 1424, 127–133. https://doi.org/10.1016/j.chroma.2015.10.098.

Freye, C. E.; Synovec, R. E. High Temperature Diaphragm Valve-Based Comprehensive Two-Dimensional Gas Chromatography with Time-of-Flight Mass Spectrometry. Talanta 2016, 161, 675–680. https://doi.org/10.1016/j.talanta.2016.09.002.

Freye, C. E.; Bahaghighat, H. D.; Synovec, R. E. Comprehensive Two-Dimensional Gas Chromatography Using Partial Modulation via a Pulsed Flow Valve with a Short Modulation Period. Talanta 2018, 177, 142–149. https://doi.org/10.1016/j.talanta.2017.08.095.

de Geus, H.-J.; de Boer, J.; Brinkman, U. A. Th. Development of a Thermal Desorption Modulator for Gas Chromatography. J. Chromatogr. A 1997, 767 (1), 137–151. https://doi.org/10.1016/S0021-9673(97)00038-1.

Ghosh, A.; Johnson, J. E.; Nuss, J. G.; Stark, B. A.; Hawkins, A. R.; Tolley, L. T.; Iverson, B. D.; Tolley, H. D.; Lee, M. L. Extending the Upper Temperature Range of Gas Chromatography with All-Silicon Microchip Columns Using a Heater/Clamp Assembly. J. Chromatogr. A 2017, 1517, 134–141. https://doi.org/10.1016/j.chroma.2017.08.036.
Giddings, J. C. Unified Separation Science; Wiley: New York, 1991.

Ghosh, A.; Foster, A. R.; Johnson, J. C.; Vilorio, C. R.; Tolley, L. T.; Iverson, B. D.; Hawkins, A. R.; Tolley, H. D.; Lee, M. L. Stainless-Steel Column for Robust, High-Temperature Microchip Gas Chromatography. Anal. Chem. 2019, 91 (1), 792–796. https://doi.org/10.1021/acs.analchem.8b04174.

de Godoy, L. A. F.; Hantao, L. W.; Pedroso, M. P.; Poppi, R. J.; Augusto, F. Quantitative Analysis of Essential Oils in Perfume Using Multivariate Curve Resolution Combined with Comprehensive Two-Dimensional Gas Chromatography. Anal. Chim. Acta 2011, 699 (1), 120–125. https://doi.org/10.1016/j.aca.2011.05.003.

Golshan, A.; Abdollahi, H.; Beyramysoltan, S.; Maeder, M.; Neymeyr, K.; Rajkó, R.; Sawall, M.; Tauler, R. A Review of Recent Methods for the Determination of Ranges of Feasible Solutions Resulting from Soft Modelling Analyses of Multivariate Data. Anal. Chim. Acta 2016, 911, 1–13. https://doi.org/10.1016/j.aca.2016.01.011.

Gough, D. V.; Bahaghighat, H. D.; Synovec, R. E. Column Selection Approach to Achieve a High Peak Capacity in Comprehensive Three-Dimensional Gas Chromatography. Talanta 2019, 195, 822–829. https://doi.org/10.1016/j.talanta.2018.12.007.

Gough, D. V.; Song, D. H.; Schöneich, S.; Prebihalo, S. E.; Synovec, R. E. Development of Ultrafast Separations Using Negative Pulse Partial Modulation to Enable New Directions in Gas Chromatography. Anal. Chem. 2019, 91 (11), 7328–7335. https://doi.org/10.1021/acs.analchem.9b01085.

Griffith, J. F.; Winniford, W. L.; Sun, K.; Edam, R.; Luong, J. C. A Reversed-Flow Differential Flow Modulator for Comprehensive Two-Dimensional Gas Chromatography. J. Chromatogr. A 2012, 1226, 116–123. https://doi.org/10.1016/j.chroma.2011.11.036.

Gross, G. M.; Prazen, B. J.; Grate, J. W.; Synovec, R. E. High-Speed Gas Chromatography Using Synchronized Dual-Valve Injection. Anal. Chem. 2004, 76 (13), 3517–3524. https://doi.org/10.1021/ac049909g.

Harynuk, J.; Górecki, T. New Liquid Nitrogen Cryogenic Modulator for Comprehensive Two-Dimensional Gas Chromatography. J. Chromatogr. A 2003, 1019 (1–2), 53–63. https://doi.org/10.1016/j.chroma.2003.08.097.

Harynuk, J.; Górecki, T. Comprehensive Two-Dimensional Gas Chromatography in Stop-Flow Mode. J. Sep. Sci. 2004, 27 (5–6), 431–441. https://doi.org/10.1002/jssc.200301649.

Izadmanesh, Y.; Garreta-Lara, E.; Ghasemi, J. B.; Lacorte, S.; Matamoros, V.; Tauler, R. Chemometric Analysis of Comprehensive Two Dimensional Gas Chromatography–Mass Spectrometry Metabolomics Data. J. Chromatogr. A 2017, 1488, 113–125. https://doi.org/10.1016/j.chroma.2017.01.052.

Jacobs, M. R.; Hilder, E. F.; Shellie, R. A. Applications of Resistive Heating in Gas Chromatography: A Review. Anal. Chim. Acta 2013, 803, 2–14. https://doi.org/10.1016/j.aca.2013.04.063.

Jacobs, M. R.; Edwards, M.; Górecki, T.; Nesterenko, P. N.; Shellie, R. A. Evaluation of a Miniaturised Single-Stage Thermal Modulator for Comprehensive Two-Dimensional Gas Chromatography of Petroleum Contaminated Soils. J. Chromatogr. A 2016, 1463, 162–168. https://doi.org/10.1016/j.chroma.2016.08.009.

James, A. T.; Martin, A. J. P. Gas-Liquid Partition Chromatography: The Separation and Micro-Estimation of Volatile Fatty Acids from Formic Acid to Dodecanoic Acid. Biochem. J. 1952, 50 (5), 679–690.

Jaumot, J.; Tauler, R. MCR-BANDS: A User Friendly MATLAB Program for the Evaluation of Rotation Ambiguities in Multivariate Curve Resolution. Chemom. Intell. Lab. Syst. 2010, 103 (2), 96–107. https://doi.org/10.1016/j.chemolab.2010.05.020.

de Juan, A.; Tauler, R. Chemometrics Applied to Unravel Multicomponent Processes and Mixtures: Revisiting Latest Trends in Multivariate Resolution. Anal. Chim. Acta 2003, 500 (1–2), 195–210. https://doi.org/10.1016/S0003-2670(03)00724-4.

Khummueng, W.; Harynuk, J.; Marriott, P. J. Modulation Ratio in Comprehensive Two-Dimensional Gas Chromatography. Anal. Chem. 2006, 78 (13), 4578–4587. https://doi.org/10.1021/ac052270b.

Kiers, H. A. L.; ten Berge, J. M. F.; Bro, R. PARAFAC2 - Part I. A Direct Fitting Algorithm for the PARAFAC2 Model. J. Chemom. 1999, 13 (3–4), 275–294. https://doi.org/10.1002/(sici)1099-128x(199905/08)13:3/4<275::aid-cem543>3.3.co;2-2.

Klee, M. S.; Cochran, J.; Merrick, M.; Blumberg, L. M. Evaluation of Conditions of Comprehensive Two-Dimensional Gas Chromatography That Yield a near-Theoretical Maximum in Peak Capacity Gain. J. Chromatogr. A 2015, 1383, 151–159. https://doi.org/10.1016/j.chroma.2015.01.031.

Klemp, M. A.; Akard, M. L.; Sacks, R. D. Cryofocusing Inlet with Reverse Flow Sample Collection for Gas Chromatography. Anal. Chem. 1993, 65 (18), 2516–2521. https://doi.org/10.1021/ac00066a020.

Krupčík, J.; Gorovenko, R.; Špánik, I.; Sandra, P.; Armstrong, D. W. Flow-Modulated Comprehensive Two-Dimensional Gas Chromatography with Simultaneous Flame Ionization and Quadrupole Mass Spectrometric Detection. J. Chromatogr. A 2013, 1280, 104–111. https://doi.org/10.1016/j.chroma.2013.01.015.

Krupčík, J.; Májek, P.; Gorovenko, R.; Špánik, I.; Sandra, P.; Armstrong, D. W. On the Determination of a Detector Response Enhancement Factor for Flow Modulated Comprehensive Two-Dimensional Gas Chromatography. *J. Chromatogr. A* 2013, *1286*, 235–240. https://doi.org/10.1016/j.chroma.2013.02.068.

Kulsing, C.; Nolvachai, Y.; Rawson, P.; Evans, D. J.; Marriott, P. J. Continuum in MDGC Technology: From Classical Multidimensional to Comprehensive Two-Dimensional Gas Chromatography. Anal. Chem. 2016, 88 (7), 3529–3538. https://doi.org/10.1021/acs.analchem.5b03839.

Lidster, R. T.; Hamilton, J. F.; Lewis, A. C. The Application of Two Total Transfer Valve Modulators for Comprehensive Two-Dimensional Gas Chromatography of Volatile Organic Compounds. J. Sep. Sci. 2011, 34 (7), 812–821. https://doi.org/10.1002/jssc.201000710.

Liu, Z.; Phillips, J. B. Comprehensive Two-Dimensional Gas Chromatography Using an On-Column Thermal Modulator Interface. J. Chromatogr. Sci. 1991, 29 (6), 227–231. https://doi.org/10.1093/chromsci/29.6.227.

Luong, J.; Gras, R.; Yang, G.; Cortes, H.; Mustacich, R. Multidimensional Gas Chromatography with Capillary Flow Technology and LTM-GC. J. Sep. Sci. 2008, 31 (19), 3385–3394. https://doi.org/10.1002/jssc.200800163.

Luong, J.; Gras, R.; Hawryluk, M.; Shellie, R. A.; Cortes, H. J. Multidimensional Gas Chromatography Using Microfluidic Switching and Low Thermal Mass Gas Chromatography for the Characterization of Targeted Volatile Organic Compounds. J. Chromatogr. A 2013, 1288, 105–110. https://doi.org/10.1016/j.chroma.2013.02.084.

Marriott, P. J. Gas Chromatography | Multidimensional Techniques. In Encyclopedia of Analytical Science (Second Edition); Editors-in-Chief: Paul Worsfold, Alan Townshend, Colin Poole, Eds.; Elsevier: Oxford, 2005; pp 39–47.

Marriott, P. J.; Chin, S.-T.; Maikhunthod, B.; Schmarr, H.-G.; Bieri, S. Multidimensional Gas Chromatography. TrAC, Trends Anal. Chem. 2012, 34, 1–21. https://doi.org/10.1016/j.trac.2011.10.013.

Megson, D.; Kalin, R.; Worsfold, P. J.; Gauchotte-Lindsay, C.; Patterson, D. G.; Lohan, M. C.; Comber, S.; Brown, T. A.; O'Sullivan, G. Fingerprinting Polychlorinated Biphenyls in Environmental Samples Using Comprehensive Two-Dimensional Gas Chromatography with Time-of-Flight Mass Spectrometry. J. Chromatogr. A 2013, 1318, 276–283. https://doi.org/10.1016/j.chroma.2013.10.016.

Mogollon, N. G. S.; Ribeiro, F. A. de L.; Lopez, M. M.; Hantao, L. W.; Poppi, R. J.; Augusto, F. Quantitative Analysis of Biodiesel in Blends of Biodiesel and Conventional Diesel by Comprehensive Two-Dimensional Gas Chromatography and Multivariate Curve Resolution. Anal. Chim. Acta 2013, 796, 130–136. https://doi.org/10.1016/j.aca.2013.07.071.

Mohler, R. E.; Prazen, B. J.; Synovec, R. E. Total-Transfer, Valve-Based Comprehensive Two-Dimensional Gas Chromatography. Anal. Chim. Acta 2006, 555 (1), 68–74. https://doi.org/10.1016/j.aca.2005.08.072.

Mucédola, V.; Vieira, L. C. S.; Pierone, D.; Gobbi, A. L.; Poppi, R. J.; Hantao, L. W. Thermal Desorption Modulation for Comprehensive Two-Dimensional Gas Chromatography Using a Simple and Inexpensive Segmented-Loop Fluidic Interface. Talanta 2017, 164, 470–476. https://doi.org/10.1016/j.talanta.2016.12.005.

Murphy, R. E.; Schure, M. R.; Foley, J. P. Effect of Sampling Rate on Resolution in Comprehensive Two-Dimensional Liquid Chromatography. Anal. Chem. 1998, 70 (8), 1585–1594. https://doi.org/10.1021/ac971184b.

Murray, J. A. Qualitative and Quantitative Approaches in Comprehensive Two-Dimensional Gas Chromatography. J. Chromatogr. A 2012, 1261, 58–68. https://doi.org/10.1016/j.chroma.2012.05.012.

Muscalu, A. M.; Edwards, M.; Górecki, T.; Reiner, E. J. Evaluation of a Single-Stage Consumable-Free Modulator for Comprehensive Two-Dimensional Gas Chromatography: Analysis of Polychlorinated Biphenyls, Organochlorine Pesticides and Chlorobenzenes. J. Chromatogr. A 2015, 1391, 93–101. https://doi.org/10.1016/j.chroma.2015.02.074.

Omar, J.; Olivares, M.; Amigo, J. M.; Etxebarria, N. Resolution of Co-Eluting Compounds of Cannabis Sativa in Comprehensive Two-Dimensional Gas Chromatography/Mass Spectrometry Detection with Multivariate Curve Resolution-Alternating Least Squares. Talanta 2014, 121, 273–280. https://doi.org/10.1016/j.talanta.2013.12.044.

Omar, J.; Vallejo, A.; Olivares, M.; Usobiaga, A.; Zuloaga, O.; Etxebarria, N. Resolution and Identification of Co-Eluting Alkylphenols in Comprehensive Two-Dimensional Gas Chromatography-Mass Spectrometry by Multivariate Curve Resolution-Alternating Least Squares. J. Chemom. 2015, 29 (4), 237–244. https://doi.org/10.1002/cem.2701.

Parastar, H.; Tauler, R. Multivariate Curve Resolution of Hyphenated and Multidimensional Chromatographic Measurements: A New Insight to Address Current Chromatographic Challenges. Anal. Chem. 2014, 86 (1), 286–297. https://doi.org/10.1021/ac402377d.

Parsons, B. A.; Pinkerton, D. K.; Synovec, R. E. Implications of Phase Ratio for Maximizing Peak Capacity in Comprehensive Two-Dimensional Gas Chromatography Time-of-Flight Mass Spectrometry. J. Chromatogr. A 2018, 1536, 16–26. https://doi.org/10.1016/j.chroma.2017.07.018.

Phillips, J. B.; Ledford, E. B. Thermal Modulation: A Chemical Instrumentation Component of Potential Value in Improving Portability. Field Anal. Chem. Technol. 1996, 1 (1), 23–29. https://doi.org/10.1002/(SICI)1520-6521(1996)1:1<23::AID-FACT4>3.0.CO;2-F.

Phillips, J. B.; Gaines, R. B.; Blomberg, J.; Wielen, F. W. M. van der; Dimandja, J.-M.; Green, V.; Granger, J.; Patterson, D.; Racovalis, L.; Geus, H.-J. de; et al. A Robust Thermal Modulator for Comprehensive Two-Dimensional Gas Chromatography. J. High Resolut. Chromatogr. 1999, 22 (1), 3–10. https://doi.org/10.1002/(SICI)1521-4168(19990101)22:1<3::AID-JHRC3>3.0.CO;2-U.

Pierce, K. M.; Kehimkar, B.; Marney, L. C.; Hoggard, J. C.; Synovec, R. E. Review of Chemometric Analysis Techniques for Comprehensive Two Dimensional Separations Data. J. Chromatogr. A 2012, 1255, 3–11. https://doi.org/10.1016/j.chroma.2012.05.050.

Pinkerton, D. K.; Parsons, B. A.; Synovec, R. E. Method to Determine the True Modulation Ratio for Comprehensive Two-Dimensional Gas Chromatography. J. Chromatogr. A 2016, 1476, 114–123. https://doi.org/10.1016/j.chroma.2016.11.015.

Prebihalo, S. E.; Berrier, K. L.; Freye, C. E.; Bahaghighat, H. D.; Moore, N. R.; Pinkerton, D. K.; Synovec, R. E. Multidimensional Gas Chromatography: Advances in Instrumentation, Chemometrics, and Applications. Anal. Chem. 2018, 90 (1), 505–532. https://doi.org/10.1021/acs.analchem.7b04226.

Rajalahti, T.; Kvalheim, O. M. Multivariate Data Analysis in Pharmaceutics: A Tutorial Review. Internat. J. Pharm. 2011, 417 (1–2), 280–290. https://doi.org/10.1016/j.ijpharm.2011.02.019.

Reid, V. R.; McBrady, A. D.; Synovec, R. E. Investigation of High-Speed Gas Chromatography Using Synchronized Dual-Valve Injection and Resistively Heated Temperature Programming. J. Chromatogr. A 2007, 1148 (2), 236–243. https://doi.org/10.1016/j.chroma.2007.03.029.

Seeley, J. V.; Kramp, F.; Hicks, C. J. Comprehensive Two-Dimensional Gas Chromatography via Differential Flow Modulation. Anal. Chem. 2000, 72 (18), 4346–4352. https://doi.org/10.1021/ac000249z.

Seeley, J. V.; Micyus, N. J.; Bandurski, S. V.; Seeley, S. K.; McCurry, J. D. Microfluidic Deans Switch for Comprehensive Two-Dimensional Gas Chromatography. Anal. Chem. 2007, 79 (5), 1840–1847. https://doi.org/10.1021/ac061881g.

Seeley, J. V. Recent Advances in Flow-Controlled Multidimensional Gas Chromatography. J. Chromatogr. A 2012, 1255, 24–37. https://doi.org/10.1016/j.chroma.2012.01.027.

Seeley, J. V.; Seeley, S. K. Multidimensional Gas Chromatography: Fundamental Advances and New Applications. Anal. Chem. 2013, 85 (2), 557–578. https://doi.org/10.1021/ac303195u.

Seeley, J. V.; Schimmel, N. E.; Seeley, S. K. The Multi-Mode Modulator: A Versatile Fluidic Device for Two-Dimensional Gas Chromatography. J. Chromatogr. A 2018, 1536, 6–15. https://doi.org/10.1016/j.chroma.2017.06.030.

Semard, G.; Gouin, C.; Bourdet, J.; Bord, N.; Livadaris, V. Comparative Study of Differential Flow and Cryogenic Modulators Comprehensive Two-Dimensional Gas Chromatography Systems for the Detailed Analysis of Light Cycle Oil. J. Chromatogr. A 2011, 1218 (21), 3146–3152. https://doi.org/10.1016/j.chroma.2010.08.082.

Siegler, W. C.; Crank, J. A.; Armstrong, D. W.; Synovec, R. E. Increasing Selectivity in Comprehensive Three-Dimensional Gas Chromatography via an Ionic Liquid Stationary Phase Column in One Dimension. J. Chromatogr. A 2010, 1217 (18), 3144–3149. https://doi.org/10.1016/j.chroma.2010.02.082.

Siegler, W. C.; Fitz, B. D.; Hoggard, J. C.; Synovec, R. E. Experimental Study of the Quantitative Precision for Valve-Based Comprehensive Two-Dimensional Gas Chromatography. Anal. Chem. 2011, 83 (13), 5190–5196. https://doi.org/10.1021/ac200302b.

Sinha, A. E.; Prazen, B. J.; Fraga, C. G.; Synovec, R. E. Valve-Based Comprehensive Two-Dimensional Gas Chromatography with Time-of-Flight Mass Spectrometric Detection: Instrumentation and Figures-of-Merit. J. Chromatogr. A 2003, 1019 (1–2), 79–87. https://doi.org/10.1016/j.chroma.2003.08.047.

Sinha, A. E.; Hope, J. L.; Prazen, B. J.; Fraga, C. G.; Nilsson, E. J.; Synovec, R. E. Multivariate Selectivity as a Metric for Evaluating Comprehensive Two-Dimensional Gas Chromatography-Time-of-Flight Mass Spectrometry Subjected to Chemometric Peak Deconvolution. J. Chromatogr. A 2004, 1056 (1-2 SPEC.ISS.), 145–154. https://doi.org/10.1016/j.chroma.2004.06.110.

Sinha, A. E.; Fraga, C. G.; Prazen, B. J.; Synovec, R. E. Trilinear Chemometric Analysis of Two-Dimensional Comprehensive Gas Chromatography-Time-of-Flight Mass Spectrometry Data. J. Chromatogr. A 2004, 1027 (1–2), 269–277. https://doi.org/10.1016/j.chroma.2003.08.081.

Stein, S. E.; Scott, D. R. Optimization and Testing of Mass Spectral Library Search Algorithms for Compound Identification. J. Am. Soc. Mass Spectrom. 1994, 5 (9), 859–866. https://doi.org/10.1016/1044-0305(94)87009-8.

Tauler, R. Chemometrics and Intelligent Laboratory Systems Multivariate Curve Resolution Applied to Second Order Data. Chemom. Intell. Lab. Syst. 1995, 30 (95), 133–146.
Tauler, R.; Smilde, A.; Kowalski, B. Selectivity, Local Rank, Three-Way Data Analysis and Ambiguity in Multivariate Curve Resolution. J. Chemom. 1995, 9 (1), 31–58. https://doi.org/10.1002/cem.1180090105.

Tessarolo, N. S.; dos Santos, L. R. M.; Silva, R. S. F.; Azevedo, D. A. Chemical Characterization of Bio-Oils Using Comprehensive Two-Dimensional Gas Chromatography with Time-of-Flight Mass Spectrometry. J. Chromatogr. A 2013, 1279 (2013), 68–75. https://doi.org/10.1016/j.chroma.2012.12.052.

Tranchida, P. Q.; Purcaro, G.; Dugo, P.; Mondello, L. Modulators for Comprehensive Two-Dimensional Gas Chromatography. TrAC, Trends Anal. Chem. 2011, 30 (9), 1437–1461. https://doi.org/10.1016/j.trac.2011.06.010.

Tranchida, P. Q.; Purcaro, G.; Visco, A.; Conte, L.; Dugo, P.; Dawes, P.; Mondello, L. A Flexible Loop-Type Flow Modulator for Comprehensive Two-Dimensional Gas Chromatography. J. Chromatogr. A 2011, 1218 (21), 3140–3145. https://doi.org/10.1016/j.chroma.2010.11.082.

Tranchida, P. Q.; Salivo, S.; Franchina, F. A.; Mondello, L. Flow-Modulated Comprehensive Two-Dimensional Gas Chromatography Combined with a High-Resolution Time-of-Flight Mass Spectrometer: A Proof-of-Principle Study. Anal. Chem. 2015, 87 (5), 2925–2930. https://doi.org/10.1021/ac5044175.

Tranchida, P. Q.; Maimone, M.; Franchina, F. A.; Bjerk, T. R.; Zini, C. A.; Purcaro, G.; Mondello, L. Four-Stage (Low-)Flow Modulation Comprehensive Gas Chromatography□ quadrupole Mass Spectrometry for the Determination of Recently-Highlighted Cosmetic Allergens. J. Chromatogr. A 2016, 1439, 144–151. https://doi.org/10.1016/j.chroma.2015.12.002.

Trinklein, T. J.; Gough, D. V.; Warren, C. G.; Ochoa, G. S.; Synovec, R. E. Dynamic Pressure Gradient Modulation for Comprehensive Two-Dimensional Gas Chromatography. J. Chromatogr. A 2019, 460488. https://doi.org/10.1016/j.chroma.2019.460488.

Wang, A.; Tolley, H. D.; Lee, M. L. Gas Chromatography Using Resistive Heating Technology. J. Chromatogr. A 2012, 1261, 46–57. https://doi.org/10.1016/j.chroma.2012.05.021.

Wang, A.; Hynynen, S.; Hawkins, A. R.; Tolley, S. E.; Tolley, H. D.; Lee, M. L. Axial Thermal Gradients in Microchip Gas Chromatography. J. Chromatogr. A 2014, 1374, 216–223. https://doi.org/10.1016/j.chroma.2014.11.035.

Watson, N. E.; Siegler, W. C.; Hoggard, J. C.; Synovec, R. E. Comprehensive Three-Dimensional Gas Chromatography with Parallel Factor Analysis. Anal. Chem. 2007, 79 (21), 8270–8280. https://doi.org/10.1021/ac070829x.

Watson, N. E.; Bahaghighat, H. D.; Cui, K.; Synovec, R. E. Comprehensive Three-Dimensional Gas Chromatography with Time-of-Flight Mass Spectrometry. Anal. Chem. 2017, 89 (3), 1793–1800. https://doi.org/10.1021/acs.analchem.6b04112.

Watson, N. E.; Prebihalo, S. E.; Synovec, R. E. Targeted Analyte Deconvolution and Identification by Four-Way Parallel Factor Analysis Using Three-Dimensional Gas Chromatography with Mass Spectrometry Data. Anal. Chim. Acta 2017, 983, 67–75. https://doi.org/10.1016/j.aca.2017.06.017.

Welke, J. E.; Manfroi, V.; Zanus, M.; Lazzarotto, M.; Zini, C. A. Differentiation of Wines According to Grape Variety Using Multivariate Analysis of Comprehensive Two-Dimensional Gas Chromatography with Time-of-Flight Mass Spectrometric Detection Data. Food Chem. 2013, 141 (4), 3897–3905. https://doi.org/10.1016/j.foodchem.2013.06.100.

Wilson, R. B.; Hoggard, J. C.; Synovec, R. E. High Throughput Analysis of Atmospheric Volatile Organic Compounds by Thermal Injection – Isothermal Gas Chromatography – Time-of-Flight Mass Spectrometry. Talanta 2013, 103, 95–102. https://doi.org/10.1016/j.talanta.2012.10.013.

Zeng, Z.; Li, J.; Hugel, H. M.; Xu, G.; Marriott, P. J. Interpretation of Comprehensive Two-Dimensional Gas Chromatography Data Using Advanced Chemometrics. TrAC, Trends Anal. Chem. 2014, 53, 150–166. https://doi.org/10.1016/j.trac.2013.08.009.